Isomeric States in the Rapid Neutron Capture Process

Master's Thesis, 8 April 2024

Author:

Miikka Winter

Supervisor:

Prof. Anu Kankainen
Dr. Stylianos Nikas

UNIVERSITY OF JYVÄSKYLÄ
DEPARTMENT OF PHYSICS

Abstract

Winter, Miikka
Isomeric States in the Rapid Neutron Capture Process
Master's thesis
Department of Physics, University of Jyväskylä, 2024, 140 pages.

The rapid neutron capture process, the r-process, is responsible for creating around a half of the nuclei above $A \approx 60$. The r-process nucleosynthesis is simulated with a nuclear reaction network that evolves the system according to the given parameters. The nuclear reaction networks involve thousands of different nuclides, but in general, they only utilise the ground state nuclei, and not isomeric states, i.e. the metastable states of the nuclei. However, in recent years, there has been research on isomers and their effect on the r-process nucleosynthesis. The so-called astromers are isomers that potentially have the greatest effect on the outcome of the r-process nucleosynthesis.

In this thesis, for the first time, a wide selection of isomers were added to a nuclear reaction network. The original code was modified to include isomeric states, and the results obtained with isomers were compared with the results without isomers. The nucleosynthesis code was run with five different initial conditions. Abundances of elements were compared at $t = 1$ Ga, and the total heating was compared during the first 1000 days after the r-process. The obtained results show not only that the code works with the added isomers but also that the results with the added isomers show some expected differences to the reference results without isomers. The differences are subtle, and especially the location of the added isomers with respect to the r-process path determine, what is the effectiveness of the isomers to the results.

Keywords: Nuclear astrophysics, r-process, isomer, astromer, nucleosynthesis

Tiivistelmä

Winter, Miikka
Isomeeritilat nopeassa neutronisieppausprosessissa
Pro gradu -tutkielma
Fysiikan laitos, Jyväskylän yliopisto, 2024, 140 sivua

Nopea neutronisieppausprosessi eli r-prosessi tuottaa noin puolet massalukua $A \approx 60$ raskaammista ytimistä. R-prosessiydinsynteesiä voidaan simuloida ydinreaktioverkolla, joka kehittää järjestelmää annettujen parametrien mukaisesti. Ydinreaktioverkoissa on tuhansia eri nuklideja, mutta ne ovat pääasiassa ainoastaan perustilalla, eikä isomeeritiloja eli metastabiileja ytimen tiloja käytetä. Viime vuosina on kuitenkin ollut tutkimusta isomeerien vaikutuksesta r-prosessiydinsynteesiin. Niin kutsutut astromeerit ovat isomeereja, joilla potentiaalisesti on suurin vaikutus r-prosessiydinsynteesin lopputulemaan.

Tässä tutkielmassa on ensimmäistä kertaa lisätty laajalti isomeereja ydinreaktioverkkoon. Alkuperäistä koodia muokattiin sisältämään isomeerit, ja saatuja tuloksia isomeerien kanssa verrattiin ilman isomeeereja saatuihin tuloksiin. Ydinsynteesikoodia suoritettiin viiden eri alkuarvon kanssa. Alkuaineiden pitoisuuksia verraattiin ajanhetkellä $t = 1$ Ga ja kokonaisenergiantuottoa verrattiin ensimmäisten 1000 päivän aikana r-prosessin jälkeen. Saadut tulokset osoittivat paitsi sen, että koodi toimii lisättyjen isomeerien kanssa, mutta myös sen, että saadut tulokset isomeerien kanssa tuottavat odotettuja eroja ilman isomeereja oleviin tuloksiin nähden. Erot ovat vähäisiä, ja etenkin lisättyjen isomeerien sijoittuminen r-prosessin polun suhteen määrittävät isomeerien vaikutusta tuloksiin.

Avainsanat: Ydinastrofysiikka, r-prosessi, isomeeri, astromeeri, ydinsynteesi

Acknowledgements

First and foremost, I would like to thank the supervisors of this thesis, Professor Anu Kankainen and Doctor Stylianos Nikas, for introducing me to the fascinating world of nuclear astrophysics and to the topic of this thesis. Additionally, special thanks to Prof. Kankainen for the valuable feedback on the thesis and Dr. Nikas for providing me reaction rates and other useful material for the thesis work. I would also like to acknowledge CSC - IT Center for Science, Finland, for computational resources used in testing and running the network code for this thesis as without their servers this thesis would not have been possible.

Jyväskylä 8 April 2024

Miikka Winter

Contents

1 Introduction

The advances in subatomic physics in the late 19th century and the early 20th century paved the way to the modern nuclear astrophysics. Works of Sir Arthur Eddington, Hans Bethe, Charles Critchfield, and Carl Friedrich von Weizsäcker, among others, opened new insights in stellar energy production and the origin of elements in the first decades of the 20th century. [1–4] The stellar fusion reactions, like the proton-proton chain and the CNO (carbon-nitron-oxygen) cycle solved the first burning stage, the hydrogen burning, in stars. In 1953, Fred Hoyle proved the existence of a resonance at 7.6 MeV in a carbon-12 nucleus (the so-called Hoyle state) [5], based on the work of Edwin Salpeter and others [6, 7]. The state was later experimentally confirmed, and the suggested process, the triple-alpha process, explained how nucleosynthesis paths can bypass the instability of ^{8}Be and create elements heavier than ^{4}He in stars.

Even though processes for stellar nucleosynthesis were known, the abundances of elements could be only partially explained. In the mid-1940s, George Gamow had theorised that all elements were created in the Big Bang nucleosynthesis. [8] Hoyle had proposed in 1946 that all nuclei heavier than lithium were produced in stars, and he expanded upon this in 1954. [5, 9] A whole new insight was given in 1957 when *Synthesis of the Elements in Stars* was published. This is often referred as the B^{2}FH paper after its authors Margaret Burbidge, Geoffrey Burbidge, William A. Fowler, and Fred Hoyle. [10] At the time the paper was revolutionary, as it claimed that only hydrogen, helium, and lithium were synthesised during the Big Bang, and the heavier elements were created in stars. The paper proposed eight different processes to explain the abundances of heavy elements. These processes included the slow and the rapid neutron-capture processes, also known as the s- and r-processes. With these processes the creation of the heaviest elements could be explained as neutrons are not affected by the Coulomb barrier in the nucleus and the reactions involving only neutrons as projectile are far more likely than those involving protons and charged particles, like α particles. [11]

Nowadays, it is known that hydrogen (^{1}H) and helium (^{4}He) are the main

primordial elements, formed in the Big Bang. They are also the most abundant of the elements, accounting for around 98% of the total abundance of baryonic matter. [11, 12] In the Big Bang, also traces of ^{2}H, ^{3}He, and ^{7}Li were formed. All the other elements have been created after the primordial nucleosynthesis, starting from the elements created in the Big Bang. The fusion reactions in stars can produce elements up to mass number $A \approx 60$, i.e. the iron peak elements, during the lifetime of the most massive stars. [11] The elements in the iron peak are the most bound ones, with ^{62}Ni having the highest binding energy per nucleon. [13, 14] Figure 1 illustrates the nuclear binding energy per nucleon as a function of mass number. Like the B^{2}FH paper suggested, most of the heavier than iron peak elements are formed in the s- and r-process nucleosynthesis. Some contribution also comes from other processes, like νp-, ν-, and p-processes, where ν and p stand for neutrino and proton respectively. [15, 16]

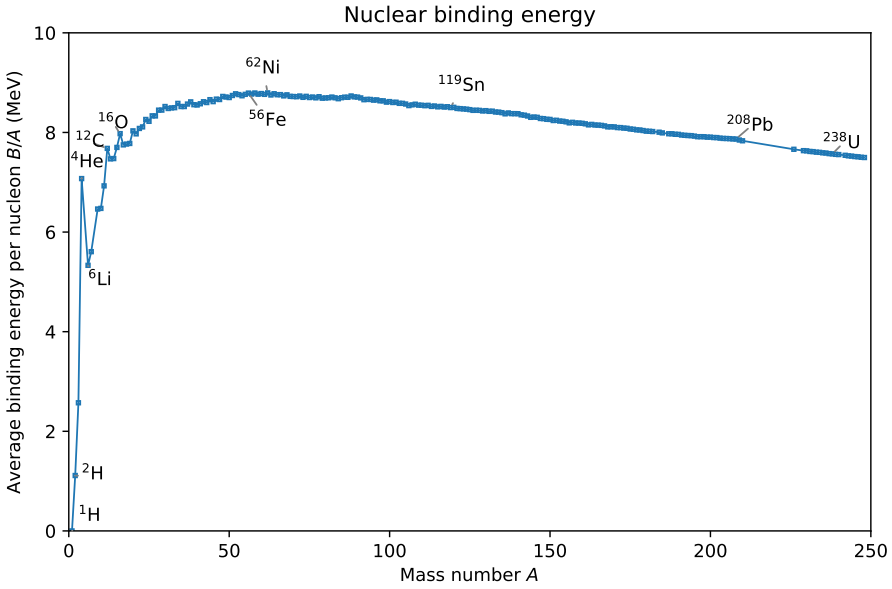

Figure 1. Average nuclear binding energy per nucleon B/A as a function of mass number A. The binding energy data has been obtained from AME2020 [17].

For a long time, the r-process was known to exists and widely theorised, but there had been no observations of an astrophysical site where the r-process could occur. In 2017, a gravitational wave signal, named GW 170817 after its observation date (17th August 2017), was detected by LIGO and Virgo gravitational-wave detectors. This signal originated from the galaxy NGC 4993, and it resulted from a binary

pair of neutron stars spiralling towards each other and finally merging. [18, 19] After merging, the formed neutron star is assumed to have promptly collapsed into a black hole as there was no evidence of ejecta being powered by a spin-down of a supermassive neutron star. [20] The merger also produced an electromagnetic signal which was registered in observatories around the Earth. [21] This signal was analysed, and combined with the gravitational wave signal, it corresponded to that of a so-called kilonova, resulting from a merger of two neutron stars. [22] The kilonova signal contained spectroscopic evidence of decaying material ejected from the merger that could only be explained with r-process nucleosynthesis. For the first time, direct evidence of the astrophysical site of the r-process was obtained and measured. [23–25]

While the r-process was already outlined in the 1950s, the exact model how to describe it was not fully understood. There were several scenarios how the r-process should evolve and which could be the possible astrophysical sites where conditions for the r-process nucleosynthesis would be suitable. As the name, the rapid neutron capture process, suggests, consecutive neutron captures have to be fast enough to overcome beta decay rate, the opposite of the s-process. This leads to very neutron-rich nuclei that are far from the valley of stability. As these nuclei are very short-lived, their nuclear properties have uncertainties regarding masses, half-lives, and fission barriers. These, in turn, lead to uncertainties in reaction rates that affect the modelling of the r-process which is done with a nuclear reaction network code. [26]

So far, the r-process calculations done with reaction network codes have been using only the ground states of involved nuclei in a full scale r-process simulation. However, there have been research in the recent years [27, 28] that shows adding metastable excited states of nuclei, isomers, to the network could potentially alter the outcome of the r-process nucleosynthesis. In this thesis, this was investigated by modifying an existing network code, GSINet, by adding isomeric states to the network. The results are then compared to the outcome of the default network code, i.e. the one without isomers.

In Chapter 2, theoretical background of the r-process nucleosynthesis is given. Some parameters relevant to the r-process nucleosynthesis are introduced in Section 2.1, and an overview of the different phases of the nucleosynthesis in the r-process is given in Section 2.2. Binary neutron star mergers and other possible r-process sites are presented in Section 2.3. Nuclear isomers, and a special case of astromers,

are discussed in the last part of Chapter 2. An introduction to nuclear network codes, and in particular to GSINet, is given in Chapter 3, as well as description of supplemental codes and input files used in this thesis. The modifications done to the original network code are also described. In Chapter 4, the obtained results using the modified code with isomers are compared to the results obtained using the unmodified code. In Chapter 5, an overview of the work with a recap of results is given, and in the outlook section, possible future improvements and further modifications to the code are presented. At the end of the thesis, the isomers used in the calculations are listed in Appendix A, and some of the self-written codes used in the network are presented in Appendix B. In Appendix C, snapshots of different moments of the r-process nucleosynthesis are provided with different initial conditions.

2 Nuclear Astrophysics

2.1 Parameters

The r-process nucleosynthesis is sensitive to a few parameters regardless of the astrophysical site where the r-process is occurring. The initial electron abundance Y_e, entropy S, and the expansion timescale τ determine the composition of the material at the time of the freeze-out phase (see Section 2.2.2) during the r-process nucleosynthesis, and thus they directly affect the outcome of the process. [29]

2.1.1 Abundance

The abundance Y_i of a species i describes the occurrence of the species i relative to all other species in the system. It can be given as a ratio of number density of the species i to the number density of baryons (e.g. [11])

$$Y_i = \frac{n_i}{n}, \tag{1}$$

where n_i and n are the number density of species i and baryons respectively. Number density can be defined as

$$n_i = \frac{X_i \rho}{m_i}, \tag{2}$$

where X_i is the mass fraction of the species i, ρ is the mass density, and m_i is the mass of a nucleus of species i. The mass of the species i can be approximated using the atomic mass unit m_u as $m_i \approx A_i m_u$, where A_i is the mass number of the species i. On the other hand, mass fraction can be written as a ratio of the mass of the species i and the total mass, or equivalently as a ratio of the density of species i and the total mass density ρ:

$$X_i = \frac{m_i}{\sum_i m_i} = \frac{\rho_i}{\rho}. \tag{3}$$

Now the abundance of species i can be given with

$$Y_i = \frac{X_i}{A_i}. \tag{4}$$

Naturally, the sum over all mass fractions in the system is 1:

$$\sum_i X_i = 1. \tag{5}$$

However, as a direct consequence from the definition in Equation (4), the sum over abundances is less than 1, as $Y = X/A \leq X$:

$$\sum_i Y_i < 1. \tag{6}$$

The electron abundance, Y_e, or the proton-to-nucleon ratio, is one of the parameters that determine the initial conditions in the r-process nucleosynthesis. It describes how neutron-rich or neutron-deficient the matter in the system is. It can be written as

$$Y_e = \sum_i Z_i Y_i = \sum_i Z_i \frac{X_i}{A_i} = \sum_i \frac{Z_i}{A_i} X_i, \tag{7}$$

where Z_i and A_i are the number of protons and nucleons of the species i respectively. If $Y_e = 1$, there are equal number of electrons and baryons, so practically this would correspond to the case of 100% ^{1}H, as the system has a zero net charge. If $Y_e = 0.5$, there are equal number of protons and neutrons, and if $Y_e = 0$, the system would be composed of pure neutron matter. In the r-process nucleosynthesis, lower Y_e means there are more neutrons available for each pre-existing seed nucleus for neutron captures in the r-process, and thus the neutron-to-seed ratio is higher. This leads to potentially heavier nuclei. [29]

2.1.2 Entropy

The conditions in which the r-process takes place are extreme in many ways. In a binary neutron star merger, matter density and temperature are initially very high. The hot and dense matter starts to expand and cool down quickly after the merger has occurred. Performing the r-process simulations require that the time dependence of neutron number density n_n, i.e. the number of neutrons per volume unit $n_n = N/V$, and temperature T is modelled depending on the specific astrophysical site and and event type. Electron abundance Y_e determines the neutron richness of the matter. As the r-process site in an explosive environment with rapid expansion and cooling, adiabatic expansion of hot matter is a realistic assumption to describe it. [30, 31]

Thus n_n and T can be related to each other by using entropy S [30]

$$S = -\left(\frac{\partial \Phi_G}{\partial T}\right)_{\overline{V},\mu_c^{\mathrm{tot}}}, \tag{8}$$

where Φ_G is the grand canonical potential, T temperature, $\overline{V}$ the specific volume, and μ_c^{tot} the chemical potential. At high temperature entropy is dominated by radiation, and the equation for S per nucleon can be given as [30]

$$S \approx S_\gamma \approx \frac{4 m_u \tilde{a}}{3}\frac{T^3}{\rho}, \tag{9}$$

where m_u is the atomic mass constant, and, ρ the density of matter. $\tilde{a}$ is the radiation density constant given by [30]

$$\tilde{a} = \frac{\pi^2 k_{\mathrm{B}}^4}{15\,(\hbar c)}, \tag{10}$$

where $\mathrm{k_B}$ is the Boltzmann constant, $\hbar$ the reduced Planck constant, and c the speed of light. A numerical value is $\tilde{a} \approx 7.565 \times 10^{-16}$J K^{-4} m^{-3}. However, if the density is low while temperature is high, the pressure contribution from electron-positron pairs need to be considered as well. Including this to Equation (10) gives [30]

$$S = S_\gamma \left[1 + \frac{7}{4} f_{\mathrm{ent}}(T)\right], \tag{11}$$

where f_{ent} is a smoothly varying function with $f_{\mathrm{ent}} \in [0,1]$ giving the contribution from ultra-relativistic particles. The factor 7/4 is due to the difference between Bose-Einstein and Fermi-Dirac statistics. [30]

The entropy results given in Equations (8)–(11) have been derived and discussed in detail in [30].

2.1.3 Timescale

The third parameter that affects the outcome of the r-process nucleosynthesis is the expansion timescale. In the adiabatic expansion, where $S = \text{const.}$, the timescale τ can be written with density ρ as [32]

$$\tau = \left|\frac{1}{\rho}\frac{d\rho}{dt}\right|, \tag{12}$$

where $d\rho/dt$ is the derivative of density over time. This is the e-folding time of the density, i.e. $\rho(\tau) = \rho_0/e$, where ρ_0 is the initial density, and e is Euler's number. Another way of defining the expansion timescale is to use expansion velocity v_{ex}:

$$\tau = \frac{R_0\,(e-1)}{v_{\mathrm{ex}}}, \tag{13}$$

where R_0 is the initial radius of the expanding material. [30]

2.2 The r-process nucleosynthesis

The r-process and the s-process are both neutron capture processes, but the difference lies in the astrophysical site and conditions that affect the outcome of the process. Typical neutron number densities are in the s-process around 10^8 neutrons/cm^3, and in the r-process around 10^{18}–10^{22} neutrons/cm^3. [30] This directly affects the rate at which neutron captures take place. In the s-process neutron captures are several orders of magnitude slower compared to the r-process. The r-process neutron capture timescales are typically less than milliseconds [33] while in the s-process the capture timescale is in general from days to years, even decades [34]. Due to the difference in how quickly the consecutive neutron captures take place, in the s-process, after each neutron capture the nucleus has time to undergo beta decay. In the r-process, several consecutive neutron captures occur before the nucleus undergoes a β-decay. As a consequence, the r-process operates rather far from the bottom of the valley of stability, and it produces the most neutron-rich isotopes. It is also responsible for the heaviest elements in the solar system as the s-process cannot produce elements heavier than A = 209 as it is the heaviest "stable" isotope ("stable" in an astrophysical sense as $t_{1/2}\left(^{209}\mathrm{Bi}\right) \approx 2.0 \times 10^{19}$ years [35]). The s-process is terminated by α-unstable isotopes ^{210}Po, ^{211}Po, and ^{211}Bi that follow ^{209}Bi in the neutron capture-β-decay chain. α-decays return the neutron capture flow back to ^{206}Pb and ^{207}Pb from which the cycle continues to ^{209}Bi, and the s-process is effectively terminated in this loop. [36] Figure 2 shows the approximate paths of the s- and r-processes in nuclear chart.

The elements heavier than those in the iron peak but lighter than ^{209}Bi can have origins in both s- and r-process, or be solely s- or r-only isotopes. Of the solar material above $A \approx 60$, around one half comes from the s-process, and the other half from the r-process [29]. In comparison, the p-process produces only about 0.001 to 0.01 of the abundances of the s- and r-isobars [29]. Figure 3 illustrates the origin

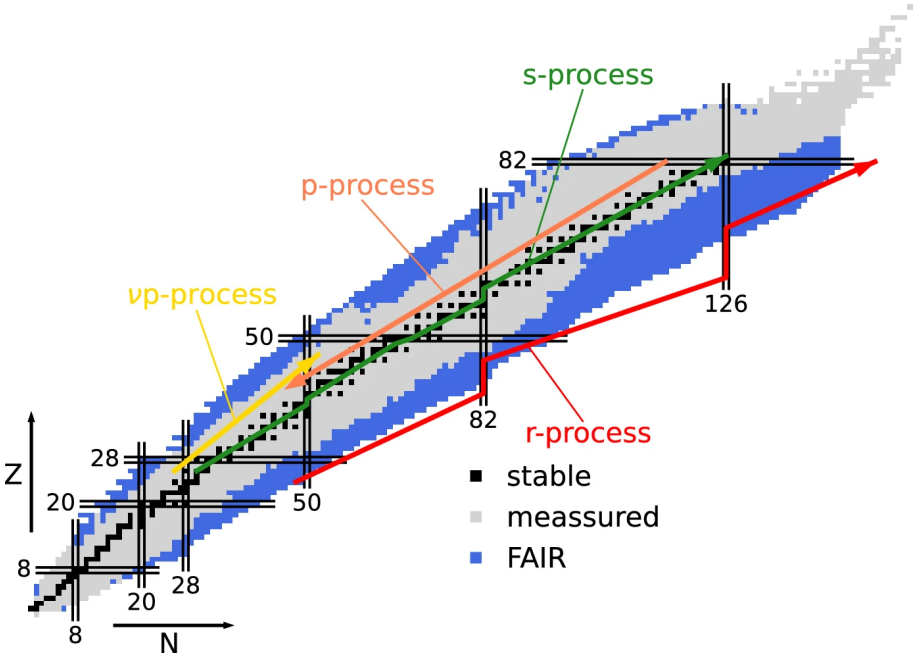

Figure 2. Nuclear chart showing the paths of the s- and r-processes as well as the p- and νp-process paths. The black squares are stable isotopes, while grey squares mark the unstable nuclei that are produced in the laborary. Blue squares indicate the isopes researched in FAIR (Facility for Antiproton and Ion Research). Horizontal and vertical black lines with values 8, 20, 28, 50, 82, and 126 show the magic numbers for protons and neutrons. From [12], by A. Arcones and F.-K. Thielemann, CC BY 4.0

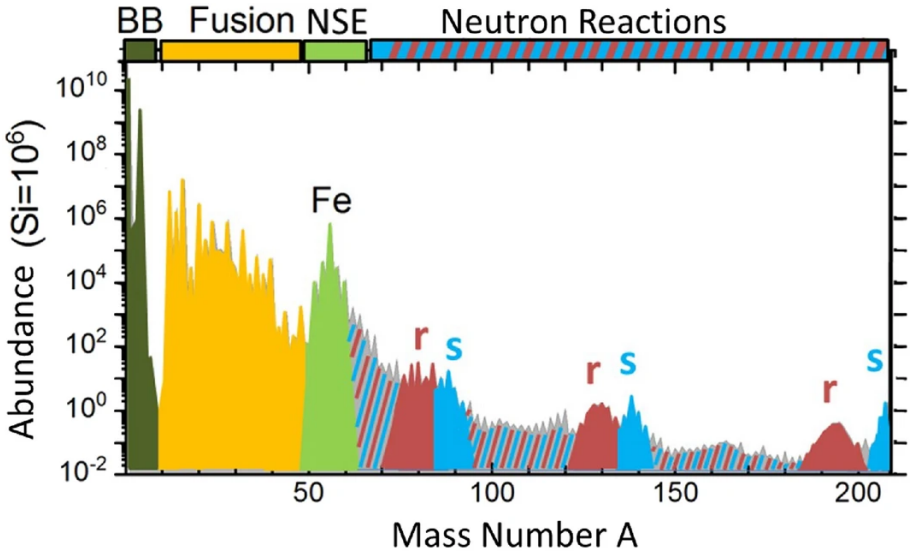

Figure 3. Solar abundances of elements as a function of mass number A. The lightest elements are primordial from the Big Bang, marked with a brownish colour. Elements originating from previous stars are marked in yellow, and the iron peak elements are marked with green. Both the r- and s-processes produce element beyond the iron peak, but there are certain peaks visible in the graph which are mainly created by the r- or s-processes. P-process abundances are minimal, and thus not shown in the graph. From [12], by A. Arcones and F.-K.Thielemann, figure originally courtesy of F. Käppeler, CC BY 4.0

of elements, showing the s- and r-process peaks. Note that the heaviest elements beyond the s-process ($A > 209$) are not visible. As the r-process operates rather far from the bottom of the valley of stability, it can only produce those stable elements that are not shielded by any beta-stable isotopes. On the other hand, the s-process cannot advance from isotopes that have longer neutron capture timescale than the beta decay half-live. Isotopes shielded by these are the r-only isotopes. This is also true for the heaviest isotopes, like ^{232}Th, ^{235}U, and ^{238}U which are not reached by the s-process nucleosynthesis. [30]

While the s-process occur in stars, mostly in asymptotic giant branch stars [11], over periods of thousands of years, the r-process requires explosive conditions which may last only days. High enough neutron density and temperature can be reached e.g. in neutron star mergers. For a long time there were several candidates for r-process sites, like core-collapse supernovae and He-layers of massive stars [37], but the observed isotopes in the neutron star merger in 2017 proved that at least kilonovas are potential sites for the r-process. [37] Other proposed sites include

the inner regions of massive-star supernova explosions. [26] The r-process sites are discussed in Section 2.3.

2.2.1 Nuclear statistical equilibrium

Initially, e.g. after a neutron star merger, the material in the r-process site is dense and hot, $T > 10$ GK. [38] The temperature and density are high enough so that all possible forward and inverse strong and electromagnetic reactions both have high rates, and the material is in so-called nuclear statistical equilibrium (NSE). This means that every nuclide is in the network is in equilibrium via strong and electromagnetic interactions [39]:

$$N \times n + Z \times p \rightleftharpoons X(N,Z) + \gamma, \tag{14}$$

where N and Z are the neutron and proton numbers respectively, and $X(N,Z)$ is a nucleon with N neutrons and Z protons. Equation (14) can also be written in terms of chemical potentials:

$$N \times \mu_n + Z \times \mu_p = \overline{\mu}(N,Z) \equiv \mu_{N,Z}, \tag{15}$$

where μ_n and μ_p are the chemical potentials of neutrons and protons respectively, and $\mu_{N,Z}$ is the chemical potential of a nucleus with N neutrons and Z protons. Neglecting the screening effect caused by electrons (see e.g. [40]) and assuming that nuclei obey Maxwell-Boltzmann statistics, the chemical potential can be written as [41]:

$$\mu_i = m_i c^2 + k_B T \ln \left[\rho N_{\mathrm{A}} \frac{Y_i}{G_i} \left(\frac{2\pi\hbar^2}{m_i k_B T} \right)^{\frac{3}{2}} \right], \tag{16}$$

where $m_i c^2$ is the rest mas of the nucleus, k_B the Boltzmann constant, N_{A} the Avogadro constant, ρ the baryon density, and G_i the partition function. Substituting Equation (16) into Equation (15), the abundance Y_i can be solved and expressed in terms of the abundances of the free protons Y_p and neutrons Y_n [41]:

$$Y(N,Z) = G_{N,Z} \left(\rho N_A\right)^{N+Z+1} \frac{(N+Z)^{\frac{3}{2}}}{2^{N+Z}} \left(\frac{2\pi\hbar}{m_u k_B T} \right)^{\frac{3}{2}(N+Z+1)} \times \exp\left\{ \left(\frac{B_{N,Z}}{k_B T} \right) \right\} Y_n^N Y_p^Z, \tag{17}$$

where $Y(N,Z)$ is the abundance, $G_{N,Z}$ the partition function of the nucleus, m_u the atomic mass, and $B_{N,Z}$ is the binding energy of the nucleus. The binding energy is defined as:

$$B_{N,Z} = (N \times m_n + Z \times m_p - m_{N,Z})\, c^2, \tag{18}$$

where m_n and m_p are the mass of neutron and proton respectively. Equation (17) is by itself inadequate to determine $Y(N,Z)$ as Y_n and Y_p are unknown. Conservation of mass, Equation (5), written as [11]

$$\sum_i X_i = \frac{\sum_i n_i M_i}{\rho N_A} = 1, \tag{19}$$

where n_i is the number density of nucleus i, and M_i its mass, can be used as a constraint. Also the total charge is conserved, as per Equation (7). Using Equations (17), (19), and (7), the composition of matter can be determined by the temperature T, density ρ (or equivalently entropy S, following Equation (9)), and electron abundance Y_e, as long as the binding energies $B_{N,Z}$ and partition functions $G_{N,Z}$ are known. [11, 41]

Reactions involving the weak interaction, i.e. β-decays, electron captures, and charged-current neutrino interactions, change the proton-to-neutron ratio Y_e and occur on longer time scales than capture and photodisintegration reactions. They have to be followed explicitly as they are not necessarily in equilibrium. Using densities ρ, temperatures T, and Y_e as functions of time, $\rho(t), T(t),$ and $Y_e(t)$ with the total mass conservation, and determining Y_e by following the weak interactions, Equations (4) and (7) can be written as [37]:

$$\sum_i A_i Y_i = Y_n + Y_p + \sum_{i,(A_i>1)} (Z_i + N_i)\, Y_i\,(\rho,T,Y_n,Y_p) = 1, \tag{20}$$

and

$$\sum_i Z_i Y_i = Y_p + \sum_{i,(Z_i>1)} Z_i Y_i\,(\rho,T,Y_n,Y_p) = Y_e, \tag{21}$$

where Y_i is now also dependent on time.

There can be cases when groups of nuclei are in statistical equilibrium, and NSE holds within that group. However, the different groups might not be in statistical equilibrium, instead, groups might be connected by comparatively slow reactions that are not in equilibrium. In such a case, these connecting rates need to be known.

Aforementioned case is called quasi-statistical equilibrium (QSE). One example of QSE is the triple-α reaction that is responsible for ^{12}C creation is stars. [30] QSE occurs also before and after the conditions for NSE are fulfilled. [37]

2.2.2 The NSE freeze-out

As the material at the r-process site expands, it cools and the density drops. The NSE holds as long as all the nuclei are in equilibrium as in Equation (14). As the temperature keeps falling, the slowest reactions begin to fall out of the equilibrium. Photodisintegration reactions freeze-out faster than the corresponding capture reactions. Hydrodynamical conditions, entropy S and the expansion timescale τ, determine how fast the freeze-out is. It occurs at $T \approx 6$ GK in explosive events like neutron star merger. [11, 30, 37] Initially, before the freeze-out, the material is α-rich. The full NSE starts to break down as some of the charged-particle reactions become slower relative to the expansion timescale, and thus QSE clusters are formed. Internally, these are still in NSE, but externally different clusters are no longer in equilibrium. In its early stages, the QSE phase is dominated by two clusters: a light cluster containing neutrons and α-particles, and traces of protons, and a heavy cluster containing ^{12}C and heavier elements. The heavy cluster is primarily determined by the $\alpha + \alpha + n$ reaction. [29, 42] The heavier cluster can further divide into to smaller clusters: Fe-group above Ca (N,$Z = 20$), and Si-group between Ne (N,$Z = 10$) and Ca. [37]

As the temperature decreases, the QSE clusters are fragmented into smaller clusters until the QSE approximation breaks altogether. After this point, a full nuclear reaction network is needed to calculate abundances. (α, γ) and (α, n) with neutron capture reactions(n, γ) dominate the α-rich environment, resulting nuclei mass numbers upwards from iron ($A \approx 56$). As the temperature keeps falling, in the end there are only neutron captures left. As the $(\alpha\alpha n)$ reaction is heavily dependant on the density (ρ^3-dependency), the decreasing density of the expanding matter further speeds up the freeze-out. [29]

The nuclei present at the freeze-out are seed nuclei for the r-process. The initial electron fraction Y_e, the entropy S, and the dynamical timescale τ_{dyn} determine the composition of the material at the time of freeze-out. The neutron-to-seed ratio determines how heavy the elements created in the r-process nucleosynthesis can become, e.g. in order to produce a nuclei with $A = 180$ when the seed nucleus has

$A = 80$, there has to be in average 100 neutrons available. A high enough neutron-to-seed ratio can be obtained by multiple ways: the entropy has to be high enough with high enough temperatures and low enough densities, with lower entropies, if electron fraction is low enough, or the temperature decreases fast enough and thus preventing the creation of heavy seeds. [29] As can be seen from Equation (17), density ρ has a high power directly dependent on the mass number A: ρ^{A-1} which leads to heavier nuclei. Similarly, light nuclei are preferred in high temperature environments, due to $(k_B T)^{-3/2(A-1)}$. The exponential term $\exp(B/k_B T)$ favours tightly bound nuclei, i.e. the Fe group nuclei, in the intermediate regime. Temperature then determines how widely is the composition distributed over the mass range in the Fe group. [43]

Due to the high dependency of $(\alpha\alpha n)$ reaction on density, in low densities at the freeze-out there is an overabundance of α particles which hinders the creation of heavier nuclei in the r-process after the freeze-out. Thus, the abundance of heavier than ^{4}He nuclei is reduced compared to their NSE abundances. On the other hand, the abundance maximum of the heavy nuclei is shifted, due to final α captures, to heavier nuclei when compared to the NSE. Instead of the maximum being in the iron peak ($A = 50$–60), it can even reach $A \approx 90$. [43] As the total entropy is dominated by electromagnetic radiation in hot environments, with $S \sim T^3/\rho$ [44, 45], high entropies are thus reached with high temperatures and low densities. As a consequence, high entropies cause α-rich freeze-out, and only relatively small amounts of the iron peak elements are produced. [43]

The r-process can produce actinides or heavier (i.e. $Z \geq 89$) if the neutron-to-seed ratio is around 150, if the seeds have $A = 50$–100. This can be reached with lower entropies, as there are more neutrons available and the seeds are, in general, heavier than in a high entropy case. Lower entropies are found i.e. in the expansion of relatively cold and high-density matter, i.e. in the ejecta of a neutron star merger. In order to have a neutron-to-seed ratio of 150, Y_e has to be less than 0.1.[43] A more detailed analysis of the entropy-electron abundance dependency in the creation of heavy elements can be found e.g. in [46, 47].

2.2.3 The r-process

After the NSE freeze-out, Equation (17) is no longer valid, and all the nuclear reactions need to be considered. This is done in a nuclear reaction network. The evolution of the abundance Y_i for each element i over time can be obtained by solving a sum of ordinary differential equations. Each of these differential equations represent reactions that either produce or destroy abundances Y_i [41, 43]:

$$\frac{\mathrm{d}Y_i}{\mathrm{d}t} = \overbrace{\sum_j N_j^i \lambda_j Y_j}^{\substack{\text{decays and} \\ \text{photodisintegrations}}} + \overbrace{\sum_{j,k} \frac{N_{j,k}^i}{1+\delta_{jk}} \rho N_\mathrm{A} \langle \sigma v \rangle_{j,k} Y_j Y_k}^{\text{two-body reactions}} + \underbrace{\sum_{j,k,l} \frac{N_{j,k,l}^i}{1+\Delta_{jkl}} \rho^2 N_\mathrm{A}^2 \langle \sigma v \rangle_{j,k,l} Y_j Y_k Y_l}_{\text{three-body reactions}}, \quad (22)$$

where the first part includes all the reactions that create or destroy particles, the middle part includes all the two-body reactions, and the last part includes all the three-body reactions with the element i. Indices j,k, and l denote the other particles taking part in the reaction with the element i. N^i is the number of nuclei i that are either destroyed or created, with a negative or positive sign denoting destruction and creation respectively. λ_j is the decay rate of element j, including decays, photodisintegrations, electron captures, and neutrino-induced reactions. N_A is the Avogadro constant, and $\langle \sigma v \rangle$ denotes the thermal average of the product of the reaction cross section σ and the relative velocity v between the nuclei j and k and j,k, and l, depending on the number of subscripts. δ_{jk} and $\Delta - jkl$ are correction terms to prevent multiple counting of particles if the projectile and target are identical. δ_{jk} is the ordinary Kronecker delta, and Δ_{jkl} is defined as [43]:

$$\Delta_{jkl} \equiv \delta_{jk} + \delta_{kl} + \delta_{jl} + 2\delta_{jkl}. \quad (23)$$

True three-body reactions in Equation (22) are negligible in astrophysical conditions, but a sequence of two two-body reactions, where the first two-body reaction forms a short-lived intermediate nucleus, is often written as a three-body reaction. [37, 48] For more detailed discussion and derivation of Equation (22), see e.g. [41, 49, 50]. To calculate abundances from Equation (22), it has to be solved numerically. As can involve many orders of magnitudes for different reactions, it is a so-called stiff initial

value problem that has to be solved with an implicit method. [41, 51] This is done with nuclear reaction network codes, and in this thesis, GSINet is used (Section 3.2).

Charged-particle reactions are frozen at ≈ 3 GK, after which the isotopic chains are connected only by β^--decays, apart from α-decays and fission reactions in the heaviest ($A > 200$) elements. As the neutron density is still high, the time scales for neutron captures are much faster than those for β^--decays. At around 1 GK, photodisintegration reactions (γ, n) are still rapid for small neutron separation energies, as the photodisintegration reactions dominate already at temperatures related to $\approx 30 k_\mathrm{B} T \geq S_n$, where S_n is the neutron separation energy, i.e. the minimum energy required to remove a neutron from a nucleus [43]. Both the (n, γ) and the (γ, n) reactions are faster than the expansion timescale and the β-decay rates, so a chemical equilibrium is set in between the neutron captures and photodisintegrations. [43] This is the so-called waiting point approximation. [29] These (quasi-)equilibrium clusters that are formed in the waiting point approximation can be described similarly as in the NSE. Figure 4 shows a schematic of the waiting point approximation, with the red square marking the waiting point. While this is an approximation, and there are more complicated models to describe the r-process evolution, the waiting point approximation often holds rather well, if the temperature and the neutron number density are very high. [37] The abundance ratio between the two isotopes of element X, $^{\mathrm{A}}\mathrm{X}$ and $^{\mathrm{A+1}}\mathrm{X}$, can be obtained with [37, 43]

$$\frac{Y(Z,A+1)}{Y(Z,A)} = n_n \frac{G(Z,A+1}{2G(Z,A)} \left[\frac{A+1}{A}\right]^{\frac{3}{2}} \left[\frac{2\pi\hbar^2}{m_u k_\mathrm{B} T}\right]^{\frac{3}{2}} \exp\left\{\frac{S_n(Z,A+1)}{k_\mathrm{B} T}\right\} \qquad (24)$$

where n_n is the neutron number density, G denotes partition function of the nucleus, m_u is the atomic mass unit, and k_B is the Boltzmann constant. This can be obtained similarly as Equation (17) in the NSE case, see e.g. in [37]. The abundance ratio depends only on $n_n = \rho Y_n / m_u$, T, and S_n. The neutron separation energy S_n itself includes the mass dependency on nuclear masses. In practice, as no experimental data exists for very neutron-rich, highly unstable nuclei, theoretical mass-models are used. As the waiting point approximation was assumed, the neutron capture cross-sections are not needed to be known. [37]

Assuming the ratio $Y(Z,A+1)/Y(Z,A) \approx 1$ at the maximum, and the partition functions $G(Z,A+1) \approx G(Z,A)$, S_n has to be the same in all isotopic chains. This defines the so-called r-process path, along the waiting points. [37] The r-process

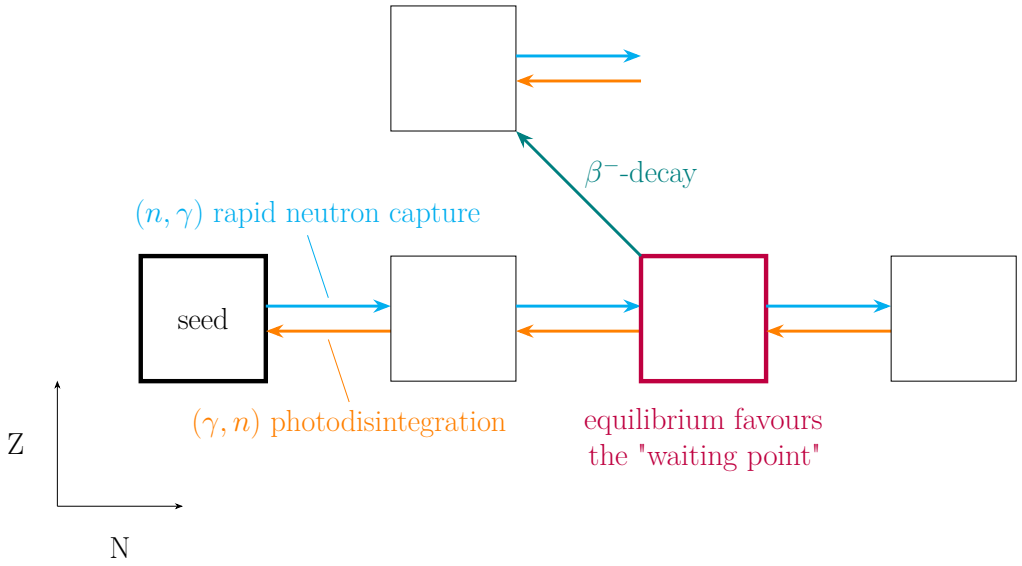

Figure 4. A schematic figure showing the waiting point approximation principle. At the waiting point (in red), photodisintegration reactions (in orange) and neutron capture reactions (in cyan) are in equilibrium, and there is sufficient time for β-decay (in teal) to take place. The seed serves as the starting point of the r-process neutron captures.

advances rapidly via neutron capture reactions, with increasing photodisintegration rates as the neutron excess increases, or equivalently, the associated neutron separation energy S_n decreases. [29] This leads to neutron-rich nuclei that have neutron separation energies S_n of 2 MeV and lower, i.e. the Q value for reaction (γ, n) is $Q_{(\gamma,n)}(Z,A) = S_n(Z,A+1)$. Neutron separation energies go down to zero at the neutron drip line where neutron captures can no longer advance as the reaction no longer releases energy. Thus, this means the theoretically heaviest possible isotope for each element is the one before the drip line. [37, 43]

Before the drip line, the r-process flow reaches a waiting point as the neutron capture and photodisintegration reactions become in equilibrium. At these points, β^--decay has enough time to occur. The closed neutron shells hinder the r-process flow as the particularly low neutron separation values S_n occur just past these closed shells, and thus waiting points tend to occur at the closed neutron shells. Neutron numbers, at which these closed shells are located, are called neutron magic numbers. They are a consequence from the nuclear shell model that is used to describe nuclear structure. For neutrons, these numbers are $N = 2, 8, 20, 28, 50, 82, 126, 184, \ldots$ [29] Consecutive neutron captures and β-decays can occur as long as the β-decays are more rapid than the neutron captures, with basically constant N and one-by-one

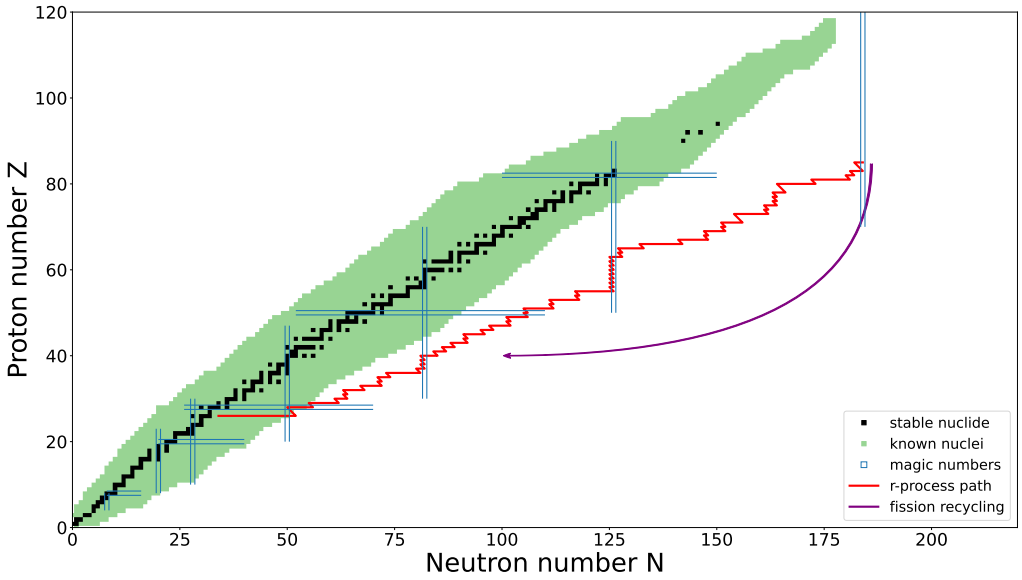

Figure 5. An illustration of an approximate r-process path (in red), starting from ^{56}Fe as a seed and ending at the closed shell at $N = 184$. At that point fission occurs, and in the so-called fission recycling (in purple), the formed daughter nuclei act as new seeds to the r-process neutron captures. The known nuclei listed in NUBASE2020 [52] are marked in green, and the stable ones in black. Vertical and horizontal blue lines mark the magic numbers. The path is based on the simulation with the code used in this work, see Figure 26 in Appendix C for an illustration of abundance evolution during the r-process nucleosynthesis.

increasing Z, forming a zigzag-like pattern. In Figure 5, the r-process path is marked with a red line. The vertical zigzag patterns occur at the neutron magic numbers. As the r-process path gets closer to the stability, S_n eventually becomes large enough so that the neutron capture reactions become more rapid than the β-decays. The capture reactions then continue, until the next waiting point is reached. [29] In waiting point approximation β^--decays are neglected along the path before the waiting point. If the conditions for the waiting point approximation are not met, i.e. either the neutron flux or the temperature is not very high, and thus the waiting point is not near the valley of stability, β^--decays deplete steadily the flow of nuclei toward higher neutron number N, and only a small fraction can reach a waiting point (that still occurs at the point where $(n,\gamma) \rightleftharpoons (\gamma,n)$). [53]

In the early phase of the r-process, the r-process path is mainly determined by the two-neutron separation energy S_{2n}, instead of S_n, due to the pairing effect preferring even neutron numbers. S_{2n} values decrease with increasing neutron excess, but a noticeable drop in S_{2n} values is caused again by closed neutron shells. There can also be seen a constant value or a saddle point behaviour just before or after closed shells, where a shape transition from a deformed to a spherical shape occurs, in several mass models. [37]

If the neutron-to-seed ratio is high enough, the r-process can continue to nuclei with a neutron number up to $N = 184$. At this point, a neutron shell becomes closed, and fission becomes a dominant reaction that terminates the r-process. For the extremely heavy nuclei, fission is basically the only decaying method. [37] The daughter nuclei formed in a fission reaction become new seeds for the r-process, and the cycle continues. This is the so-called fission recycling, and an illustration of it can be found in Figure 5, in which the fission recycling is marked with a curved purple arrow. Fission can be spontaneous, or it can also be induced by β^--decay, or by capturing a neutron (neutron-induced fission). [54] For heavy (A $\gtrsim$210) translead nuclei, α-decay is also possible, but, in general, β^--decays dominate. [37, 55] This does not take into account the nuclear isomeric states, discussed in Section 2.4 and with calculation results in Section 4. These, however, can be more impactful after neutron capture reactions have ended, and the formed nuclei decay towards stability due to differing nuclear properties like half-lives. [28] Apart from β^--decay, these can decay by releasing a photon without changes in the proton or neutron numbers via electromagnetic transition. [56]

As the neutron density falls during the expansion of the material, β^--decays and neutron captures start to operate on similar time scales, until the neutron source is depleted. This is the so-called r-process freeze-out. The transition from neutron-capture dominated phase to freeze-out occurs when neutron-to-seed ratio becomes close to one. After neutrons have been depleted, only β^--decays are present, with α-decay and fission being possible for the translead nuclei. [37] The abundance maxima tend to occur at the top end of the kinks in the r-process path at neutron shell closures $N = 50, 80,$ and 126. At the end of the r-process, after decaying to stability, these maxima are located at the corresponding mass numbers A. [37] The final abundances are also affected by the β-delayed neutron emission during the freeze-out as it acts as a source for neutrons, and shifts masses to lighter ones. Rarely, even a β-delayed two-neutron emission may occur. β-delayed neutron emission is dominating if the neutron-to-seed ratio is less than 150. With higher neutron-to-seed ratios also neutrons produced in fission reactions become significant. [37] Neutron emission during decay smoothens the odd-even staggering which occurs during the r-process neutron captures. [57]

The competition between β-decays and neutron captures smoothens the r-process abundances in comparison what could be expected from solely decaying matter during freeze-out. [37] The rare-earth peak ($A \approx 160$) is formed during the r-process freeze-out. With a low neutron-to-seed ratio the competing β^--decays and neutron captures cause the formation of the rare-earth peak [58], while with a higher neutron-to-seed ratio importance of fission increases [59, 60]. The r-process also has a strong effect on abundances at the 2nd r-process peak, at $A \approx 130$, and the 3rd peak at $A \approx 195$. [61] In a high neutron-to-seed case, material accumulates at $N = 184 (A \approx 280)$ which then by undergoes fission that produces nuclei with $A \lesssim 140$ and free neutrons. This can lead to different results in the final abundances, depending on the fission rates and yields. [59, 62, 63] The neutrons produced in fission have a strong impact on the 3rd r-process peak abundances. [61] The first r-process peak at $A \approx 80$ results from the accumulation of matter at the closed neutron shell $N = 50$. [64] Figure 6 shows the location of the three r-process peaks.

In this section, the waiting point approximation was assumed. However, there are also dynamical models that have time-dependent neutron number density $n_n(t)$, and temperature $T(t)$. These also discard the equilibrium requirement $(n, \gamma) \rightleftharpoons (\gamma, n)$ used in the waiting point approximation. Dynamical calculations have shown that

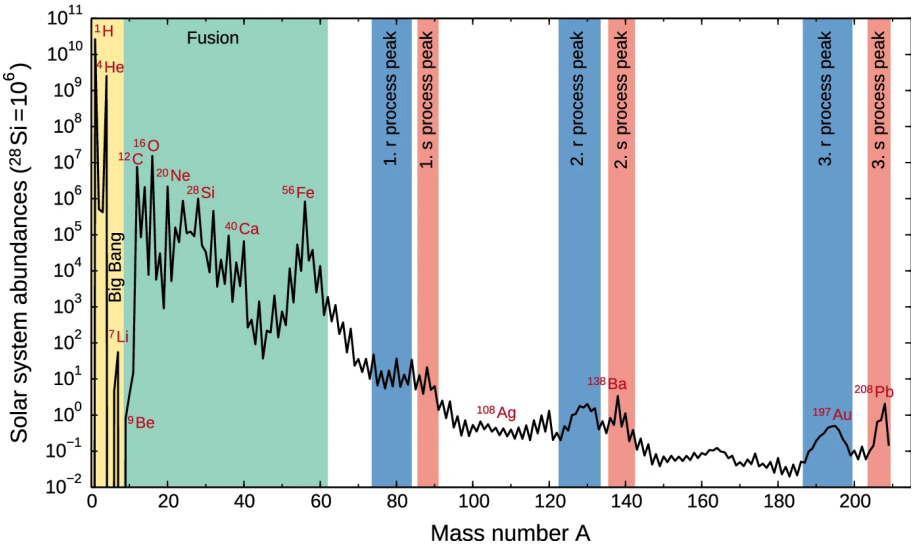

Figure 6. Solar system abundances as a function of mass number A, normalised to Si at 10^6. Elements with primordial and stellar fusion origins are highlighted with yellow and green respectively. The r- and s-process peaks are highlighted with blue and red respectively. The rare-earth peak at $A \approx 160$ is not highlighted in the graph. Data based on Ref. [65]; from [12], by A. Arcones and F.-K. Thielemann, CC BY 4.0

the r-process can operate in two different regimes with different physical requirements [66, 67]: a "hot" r-process with temperatures high enough to reach $(n, \gamma) \rightleftharpoons (\gamma, n)$ equilibrium, and a "cold" r-process with temperatures so low that photodisintegration reactions are irrelevant. [37] Here "hot" and "cold" refer to the temperature conditions during the neutron capture phase, e.g. initially material could be very hot, but due to expansion it can cool to produce a cold r-process. There are a broad range of conditions in which both high and low temperatures are reached. In some cases, the neutron density becomes so small, that free neutrons are present after the r-process. [68]

2.3 The r-process sites

Before the observation of GW 170817 there were only predictions of possible r-process sites. It was already known that neutron star mergers are a potential site, but there were also other possibilities, like the innermost ejecta of regular core-collapse supernovae (CCSNe). [37] Even though the binary neutron star merger can explain the total amount of solar r-process matter and also the abundances, within in the given uncertainties, there have to exists other r-process sites. [43] The r-process

simulations correctly produce the double peak structure near closed neutron shells in heavy element abundances. However, the observed r-only elements of stars with low metallicity, originating from the early universe, indicate that there are two types of r-process events [26]: a rare event, producing the heavy r-process abundances in solar proportions, a so-called "strong" or main r-process, and a more frequent event producing the lighter r-process abundances, a so-called "weak" r-process [37, 69, 70]. The main r-process is responsible for production of nuclides with $A \gtrsim 130$, and the weak r-process elements have $A \lesssim 130$. [71] Metallicity in astrophysical context refers to the fraction of elements heavier than hydrogen or helium, i.e. "metals" are not only the metals based on the conductivity but also all the nonmetals heavier than helium. [11] Metallicity is often defined by the ratio [29]:

$$\left[\frac{\mathrm{Fe}}{\mathrm{H}}\right] = \log_{10}\left(\frac{N(\mathrm{Fe})}{N(\mathrm{H})}\right)_{\star} - \log_{10}\left(\frac{N(\mathrm{Fe})}{N(\mathrm{H})}\right)_{\odot}, \tag{25}$$

where $N(\mathrm{X})$ is the abundance by number of element X, and indices $\star$ and $\odot$ refer to a given star and to the Sun respectively.

The conditions required from an r-process site are a combination of entropy S, expansion time scale τ, and electron abundance Y_e in the ejecta, and as a minimum requirement there should be a high enough neutron-to-seed ratio. [37] Neutron stars have the required neutron abundance, but due to the extreme gravitation, there has to be a cataclysmic event that allows the neutron-rich ejecta escaping the gravitational well of a neutron star. Such an event could be the birth of a neutron star in a supernova explosion, or a binary merger involving a neutron star. [37] A neutron star merger could potentially be a site for both the weak and the main r-process. The weak r-process could potentially occur in the late ejecta affected by neutrino interactions, while the main r-process has been already proven to occur in the early dynamic ejecta. [37]

Neutrinos can cool the matter when the matter reaches temperatures high enough that nuclei are dissociated into free nucleons. The other way how neutrinos affect the matter is the reactions between nucleons and neutrinos, in particular electron neutrinos [37]:

$$\nu_e + n \rightleftharpoons p + e^-, \text{ and} \tag{26}$$

$$\bar{\nu}_e + p \rightleftharpoons n + e^+, \tag{27}$$

where ν_e and $\bar{\nu}_e$ are the electron neutrino and antineutrino respectively. As neutrino reactions can protonize matter, Y_e is affected, which impacts the r-process nucleosynthesis. [37]

2.3.1 r-process sites related to massive stars

There are different scenarios related to the final moments of massive star evolution that are potentially r-process sites. Stellar evolution depends on the initial mass of the star, and if the initial mass is less than 8 solar masses, the final stage of stellar evolution is a white dwarf. For initial masses $8\ M_\odot \lesssim M \lesssim 10\ M_\odot$, evolution is more complicated, and after the fusion reactions have ended, the resulting object can be a white dwarf, or a supernova explosion following the ONeMg core collapse. In the most massive stars, with $M \gtrsim 10\ M_\odot$, fusion reactions lead to the formation of Fe-core. This is followed by a core collapse and a supernova explosion. [11, 72]

Core collapse results when silicon has been exhausted in the core of a massive star, and there is a high abundance of iron peak element in the core, like ^{56}Fe and ^{52}Cr, and the star has a shell structure with layers of different compositions separated by thin nuclear burning shells. Figure 7 illustrates the schematic structure of a massive star before core collapse. The electron degenerate core can no longer advance in nuclear burning and thus is lacking in nuclear energy generation. The mass of the core still increases, as the overlaying nuclear burning shells contribute nuclear ashes. When the mass of the core exceeds the Chandrasekhar limit ($\approx 1.4 M_\odot$), the electron degeneracy pressure can no longer counteract gravity which leads to core collapse. This is accelerated by increasing electron density, as the electrons are captured by the iron peak nuclei in the core which decreases the electron degeneracy pressure. [11, 72] Also, in stars with the initial mass of $8\ M_\odot \lesssim M \lesssim 10\ M_\odot$, the electron captures trigger the collapse of a degenerate ONeMg core. [72] At temperatures around 5 GK, the core reaches NSE. This removes energy that could have provided pressure, thus accelerating the collapse further. At this point, the core is essentially free-falling until the density reaches values of order the nuclear density $\left(\approx 10^{14}\ \mathrm{g/cm^3}\right)$. As the matter has become so dense, the nuclei and free nucleons are affected by repulsive nuclear force. This leads to a rebounce of the core matter, and when encountering the infalling matter, gives rise to an outward moving shock wave. The remaining inner core has become a proto-neutron star.[11, 72]

Photodisintegrations of the iron peak nuclei in the shock wave and the emission

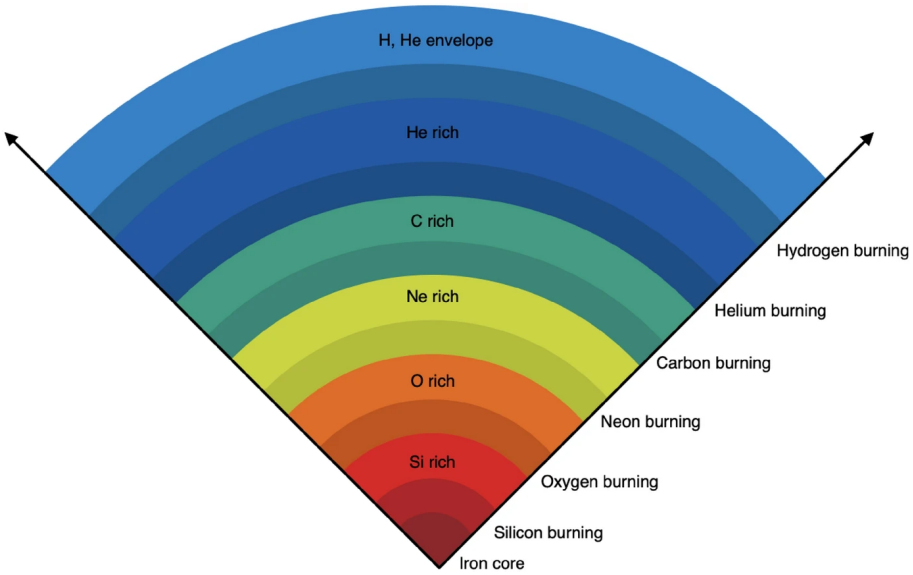

Figure 7. The schematic structure of a massive star before core-collapse supernova. On the right-hand side, thin burning shells are marked between different composition layers. From [12], by A. Arcones and F.-K. Thielemann, CC BY 4.0

of neutrinos with pressure from infalling material lead to stalling of the shock wave at 2×10^7 cm at the outer edge of the core. [11, 72] However, neutrinos and antineutrinos emitted by the hot proto-neutron star are believed to revive the stalled wave [73] The revived shock wave then propagates further, and compresses and heats the overlying shells of the star, leading to explosive nuclear burning in some shells. In the end, the the overlying shells are ejected into space, and the deepest regions ejected have a large abundance of free neutrons, possibly leading to r-process nucleosynthesis. [11] Six of the potential r-process sites related to supernovae are listed here, following Ref. [37] by Conan et al. Numerous references to the original research and in-depth discussion can be found in the the aforementioned paper.

1. **Neutrino winds from core-collapse supernovae:** Hydrodynamic simulations have shown that the weak r-process is possible. [74, 75] Further research, with neutrino radiation hydrodynamics simulations [76] and improved treatment of neutrino opacities in decoupling region [77], has shown that most or all of the ejecta are proton-rich [78], leading to νp-process nucleosynthesis [15], and thus producing neutron-deficient nuclei, like ^{92}Mo [79]. It is understood that matter is ejected by neutrino energy deposition and subjected to neutrino reactions. [37]

2. **Electron-capture supernovae:** As neutrino reactions turn neutron-rich matter to proton-rich, the so-called electron-capture supernovae, with 8 to 10 solar masses, could be a solution as the matter is promptly ejected with little exposure to neutrinos. [37, 80] A weak r-process could take place there [81], producing nuclei up to Eu ^{153}Eu, but not up to the third r-process peak ($A \approx 196$) [78]. Based on multidimensional hydrodynamic simulations [82] and data on the electron capture rate on ^{20}Ne [83], there are strong indications that electron captures on ^{20}Ne may trigger a thermonuclear supernova in intermediate-mass stars [37].

3. **Neutrino-induced r-process in the He-shell:** A low seed abundance allows a high neutron-to-seed ratio in the He-shell r-process. Even with metallicities as low as [Fe/H] ≤ 3, indicating a very low seed abundance, the neutrons produced by ^{4}He$(\bar{\nu}_e,e^+n)^3$H are enough to produce nuclei with $A \approx 200$. This can occur in stars with masses 11–15 $M_\odot$. While the high neutron-to-seed ratio allows production of heavy nuclei via neutron captures, the low neutron number density n_n shifts the abundance peaks to higher A compared to those found in the solar system. The overall abundance pattern is something between the r- and the s-processes. Thus, this process cannot explain the solar r-process abundances and the abundance patterns of low-metallicity stars. [37, 84]

4. **Quark deconfinement supernovae:** In this case, an object undergoes core-collapse and forms a central compact proto-neutron star, but the neutron emission and accreted matter is not sufficient to prevent further collapse with ongoing mass accretion. [37] With a specific equation of state [85, 86] adjusted to observed maximum neutron star masses, it could be shown [87] that in supernovae explosions in a certain mass range, an r-process can take place in the innermost ejecta. This can produce nuclei up to the third r-process peak, but the relative abundances beyond the second peak were suppressed relative to the solar r-process abundances. [87]

5. **Magneto-rotational supernovae with jets:** Neutron stars with extremely high magnetic fields can result from core-collapses with fast rotation and strong magnetic fields. [88] The related supernovae, induced by strong magnetic fields and/or fast rotation of the stellar core, could provide an alternative astronomical source for the r-process. One example of such supernovae are

magneto-rotational supernovae, MHD-SNe. [89, 90] Studies based on MHD simulations exhibited an r-process in jet-like explosions, and results with a successful r-process beyond the third r-process peak have been achieved. [91] The prerequisite of high initial magnetic fields combined with high rotation rates in order to achieve an early jet-like ejection of neutron-rich matter is the major constraint in this scenario. [37] Different rotation rates, initial magnetic fields, and ratios of neutrino luminosities vs. magnetic field strengths can lead to differing outcomes, varying from a main r-process with nuclei beyond the 3rd r-process peak, over a weak r-process without the third r-process peak nuclei, down to no r-process at all. [37, 92]

6. **Collapsars, hypernovae, long-duration gamma-ray bursts:** Very energetic supernovae with $E > 10^{52}$ erg[1], or the so-called hypernovae, are linked to long-duration gamma-ray bursts (lGBRs). The question is which features should be related in these events, and what is the stellar mass range. Non-rotating massive stars lead to regular supernovae, but rotating black holes and the formation of accretion disks can lead to lGRBs or hypernovae, also called as collapsars, i.e. the supernova-triggering collapse of rapidly rotating massive stars. [37, 93] The ejecta from hypernovae can have up to 0.5 $M_\odot$ of ^{56}Ni. High entropies and a strong α-rich freeze-out can result due to high explosion energies. α-rich freeze-out leads to large amounts of ^{45}Sc that is difficult to produce in other environments, and Fe-group elements. Self-consistent modelling of the full event has been challenging, and there is uncertainty if r-process ejecta can be produced in the same event with large amounts of ^{56}Ni. [37, 93]

It is possible that core-collapse supernovae can produce r-process elements but they might not support the main r-process up to the third r-process peak. [37]

[1] 1 erg = 10^{-7} J. The erg is an often-used unit in astrophysics, and it is a part of the Centimetre-gram-second system of unit (CGS). [11]

2.3.2 Binary neutron star mergers and neutron star-black hole mergers

Neutron stars are some of the densest massive objects in the universe. They result from the gravitational collapse of the core of a massive star ($> 8\ M_\odot$) in a supernova explosion at the end point of the evolution of a star. [94] If the mass of the core of a stellar remnant exceeds $\approx 1.44\ M_\odot$ (the Chandrasekhar limit), the electron degeneracy cannot prevent further collapse of the core to a neutron star. As the remains of a star collapse, the Fermi energy of the electrons increases. It becomes energetically favourable for electrons to combine with protons to form neutrons in electron capture:

$$p + e^- \longrightarrow n + \nu_e, \tag{28}$$

where ν_e is the electron neutrino. As the density increases, neutron degeneracy pressure with the short-distance repulsion of the nucleon-nucleon interaction halt the collapse, and the flux of neutrinos push the falling outer envelope outwards. Neutron degeneracy pressure alone is enough to prevent further collapse if the mass of the core is less than $0.7\ M_\odot$. If the stellar core is heavier, repulsive nucleon-nucleon interactions become essential to support a massive neutron star from collapsing into a black hole. If the mass of the core exceeds $\approx 2.4\ M_\odot$ (corresponding a core mass of approximately $15\ M_\odot$, depending on the metallicity of the star [95]), the repulsive forces and degeneracy pressure are not sufficient to prevent further collapse, and a black hole is formed. [96]

Neutron star masses are typically on the order of $1.5\ M_\odot$, and they have a radius $R \approx 12$ km. [94] The density varies in different layers of the neutron star, and in the core it can reach 5 to 10 times the nuclear matter saturation density of $n_0 = 0.15\ \text{fm}^{-3}$, corresponding to a mass density of $\rho_0 \approx 10^{14}\ \text{g/cm}^3$. [94, 96] The outermost surface of the neutron star contains a thin atmosphere, which thickness of a few centimetres, composed of hydrogen, and possibly some heavier elements like helium and carbon. Below the atmosphere there is a thick envelope that separates the hot interior and the relatively cold surface. The matter there is not yet fully degenerate, but in the layers below, the crust and the outer and the inner core, the density increases and the composition of matter becomes more complex. At the top layers of the outer crust, it is energetically favourable for nucleons to cluster into ^{56}Fe. As the density increases in the deeper regions of the neutron star, the energetically favourable nuclei become more neutron rich. Ultimately, at the bottom layers of

the inner crust, nucleons form a so-called nuclear pasta in which the nucleons form complex structures of various topologies that are a result from "Coulomb frustration". It is due to competition between short-range attraction and long-range repulsion that are comparable in the bottom of the inner crust. These topologies are not well understood, and different models are used to describe it. [96]

The core accounts for around 90% of the size and most of the mass of the neutron star. In the outer core, neutrons, protons, electrons, and muons are in chemical equilibrium, with proton fraction being around 10%. The inner core is assumed to contain exotic forms of matter like hyperonic matter, meson condensates, deconfined quark matter, and/or colour superconductors. Hyperons are baryons containing strange quarks, and thus they are heavier than the protons and neutrons in the outer core. Mesons are bound states containing one quark and one antiquark, unlike baryons that are composed of three quarks. There is also a possiblity of deconfinement of quarks and gluons that normally are confined withing baryons and mesons. However, there are major uncertainties regarding this. [96]

If two neutron stars form a binary system, General Relativity predicts that they lose energy by emission of gravitational waves. Eventually, this leads to to a merger, with timescales of $\approx 108^8$ years in observed systems. This is dependent on the initial separations and eccentricities of the orbit. [37] Already in the 1970s, simultaneously to the discovery of binary pulsars, binary neutron star or a neutron star-black hole mergers were suggested to eject r-process nuclei ([97, 98]). This was confirmed with the observations following the Gravitational Wave event GW170817 that resulted from a binary neutron star merger. In the case of a neutron star-black hole merger, it is necessary that the black hole tidal force is larger than the self-gravity of the neutron star. Otherwise, there would be no ejection of matter. [37] An accretion disk is often formed in a neutron star-neutron star merger, as well as in some neutron star-black hole mergers, surrounding the central remnant. [99]

The main ejection channels in binary neutron star mergers are dynamic ejecta at the coalescence phase, followed by post-merger neutrino wind ejecta, and the late time viscous or secular outflow from the accretion disk. [37]

1. **Dynamic ejecta:** The are two types of dynamic ejecta: a cold component that originates from the outer regions of the neutron star and is ejected via tidal interaction in the equatorial plane, and a hotter component originating from the contact interface. [37]

The cold component consists of very neutron-rich matter, and it is the only one present in neutron star-black hole mergers. [37] The nucleosynthesis has been widely studied (e.g. [61, 100, 101]), and it has been found to be rather sensitive to the nuclear physics input [43, 61], but independent of the astrophysical conditions [102]. As the material can reach neutron-to-seed ratios of several thousands, Y_e becomes very low, and the associated nucleosynthesis becomes less sensitive to the initial composition. The neutron capture phase can have a hot or cold r-process, independent of the initial conditions. Typically, the expansion of the material is slow enough so that neutrons are completely captured. This leads to neutron-rich nuclei and several fission cycles. Very heavy ($A \approx 280$) nuclei are present at the freeze-out, and during the final freeze-out phase the final abundances of nuclei with ($A \leq 140$) are determined by the fission yields of these heaviest nuclei. [37, 63] The neutrons produced in the fission reactions are tend to be captured by the third r-process peak material. Depending on the number of neutrons produced and the rate at which they are released may shift the third peak to higher mass numbers, compared to the solar abundances. [37] Low Y_e ejecta has been shown to produce a final abundance distribution that is close to the solar abundance distribution for $A > 140$, regardless of the fission yields used in simulation. [63]

According to several studies (e.g. [55, 61, 103]), part of the material, up to 10% in mass, is ejected very fast. The density of material becomes so low that the timescale for neutron captures becomes much longer than the expansion timescale. [61] Thus, most of the neutrons are not captured, even though the neutron-to-seed ratio is large. This is a so-called "frustrated" r-process, and the final abundances do not correspond to the solar abundances. Hence, it cannot form the major component of the ejected mass, assuming mergers are a major r-process site. Nonetheless, this may have a significant contribution for nuclei around $A \sim 200$. [37]

The hot component constitutes most of the unbound material in binary neutron star mergers. [37] Weak processes operating on the shock-heated ejecta can increase Y_e to values 0.25–0.4, depending on the neutrino luminosities. This is particularly efficient in the polar region where there are high neutrino fluxes from the formed hyper massive neutron star that increases Y_e, as long as the neutron star does not collapse promptly to a black hole. [37, 104]

Dynamic ejecta from neutron star-neutron star mergers are expected to contribute to a broad range of r-process nuclei, including both light and heavy, if weak processes are considered. [104, 105] However, the predicted amount of high Y_e matter is typically a lot smaller than in accretion disk outflows. [37]

2. **Neutrino Winds:** When dynamic ejecta is directly related to the merging or collision, neutrino winds are part of the post-merger ejecta. These are found in core-collapse supernovae. In a typical merging system, the hot neutron star remnant is supported by high temperatures and differential rotation, and will not collapse to a black hole immediately, as long as the total mass of the system is less than critical mass required for prompt collapse. The remnant is surrounded by a hot and dense torus. [37] The outflowing wind occurs mainly in the polar direction [106]. As matter is exposed to neutrinos long enough for the material to reach an equilibrium between electron neutrino and antineutrino absorbtion, the initial neutron-rich condition change, and as a result Y_e can reach values above 0.5. [37] The peak of Y_e distribution is expected to be neutron-rich with $Y_e \gtrsim 0.25$ [107] which leads to a weak r-process and produces mainly matter below the second r-process peak. [37]

   The properties of neutrino-wind ejecta, Y_e in particular, are expected to be sensitive to the spectral differences of electron neutrino and antineutrino. This requires an accurate prediction of neutrino luminosities and spectra. The spectra can also be changed by neutrino flavour conversion which in turn affects Y_e. [37]

   Another wind component relates to magnetically driven winds from the remnant (e.g. [108]). However, their nucleosynthesis yields and interaction with neutrino driven winds are not well understood. [37]

3. **Accretion Disks:** At $t \approx 1 - 10$ s, viscous heating and nuclear recombination power the outflow of material from the accretion disk. [109, 110] The amount of ejected mass increases with the lifetime of the massive neutron star formed in the merger, and with a longer lifetime, also Y_e increases due to neutrino irradiation. With lifetimes $\gtrsim 1$ s, $Y_e > 0.3$. [111] This drastically changes the nucleosynthesis outcome, and in such ejecta, the nucleosynthesis is similar to the neutrino-wind ejecta. If the lifetime of a massive neutron star is short, $t \lesssim 1$ s, neutrino-irradion has less impact, and thus the nucleosynthesis is

similar in both neutron star-neutron star and neutron star-black hole mergers. [37]

Simulations have shown that disk outflows alone can produce wide range of r-process nuclei, with significant production of $A \lesssim 130$ nuclei. Most of the simulations also have reached the third peak at $A = 195$. The results are affected by the disk viscosity, the initial mass or entropy of the torus, the black hole spin, and the nuclear physical input, like the used mass model. [37]

For deeper discussion with more references to original research, see e.g. [37].

2.4 Nuclear Isomers

Each nuclear state is characterised by its excitation energy, total angular momentum, parity, and isospin. The state with the lowest energy is called the ground state, and the rest are excited states. Differing quantum properties of nuclear states affect the physical properties of states. One of the properties is the mean lifetime of a nucleus. In general, the ground state is the most stable one, either stable or with the longest half-life, while most of the excited states are very unstable, with decay timescales of picoseconds or shorter. [112] In contrast, nuclear isomers are so-called metastable excited states that are relatively long-lived, with half-lives ranging from nanoseconds to years. [56, 112] Isomers are usually denoted by 'm' after the mass number in chemical symbol, e.g. $^{180\mathrm{m}}_{73}\mathrm{Ta}$. If there are several isomers for the nuclide, a number is added to separate isomers. For example, 'm1' denotes the first isomer.

Isomer research dates back to 1917 when Frederick Soddy predicted that a single nuclide might have states with differences in stability and decay. [56, 113] In 1921 Otto Hahn observed an isomer for the first time in his study of UZ and UX_2, which nowadays are known as ^{234}Pa and $^{234\mathrm{m}}$Pa. [56, 114] However, the theoretical explanation was given not until 1936 when Carl Friedrich von Weizsäcker proved that the combination of a large angular momentum change and low transition energy could lead to a long half-life for electromagnetic decay. [56, 115, 116] Eventually, the subsequent research lead to discovery of several isomers in nuclei, and in the most recent NUBASE evaluation (NUBASE2020), there are 1938 listed isomers. [52]

While isomers are metastable states of an isotope, there is no definition of a minimum half-life that an excited state should have in order to be listed as an isomer. The half-life should be long compared to other excited states. In general, this

should be longer than 1 ns, as a nanosecond is long enough to distinguish electronic signals obtained from recoils form heavy ion reactions. [27, 117, 118] For example, in the NUBASE evaluations, the experimentally known isomers listed there have $T_{1/2} \geq 100$ ns. [52] While many of the isomers are rather short-lived, some of them can be very long-lived. In fact, ${}^{180\mathrm{m}}_{73}\mathrm{Ta}$ has a half-life over 10^{15} years, while the ground state ${}^{180}_{73}\mathrm{Ta}$ has a half-life of 8.2 hours. This is the only isomer with half-life long enough that it naturally exists on Earth, albeit in minimal traces. [52, 118]

Isomers can decay via similar modes as the ground states. For the lighter isomers, with $A < 200$, β-decay is the most common particle decay mode. On the neutron-rich side of the valley of stability in nuclear charts β^--decay is a common path towards stability, and on the proton-rich side β^+-decay, similarly to ground states. If the isomer is very close to the particle drip lines, even beta-delayed particle emission may occur, e.g. near the neutron drip line successive emission of β^--particle and one or more neutrons is likely. The heavier the isomers become, α-decay becomes more common, and the heaviest isomers can even undergo fission. It can be spontaneous, or it can be induced by a particle (e.g. β) decay or by a neutron capture. [52, 118]

In addition to particle emissions, isomers can also de-excite via internal transition to lower energy states by emitting a γ-ray or by internal conversion (IC) in which one of the orbital electrons of an atom is emitted. Internal conversion is different from β^--decay, in which an electron (β^- particle) is emitted from the nucleus with a neutrino. Naturally, if the excited atom is fully ionised, internal conversion is not possible, but otherwise internal conversion is possible if gamma decay is. γ-ray emission or internal conversion does not change the proton number Z or the neutron number N of the nucleus, unlike in particle decay. Isomeric state can de-excite directly to the ground state, but it is more common that decay proceeds through several lower-lying excited states. If the enviroment is energetic enough, i.e. the temperature is high, the de-excitation can happen by first exciting to a higher level, which in turn might decay more readily to a lower state, bypassing the isomeric state. This is can occur in astrophysical conditions in the stellar photon bath, or it can be induced with accelerator-based bremsstrahlung. [118, 119]

Isomeric properties arise from different ways, depending on the isomer. The nuclear shell structure impacts the nuclear properties, and thus also have an effect on nuclear isomers. Most isomers can be thought to have one or two unpaired nucleon orbitals in the nuclear shell model, but even up to around ten unpaired orbitals

can exist. These isomer-related orbitals couple which leads to states requiring the emission of low-energy and/or high-spin radiation to de-excite. However, it must be noted that the shell model alone is not enough to describe all the properties of nuclear isomers which can be seen for example in the decay radiation. [27, 56, 117, 118] The best known isomer types are spin traps, K isomers, and shape isomers. [118]

Spin-trap isomers are due to considerable difference between the isomeric state spin and the lower-lying states. This heavily hampers the decay to lower energy states as the emitted radiation should have a high multipolarity λ that corresponds to the angular momentum carried by photon. One of the most notable example of spin-trap isomers is $^{180\mathrm{m}}$Ta with a spin of $I = 9$. The corresponding ground state, ^{180}Ta, has a spin of $I = 1$, so the emitted radiation need to carry $\lambda = 8$. Of course, it could be possible to decay via intermediate energy states, but in this case, the isomeric state has an excitation energy of 77.1 keV, so there are only two (including the ground state) lower-lying states below it. And those, as well, are mismatched in spin. As a consequence $^{180\mathrm{m}}$Ta has a theoretical half-life of at least 7.15×10^{15} years. This is several orders of magnitude longer than the half-life of the ground state, $t_{1/2}\,(^{180}\mathrm{Ta}) = 8.154$ h [35]. The most common way of a spin-trap isomer to decay is by electromagnetic processes, gamma emission or internal conversion, there are also cases that decay by the strong interaction (alpha or proton emission), or by the weak interaction (β emission or electron capture). [56, 117]

K-isomers, or K-trap isomers, are due to both the magnitude of the nuclear spin vector and the orientation of the vector. The quantum number K is the projection of the total nuclear spin along the symmetry axis of the the nucleus. Thus this type of isomer requires axially symmetric, deformed nuclei that have open shells as closed shell nuclei favour spherical shapes. All K-trap nuclei have prolate shapes with the long axis being the axis of symmetry. In principle, the decay radiation should have multipolarity λ at least as large as the change in the K-value, but symmetry-breaking processes enable transitions that do not fulfil the K-selection rule. These so called *"K-forbidden"* transitions are hindered, which can be seen e.g. in ^{180}Hf. It has an isomer $^{180\mathrm{m}}$Hf at 1.1 MeV with $I = 8$ and $K = 8$. It has a half-life of 5.5 hours (the ground state is stable). The most probable decay occurs by a 58-keV gamma ray with $\lambda = 1$ to a state with $I = 8, K = 0$. Clearly, this violates the K-selection rule, as now $\lambda = 1 < 8 = \Delta K$. There is also a K-allowed decay path directly to the

$I = 0, K = 0$ ground state with a 1.1 MeV gamma ray, but due to high multipolarity this transition is heavily hindered. [117]

The third type of isomers are shape isomers. The ground state of a nucleus is located at the primary energy minimum. In a case of elongated nuclei, there exist other local minima that correspond to the isomeric states at different elongated shapes of the nucleus. One of the examples is ^{242}Am which has a 2.2 MeV isomer that undergoes a spontaneous fission with a half-life of 14 ms. Shape isomers are often heavy, and thus spontaneous fission is a common decay path. For some shape isomers, there is also a competing decay channel to the ground state by gamma emission. [117, 118]

There are also other types of isomers. One is the so-called yrast-trap isomers. An yrast state is the lowest energy level of a nucleus for a given angular momentum. [120] Yrast traps occur when the high-spin yrast levels of a nucleus are not allowed to decay via collective transitions that normally compete with intrinsic transitions. A spinning nucleus may be distorted into an oblate shape at some high spin. The most efficient way to achieve a given angular momentum is alignment along the axis of symmetry of independent single particles, i.e. the single-particle potential becomes axially symmetric with respect to the spin direction. With this symmetry of the potential, the individual levels do not organize into rotational bands parallel to the yrast line, and thus the decay cannot proceed via a low-multipolarity transition. This creates the yrast trap. [120, 121] One example of yrast isomers is the $J = 12^+$ state of $^{52}_{26}$Fe [122].

Another type of isomerism are the seniority isomers which arise from selection rules related to the seniority quantum number v, hindering the electromagnetic decay of the state. Seniority refers to the particles that are not pairwise coupled to total angular momentum $J = 0$. [123, 124] In general, in semi-magic nuclei (i.e. the nuclei in which either the proton number or the neutron number is a magic number) states with low seniority occur at low energies. For example, the ground state of an even-even semi-magic nucleus has $v \approx 0$, as all nucleons are coupled to $J = 0$. On the other hand, the yrast levels with $J = 2,4,6,\ldots$ have $v \approx 2$ as there is one uncoupled pair with $J \neq 0$. [123] The electric quadrupole (E2) transitions between $v = 2$ states are small when the valence shell is close to half-occupied, and thus seniority isomerism is expected to occur in semi-magic nuclei. [123, 124] Examples of seniority isomerism include $J^\pi = 8^+$ levels in $^{94}_{44}$Ru and $^{96}_{46}$Pd [123].

The different properties leading to isomers are not mutually exclusive. For example, around the aforementioned ^{180m}Hf is one of the regions of the nuclear chart with the most isomers. These isomers are due to both spin and K-trapping, and these are also rather long-lived compared to many other isomers, with half-lives over one hour. [117]

2.4.1 Astromers

Although there are 1938 listed isomers in NUBASE2020 [52], not all isomers are impactful in astrophysical nucleosynthesis. Those isomers that have influence in the outcome of astrophysical nucleosynthesis are called astrophysical isomers or "astromers". As isomers, they can have different properties in reactions compared to their associated ground states, e.g. they may have different half-lives and decay Q values, and thus nuclear networks should treat them as separate species. [27]

When calculating nucleosynthesis rates, typically only the ground state rate is used, or different levels are considered to be in a thermal-equilibrium probability distribution. If there is a metastable state, it can decrease the accuracy in both cases. [27] As a nucleus is produced in a reaction, it is often in an excited state that de-excites primarily by gamma ray emission. While releasing energy, the nucleus might reach an isomeric state that might undergo e.g. a β-decay, and in this case the ground state of the parent is never reached. The probability distribution of nuclear energy levels might also not reach thermal equilibrium due to presence of an isomeric state. [27] Isomeric state might also have destruction rate (e.g. β^--decay) that is drastically different to that of the ground state, as was seen with ^{180m}Ta in Section 2.4. If the destruction rates are fast compared to the electromagnetic transition rates between long-lived states, the state with higher destruction rate will become depopulated in relation to the thermal equilibrium population as the transition between states is not fast enough to compensate. In the previous cases an isomer can be have an impact in nucleosynthesis, and thus it can be labelled as an astromer. [27] Figure 8 illustrates a parent nucleus or a compound nucleus, an intermediate state created in a compound nuclear reaction, decaying to various states of the daughter nucleus with an isomeric state. Below the continuum of states (in blue gradient) are the discrete energy levels. The short-lived are marked with dotted lines while the isomer and the ground state are marked with solid lines. Electromagnetic transitions between states are marked with two-headed arrows. The relatively slower transitions

between the isomeric state and the lower-lying states are marked with red arrows. The isomer can also be depopulated via competing decay channels (the blue dashed arrow), like β-decay.

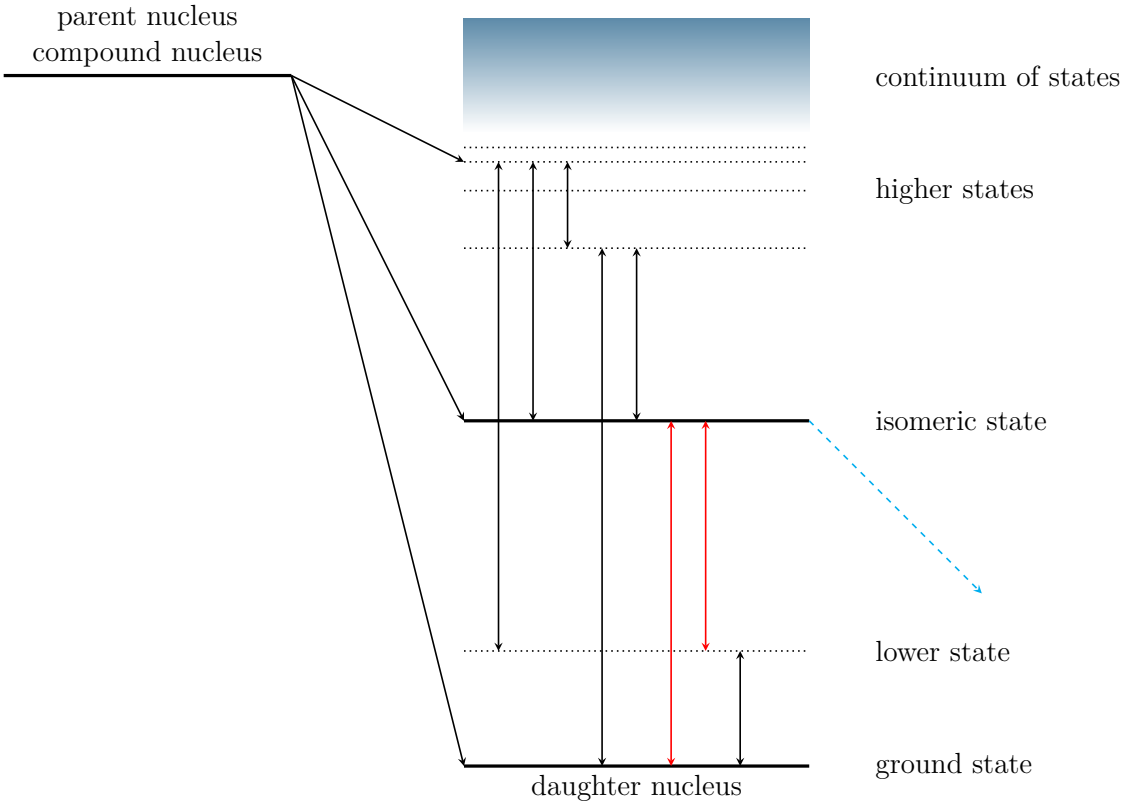

Figure 8. A decay schematic showing the parent nucleus decaying to various states of the daughter nucleus with an isomeric state. The dotted lines depict short-lived excited states that quickly decay to other states. Above the higher discrete energy states is the continuum of states (in blue gradient). The isomer has relatively slower transitions (the red arrows) to the lower-lying excited states and the ground state, while the other excited states decay relatively faster (black arrows). The isomer may be depopulated via competing decay channels (the blue dashed arrow). In astrophysical conditions thermal population of states is also possible, which is marked with two-headed transition arrows.

On the other hand, if an isomer decays mainly by gamma emission to the ground state, destruction by e.g. β-decay is not sufficient to cause deviation from thermal equilibrium. Also, even if isomers could possibly have an effect on the nucleosynthesis, the environment might prevent this. For example, in lower temperatures an isomer could prevent thermalization, but in higher temperatures, like temperatures in the s- or r-processes, equilibrium can be achieved by thermally driven transitions through

intermediate states. One example is ^{123m1}Sn with a thermalization temperature at $T \approx 25$ keV ≈ 0.29 GK which is well above the temperature at which the isotopes are expected to populate after the r-process freeze-out. [27]

In the r-process sites isomers can be thermally populated, but as the temperature starts to decrease rapidly, these isomers can be frozen out before they reach thermal equilibrium. Neutron capture reactions (n,γ) and photodisintegration reactions (γ,n) can also produce isomers [125], as well as fission reactions [126]. Isomers can also be produced by β^--decay when the neutron-rich nuclei decay [127]. In a simulation, it was shown that the direct population of nuclear isomers affects potentially the radioactive heating in the r-process events, when compared to the ground-state only case [128].

Misch et al. [27] provide a method based on [129, 130] to calculate effective transition rates between long-lived nuclear states in hot environments. The method uses intermediate, non-isomeric states between the endpoint states that can be an isomeric state and the ground state or two isomeric states that communicate through a thermal photon bath. Beta decay and other destructive reactions are then handled separately. The transition rate between states 1 and 2 is given by [27]

$$\lambda_{12} = \frac{2J_2 + 1}{2J_1 + 1} e^{\frac{E_1 - E_2}{T}} \lambda_{21}, \tag{29}$$

where λ_{12} is the transition rate between states 1 and 2, and λ_{21} is the transition rate for the reverse transition, J_i is the spin of the state i, E_i is the energy of the state i, and T is the temperature of the system.

To get an effective transition rate from state 1 to 2, one needs to include all the possible transitions between the endpoint states via intermediate states, as well as the possible direct transition rate between the endpoint states. This can be expressed with [27]

$$\Lambda_{12} = \lambda_{12} + \sum_i \lambda_{1i} P_{i2}, \tag{30}$$

where Λ_{12} is the effective transition rate from state 1 to state 2, λ_{12} is the direct transition from state 1 to state 2, λ_{1i} is the transition rate from state 1 to one of the intermediate states, and P_{i2} is the probability that the chain of transitions lead to the endpoint state 2 without passing though the state 1. The sum is then over all

the possible intermediate states i. The probability P_{i2} can be written as [27]

$$P_{i2} = \sum_s b_{is} P_{s2}, \tag{31}$$

where s denotes an intermediate state, and the summation runs over all the possible states s. b_{is} is the probability of transition from state i to state s. Equation (31) can be simplified by noting that if $s = 1$ (state 1), the transition has failed, and if $s = 2$ (state 2), the transition is fully proceeded. Thus, $P_{12} = 0$, and $P_{22} = 1$, when the first state index denotes the state s. As there is no transition from s to s, $b_{ss} = 0 \forall s$. Equation (31) can now be written as [27]

$$P_{i2} = b_{i2} + \sum_j b_{ij} P_{jB}, \tag{32}$$

where j now runs over intermediate states, but not the endpoint states 1 and 2. For a computer friendly form, Equation (32) can be written in matrix form [27]:

$$\begin{aligned} \overrightarrow{P}_{I2} &= \overrightarrow{b}_{I2} + \mathbf{b}_{II} \overrightarrow{P}_{I2} \\ (\mathbb{I} - \mathbf{b}_{II}) \overrightarrow{P}_{I2} &= \overrightarrow{b}_{I2}. \end{aligned} \tag{33}$$

Now $\overrightarrow{P}_{I2}$ is a vector with components P_{i2}, $\overrightarrow{b}_{I2}$ is a vector with components b_{i2}, and $\mathbf{b}_{II}$ is a matrix with elements b_{ij}. Indices i and j denote the intermediate states. Equation (33) now corresponds to a system with N linear equations in N variables, where N is the number of the intermediate states used in the calculation. The effective rate can be found after solving $\overrightarrow{P}_{I2}$ with a linear equation solver, and inserting the result into Equation (30). [27]

Misch et al. have applied the method described above to some of the potential astromers, ^{26}Al, ^{36}Cl, and ^{85}Kr, to obtain effective transition and beta decay rates. [27] In a following research [28], more potential astromers were investigated and rated by their importance in the r-process nucleosynthesis. Some of the most influential ones are listed in Table 1.

In the obtained results [28], some of the added isomers did not have a noticeable impact on the outcome of the r-process nucleosynthesis. Those astromers with different beta decay rates compared to the ground state rates had an impact on the r-process heating. Astromers with slower decay rates heating was decreased compared to the ground state heating rates, while those with faster rates increased

Isotope	E_m (keV)	J^π_g	J^π_m	$T_{1/2g}$ (s)	$T_{1/2m}$ (s)	$B_{m\beta}$ (%)
^{69}Zn	438.636	$1/2^-$	$9/2^+$	3.38×10^3	4.95×10^4	0.033
^{71}Zn	157.7	$1/2^-$	$9/2^+$	1.47×10^2	1.43×10^4	100
^{85}Kr	304.871	$9/2^+$	$1/2^-$	3.39×10^8	1.61×10^4	78.8
^{115}Cd	181.0	$1/2^+$	$(11/2)^-$	1.92×10^5	3.85×10^6	100
^{119}In	311.37	$9/2^+$	$1/2^-$	1.44×10^2	1.08×10^3	95.6
^{121}Sn	6.31	$3/2^+$	$11/2^-$	9.73×10^4	1.39×10^9	22.4
^{130}Sb	4.8	(8^-)	$(4,5)^+$	2.37×10^3	3.78×10^2	100
^{127}Te	88.23	$3/2^+$	$11/2^-$	3.37×10^4	9.17×10^6	2.4
^{166}Ho	5.969	0^-	7^-	9.66×10^4	3.79×10^{10}	100

Table 1. Some of the most influential astromers and their properties according to Misch et al [28]. Indices g and m denote the ground state and isomeric state respectively. E_m is the isomer energy, J^π are the spin and the parity, parentheses denote uncertain value, $T_{1/2}$ is the half-life measured in the laboratory, and $B_{m\beta}$ is the beta decay branching of isomer. The rest of the decay is via internal transition. [28].

increased heating output. However, it was noted that incomplete data of β intensities may change the outcome, as the decays with no published intensities were assumed to always end in the ground state. This can change the feeding of isotopes in decay chain, and thus make the results inaccurate.

3 Tools

The primary code used in this thesis is the nuclear reaction network GSINet [61] which was modified to include fully β^--decaying isomers in the network. The modified network code was then used to obtain results from r-process nucleosynthesis with isomers. As there is no publicly available documentation for GSINet, documentation for a nuclear reaction network WinNet [39] is referenced instead, where applicable. The both network codes share a common origin in BasNet [39], and the principle how they function is similar, and in many cases identical. In order to obtain required input values for the added isomers in the network code, a nuclear reaction code TALYS [131] was used to calculate (n, γ) and (γ, n) reaction rates for the added isomers.

3.1 Nuclear reaction network fundamentals

Different nuclear reaction network codes are in principle the same: they all evolve the abundances of different nuclei in the system with given input. This section will follow the implementation in GSINet (and in WinNet). Equation (22) in Section 2.2.3 is often called the "nuclear reaction network equation" [39]. It is the fundamental differential equation that is solved in GSINet, and the individual terms can be identified with specific reactions. The first term for one-body reactions usually includes decays, photodisintegrations, electron or positron captures, and neutrino absorption. The second term for two-body reactions include reactions involving two reactants like fusion reactions. Similarly, the third term is for three-body reactions, including reactions with three reactants. One example is the triple-α reaction. Reactions with four or more reactants are neglected.

Reverse or backward reactions are related to the forward reaction by the so-called detailed balance theorem [132]. If the forward reaction has a positive Q-value defined as the difference between the initial and the final ground-state masses, the relation between both states can be written as [39, 132]

$$\langle\sigma\nu\rangle_{\text{backward}} = \frac{\Delta_{\text{reactants}}}{\Delta_{\text{products}}} \left(\frac{\prod_{i=1}^{N_{\text{reactants}}} G_i\left(T\right)}{\prod_{j=1}^{N_{\text{products}}} G_j\left(T\right)}\right) \left(\frac{\prod_{i=1}^{N_{\text{reactants}}} g_i}{\prod_{j=1}^{N_{\text{products}}} g_j}\right) \left(\frac{\prod_{i=1}^{N_{\text{reactants}}} A_i}{\prod_{j=1}^{N_{\text{products}}} A_j}\right)^{\frac{3n}{2}} \times \left(\frac{m_u k_{\text{B}} T}{2\pi\hbar^2}\right)^{\frac{3n}{2}} \exp\left[-Q/\left(k_{\text{B}}T\right)\right] \langle\sigma\nu\rangle_{\text{forward}}, \quad (34)$$

where Δ denotes the double counting factor for reactants and products, G are the partition functions, g is the spin factor, defined as $g = 2J + 1$, where J is the spin of the ground state, A_i is the mass of the nucleus i, Q is the Q-value of the reaction, and n is the difference between the number of reactants and the reaction products. $\langle\sigma\nu\rangle$ is the cross section with subscript indicating the forward and the backward reaction. For photodisintegration reactions, Equation (34) needs to be modified by replacing $\langle\sigma\nu\rangle_{\text{backward}}$ with $\lambda_{\text{backward}}$. As $n \neq 0$, there are additional factors from the terms with n in the exponential. In the case of three-body reactions, $\langle\sigma\nu\rangle$ needs to be replaced with $\langle ijk\rangle$. [39] Reverse rates in the JINA Reaclib are calculated by using detailed balance. [133]

When the temperature is around $T \gtrsim 6$ GK, nuclear statistical equilibrium (Section 2.2.1) is used instead of the full nuclear network. Equation (22) is one element of a set of non-linear differential equations that has to be solved in order to determine the evolution of composition. As the reaction rates and abundances can involve many orders of magnitude [134, 135], and the time scales of different reactions may differ significantly, the set of equations is a so-called stiff initial value problem that has to be solved with an implicit method. [41, 134, 136, 137] As this is a non-linear problem, an iterative solution is required. One possible method to solve this type of problems is to use the backward Euler method (also known as the implicit Euler method) which is one of the most basic numerical methods to solve ordinary differential equations (see more e.g. [41, 138]). This is used in GSINet and also in Skynet [138], but higher-order methods, like Bader-Deuflhard variable-order method [139], have been recommended. [134]

The following derivation follows the one presented in [39]. The general form for a set of coupled ordinary differential equations (ODEs) can be written as

$$\frac{\mathrm{d}y_i}{\mathrm{d}t} = \dot{y_i} = f_i\left(t,y_1,...,y_N\right), \quad (35)$$

where y_i is the abundance of species i, t is time, and N is the amount of nuclei. f_i is some unspecified function of $N + 1$ variables. Writing the derivative in Equation

(35) as a difference quotient

$$\frac{y_i\left(t+h\right)-y_i\left(t\right)}{h}=f_i\left(t+h,y_1,...,y_N\right), \tag{36}$$

with a time step h, an iterative formula for the solution of $y_i(t)$ can be derived:

$$y_i\left(t+h\right)=y_i\left(t\right)+h\cdot f_i\left(t+h,y_1,...,y_N\right). \tag{37}$$

Now $f_i\left(t+h,y_1,...,y_N\right)$ is unknown. Implicit method evaluates f_i at $t+h$ in order to get numerical stability. A root-finding algorithm, like the Newton-Raphson method, is thus needed. The Newton-Raphson method can be used to solve equations which are formulated as

$$\vec{F}\left(\vec{x}\right)=0. \tag{38}$$

Expanding Equation (38) gives

$$F_i\left(\vec{x}+\delta\vec{x}\right)=F_i\left(\vec{x}\right)+\sum_{j=1}^{N}\frac{\partial F_i}{\partial x_j}\delta x_j+\mathcal{O}\left(\delta\vec{x}^2\right), \tag{39}$$

where $\partial F_i/\partial x_j$ is one element of the Jacobian $\mathbf{J}$ which contains the partial derivatives of $\vec{F}$ and is defined as

$$J_{ij}=\frac{\partial F_i}{\partial x_j}. \tag{40}$$

Equation (22) is linearly approximated in Equation (39) as the higher order terms are discarded. The root of $\vec{F}$ can be found by applying an iteration of

$$\vec{x}^{k+1}=\vec{x}^k+\delta\vec{x}^k=\vec{x}^k-\mathbf{J}\left(\vec{x}^k\right)^{-1}\cdot\vec{F}\left(\vec{x}^k\right) \tag{41}$$

until the convergence is reached. The convergence criteria can be given by e.g. the mass conservation:

$$\left|1-\sum_{i=1}^{N}X_i\right|<\sigma, \tag{42}$$

where σ is a set tolerance, usually of the order of $\sim 10^{-6}$ [140]. When the criteria has been met, the algorithm is assumed to have converged. In order to solve the ODE, both the time integration and the root finding algorithm (in this example, the Newton-Raphson method) needs to be applied. Combining Equations (41) and (37)

gives

$$\vec{y}^{k+1}_{n+1} = \vec{y}^{k}_{n+1} - \left(\frac{1}{h} \cdot \mathbb{1} - \frac{\partial f\left(\vec{y}^{k}_{n+1}\right)}{\partial \vec{y}^{k}_{n+1}} \right)^{-1} \cdot \left(\frac{\vec{y}^{k}_{n+1} - \vec{y}_n}{h} - \vec{f}\left(\vec{y}^{k}_{n+1}\right) \right), \tag{43}$$

where the subscript denotes the backward Euler and the superscript the Newton-Raphson iteration. There is no error estimation using the higher order terms, but the next time step h' can be determined by estimating the maximum percentage of change ε of the abundances. This is based on the current derivative and the approximate change is calculated by

$$\left|\dot{\vec{y}}(t)\right| = \left| \frac{\vec{t}(t+h') - \vec{t}(t)}{h'} \right| \tag{44}$$

and

$$\varepsilon = \max\left\{ \left| 1 - \frac{\vec{t}(t+h')}{\vec{t}(t)} \right| \right\}, \tag{45}$$

where the division of vectors is component-wise and the maximum is the maximum of all the components. These lead to

$$\left|\dot{\vec{y}}(t)\right| = \left| \frac{(1-\varepsilon)\cdot\vec{t}(t) - \vec{t}(t)}{h'} \right| \Rightarrow h' = \varepsilon \cdot \min\left| \frac{\vec{y}(t)}{\dot{\vec{y}}(t)} \right|, \tag{46}$$

with typical values of $\varepsilon \approx 0.1$ [140]. The time step is also limited by the previous step size, in order to avoid rapid changes:

$$h' = \min\left\{ C \cdot h, \varepsilon \cdot \min\left| \frac{\vec{y}(t)}{\dot{\vec{y}}(t)} \right| \right\}. \tag{47}$$

The constant $C > 1$ has typical values of $C \approx 2$ [140]. Abundances use a threshold value as well, and only species with abundances over the threshold limit are included in each step. Density and temperature changes can also be restricted. [140]

In GSINet, as well as in WinNet, the calculation starts at 10 GK in NSE conditions. This then decreases and the higher temperature results are initial values for lower temperature calculations. At the starting temperature, the initial composition is assumed to consist only nucleons with $Y_n = 1 - Y_e$ and $Y_p = Y_e$. Weak reactions are evolved with a simplified reaction network that includes only reactions in Equation (22). Using charge neutrality (7), a new electron fraction is determined after each

time step. As long as the temperature is high enough, NSE is assumed and strong and electromagnetic reactions occur instantly, followed by weak interactions. [39]

Every nucleus in the system is, in principle, connected to every other nucleus by nuclear reactions. However, most of the reactions are unlikely, and can be omitted in calculations. Decays and reactions involving the lightest nuclei (n, p, α) are the most relevant ones. Fission reactions, the triple-alpha reaction, and some of the heavy ion reactions (e.g. ^{12}C(^{12}C,γ)^{24}Mg) need to be handled, as well. [140] As a result, the Jacobian presented in Equation (40) is sparse, i.e. there are only a handful of non-zero elements in the matrix. There are various ways to reduce the computational work with sparse matrices. Instead of keeping the original matrix, it can be split into smaller arrays which store the non-zero Jacobian value and the position data of the original Jacobian. [41, 140] For more details, see e.g. [41]. In GSINet, Intel PARDISO sparse matrix solver [141] is used.

The majority of the energy released by neutron captures and photodissociations in the r-process occurs within seconds. Most of this initial heating, as well as the residual energy from the merger, powers the adiabatic expansion as during the early times the outflow is highly optically thick. At the same time, the expanding material cools due to expansion. [142, 143] As the r-process produces neutron-rich unstable nuclei that decay to stability by β-, α-, and fission decays, large amounts of energy is released that mainly affects the evolution of temperature, but can also lead to observable electromagnetic emission. [37, 138, 143] When the heating is dominated by a wide distribution of nuclei decaying exponentially, a decreasing power-law dependence $\left(\dot{Q} \propto t^{-\alpha}\right)$ is expected, with $\alpha < 2$. [142] This is the case if $Y_e \lesssim 0.2$ in ejecta. An example of a low-Y_e heating rate can be seen in Figure 9, in which the heating rate closely follows a power-law $\propto t^{-1.3}$ with $Y_e \approx 0.13$. Higher Y_e ejecta causes 'bumps' in the heating rate, as a few nuclei dominate. [37, 144] The high Y_e ejecta is dominated by β-decay, and only electrons and photons are relevant as they thermalize efficiently while neutrinos cause energy loss by escaping the ejecta. [37, 145] In GSINet, heating caused by β-decays is assumed to be a half of the total energy released in *beta*-decay reactions. The other half is assumed to be lost with escaping neutrinos.

In a low-Y_e ejecta, actinides are produced, and α-decay with fission can form a notable part of the energy production. [37, 146] Fission can be spontaneous, β delayed, or induced by neutrons. The type of heating is dependent on the time passed

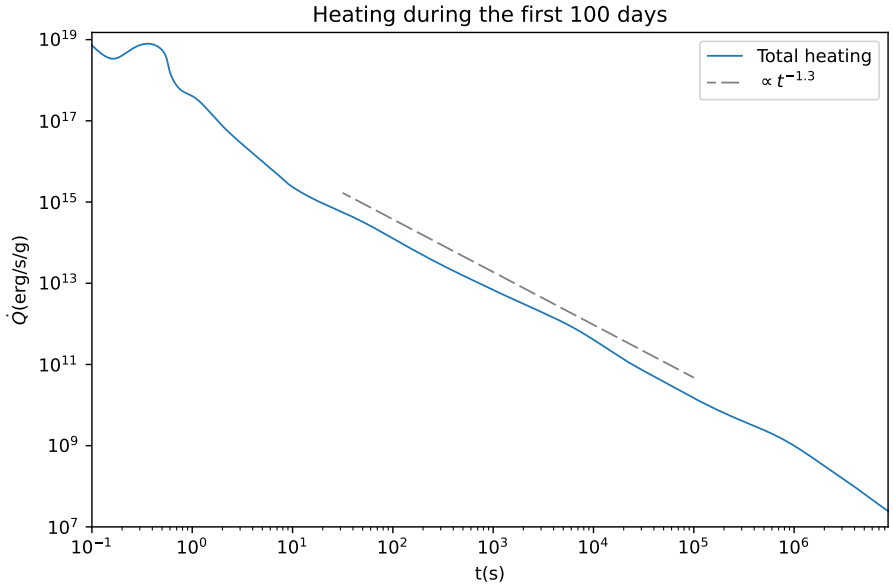

Figure 9. An example of the total heating rate during the first 100 days after the neutron star merger, with an initial $Y_e \approx 0.13$. The heating rate follows closely the power-law $\dot{Q} \propto t^{-1.3}$.

after the freeze-out of neutron captures. During the first hours, neutron decay may be dominating the heating, assuming there is a substantial amount of free neutrons still available in the outermost layers of the ejecta. [37] During the first 10 days, $\beta-$decays are the dominating in the energy production. [146] During the first 100 days, the heating is dominated by a few decays, like β^--dacays of ^{234}Th $\left(t_{1/2} = 24.10(3)\text{ d}\right)$ and ^{140}Ba $\left(t_{1/2} = 12.7527(23)\text{ d}\right)$ (see Wu et al. [145] for further examples). This is due to a limited number of nuclei with an appropriate half-life, and thus the heating may differ from the power-law dependence. [37] The abundance distribution of nuclei produced during the r-process nucleosynthesis affects heavily the heating rate at the timescale of $\tau \approx 1$–100 days. At later times of weeks to months, the decay energy production can also be dominated by several α-decays, like ^{223}Ra $\left(t_{1/2} = 11.43\text{ d}\right)$ and ^{225}Ac $\left(t_{1/2} = 10.0\text{ d}\right)$, and the fissioning isotope ^{254}Cf $\left(t_{1/2} = 60.5\text{ d}\right)$, as they release more energy per decay and thermalize more efficiently than β-decay products. [145] This is partially due to rapid decrease of γ-ray thermalization efficiency which practically becomes negligible on timescales of a few tens of days. [37]

In a hot stellar plasma, Coulomb effects can have a significant effect on fusion processes. As electrons are attracted by the positively charged nucleus, they modify the Coulomb interactions between two nuclei. This makes charged particle reactions

more likely. The shielding effect of electrons can be approximated by so-called screening corrections. [39, 147] These are dependent on the temperature and density of material. [148, 149] Usually, three different screening regimes are distinguished, separated by the ion-coupling parameter Γ_{12} [150]:

$$\Gamma_{12} = 2\frac{Z_1 Z_2}{Z_1^{1/3} + Z_2^{1/3}} \frac{e^2 (4\pi n_e)^{1/3}}{3^{1/3} k_\mathrm{B} T} \tag{48}$$

$$\approx 4.5494 \times 10^{-4} \frac{Z_1 Z_2}{Z_1^{1/3} + Z_2^{1/3}} \left(\rho Y_e\right)^{1/3} T^{-1}, \tag{49}$$

where Z_i is the number of protons of nucleus i, e is the elementary charge, $n_e \equiv \rho N_\mathrm{A} Y_e$ is the electron number density, k_B is the Boltzmann constant, T is the temperature in GK, and ρ is the density of the environment. N_A is the Avogadro constant and Y_e the electron abundance. If $\Gamma_{12} \ll 1$, it is called the weak screening regime. The intermediate regime is at $\Gamma_{12} \approx 1$, and the strong regime at larger values. [39] Screening effects are taken into account in GSINet, as well.

3.2 GSINet

A nuclear reaction network evolve the numbers of different nuclei in a system with a given set of reaction and rates for reactions transmuting nuclei into other nuclei. There are multiple different nuclear reaction networks available, however, only a few are publicly available, of which some of the most notable are Torch and SkyNet. [39, 138] GSINet is one of the non-publicly available networks. GSINet is a modular nuclear reaction network code that holds several similarities to WinNet [39]. They both have a common background in BasNet. GSINet is a so-called single-zone network code which means that it is based on tracers or zones that are unable to interact with each other. The ejecta from an astrophysical event is traced with passively advected particles that are affected by the velocity field of the fluid. These tracer particles contain information about the thermodynamical conditions in time. If diffusion of the composition is insignificant compared to the burning, tracers can be calculated separately and the total matter ejected from the event is the average over all tracer particles. [39, 151]

GSINet is written in Fortran, mainly in Fortran 90, with some parts utilising also features from more recent Fortran releases. The code is split into two main parts. The first part, the initialisation part, reads the control file where the user has

defined which nuclear reactions will be used in calculation. As the code is highly modular, the user can, for example, choose not to include beta or alpha decay, or ignore neutrino interactions. The control file also contains paths for the required input files for nuclear data and the included reactions. These can also be modified as long as they are in a suitable format. Running the first part compiles the given input data into a matrix form that is used in the second part of the code that manages the network calculation.

The second part of the code is the nuclear network part which is responsible for the calculation of the system parameters and their evolution. The simulation runs from $\sim 2 \times 10^{-2}$ s to 10^{18} s ($\approx 3.2 \times 10^{10}$ a). A control file is used to define e.g. parameters in converging conditions, but most importantly, the user need to provide a path for a trajectory file that holds the information about the evolution of the system. The trajectory file also includes the initial values e.g. for electron abundance Y_e and entropy S.

3.2.1 Modifications to GSINet

The code simulates a merger of two neutron stars, with parameters like neutron density given in a trajectory file. The trajectory file contains the required information how the system evolves as the network code advances, [61] The calculations begin at a temperature of $T = 10$ GK, and nuclear statistical equilibrium is assumed until $T = 6$ GK after which the code switches to a full network calculation. The version used for calculations in this thesis includes 7362 different nuclei with $Z = 0...110$ and $A = 1...313$, ranging from free neutron (n) to darmstadtium (Ds). The input files include reaction rates from the JINA Reaclib v2.2 reaction rate library, and both experimental and theoretical values for different decays. For the r-process, the most important reaction rates are (n,γ) and (γ,n) reactions, for neutron capture and photodisintegration respectively. The code also handles the both beta decay types, electron captures, and alpha decay, as well as fission reactions. Neutrino interactions can also be included, but in this thesis, they were not added to the reaction network. GSINet has been previously tested by comparing the obtained abundances from a full r-process network calculation to the abundances obtained with SkyNet [138], and the results have been identical. [152] Also the closely related WinNet has been widely tested [39].

In its basic form, the GSINet includes only ground states for each isotope. Also,

the JINA Reaclib includes only reactions between ground states. In order to add isomers to the code while keeping the unmodified modules still working, required a new method to name the isomers. Traditionally, isomeric states are denoted by mx, where x is the isomer number. As the goal in the modifications was to keep the code working without major changes to the structure, a different naming scheme had to be used. The added isomers were named with a Python script to give each isomer a unique two-letter chemical symbol so that the code would handle isomers and ground states as separate elements. As this was done before running the network code, the list of added names was stored in the input data files so that the network code could access it when needed. From the code point of view, isomers and ground states are different elements that happen to have same amount of neutrons and protons, with different reaction Q values and mass excesses. The two-letter names were chosen, as multiple subroutines should have been altered in order to handle longer element names. The used names are not visible in the output files, and thus they do not necessarily need to resemblance the element names,

In this thesis, of different types of radioactive decays, only beta minus decay was considered for isomers, as beta minus decay is the prevailing decay type until the heaviest isotopes above A $\sim$ 200. By limiting the mass numbers of the added isomers to below A = 200, fission reactions could also be ignored for isomers, as they are basically non-existent at mass numbers below 200. Fissions of ground states were normally included in the calculations, however, the products were always ground states, even if the daughter nuclei had both ground state and isomeric state available. Alpha decays are also negligible with mass numbers A $<$ 200, so excluding isomers in alpha decays is justifiable. As with the fission reactions, the daughter nucleus was always a ground state nucleus, even if it had also an isomeric state, Naturally, as beta plus decays and electron captures are the main decay channel in the proton rich side of the valley of stability, it is safe to ignore β^+ decay in r-process calculations, even though the network code includes it as well. Neutrino interactions are not included in the version used in the thesis, and thus they were not considered with the additional isomers either.

As the unmodified version of GSINet does not include any excited states, there are no reaction module for electromagnetic transitions, and in the case of isomers, isomeric transitions (IT). For calculations in this thesis, the added isomers were chosen so that they do not include transitions from isomeric state to the ground

state. Adding isomeric transitions to the lower-lying states suffices if temperatures are low enough, but in the astrophysical conditions at temperatures way above 1 GK, there are also excitations from lower energy states to higher states, and this could be taken into account, if a module for electromagnetic transitions were to be added into the network code. This would also require more complete excited-state data, as it would improve the transition rates between the ground state and the excited states. In particular, the measurements of intermediate state half-lifes and γ intensities would make more reliable calculations of thermally mediated transition rates possible. [28]

The major changes done in the code are in the input part that reads the input files and creates the reaction matrix. The most important changes in the code can be found in Appendix B. As the code is not publicly available, only the most notable changes made in the code are shown, with some necessary parts of original code included. The other part of the code, the network itself, was basically unaltered apart from minor changes to the output files so that the isomer labelling could be added. Thus the subroutines in Appendix B are from the input part.

Two new subroutines were added to handle isomers. Subroutine `find_iso` reads through the an added file that included the unique isomer names. The subroutine takes an element name, and returns a value that tells, if the element name belongs to a ground state (0) or to an isomer (1 for the first isomer, 2 for the second). Subroutine `iisomer` is used in beta decay. For the given proton and neutron numbers, it checks if that element has any isomers, and returns the number of isomers, using the precompiled file of isomer names. Subroutine `mapname_mod` is a heavily modded existing subroutine to include isomer handling. For the given neutron and proton numbers, and isomer index, the subroutine returns a name corresponding the input values. This subroutine reads the precompiled isomer name file, and creates a 2D-array of elements. The position of the element name is defined by the input values.

As only the beta minus decay for isomers was considered in this thesis, the source file that reads the information regarding beta decay was updated. Although each isomer was given a unique name, the beta decay part of the code does not utilise names, instead it uses neutron and proton numbers. As the ground state and isomeric states have identical proton and neutron numbers, the original input data file had to be modified so that it includes indexing for different states for each isotope. The

code was then modified so that there was an additional loop that checked for each decay if the daughter had possible isomeric states, using this added indexing in the input data file. This can be seen in subroutine `beta_exp_data`, in which the grayed parts are unmodified, and those in black have modifications. The added `do`-loop with `isom` as an end point value. There are also function calls to subroutines `iisomer` and `mapname_mod` that are required in isomer handling. The input file was also modified so that it includes beta branching ratios to the ground state and isomeric states. Without this addition there would have been double counting in a case if the beta decay had decay branching to multiple states in the daughter nucleus. As the indexing was stored alongside with the proton and neutron numbers, the ground state and isomeric states were separate isotopes even if the naming was not used in the code.

The data for isomers was obtained from an ASCII formatted file of NUBASE Evaluation - NUBASE2020. The NUBASE2020 evaluation contains the required nuclear properties for the code, and there are listed isomeric states with $t_{1/2} \geq 100$ ns. There are 1938 isomers in the listing fulfilling the criteria. [52] As the reaction rates for the isomers were not present in the original input files, they were calculated using TALYS. As there were slight differences in energy levels of the isomers between those included in TALYS and those obtained from NUBASE2020, isomers with an energy level difference greater than 4×10^{-4} times the energy level listed in TALYS were omitted. In the end, 58 isomers were added to the network; of these 52 were 1st isomeric states, and 6 were 2nd isomeric states. The mass numbers range from A = 58 to A = 175. The full list of added isomers can be found in Appendix A with their mass number A, proton and neutron number Z and N, spin J, half-life $t_{1/2}$, mass excess $\Delta M(Z,N)$, and in the case of isomers also the excitation energy E_{ex}. The excitation energy E_{ex} is obtained from mass excesses: $E_{\mathrm{ex}} = \Delta M^*(Z,N) - \Delta M(Z,N)$, where the asterisk denotes the isomeric state.

3.3 Talys

TALYS is a versatile software package for simulating nuclear reactions below 200 MeV. It is widely used, and can be used for several types of reactions, including low-energy neutron captures, high-energy particle reactions, and astrophysical reactions. There are several reaction mechanisms included in TALYS, and in this work compound nucleus model was used. The compound nucleus capture at the astrophysical energies is known to be the dominant reaction mechanism for medium- and heavy mass nuclei within the valley of β-stability. [131, 153] In compound nucleus reactions, Hauser-Feshbach statistical model [154] is used. The Hauser-Feshbach model relies on the assumption that the capture process advances via creation of an intermediate compound system, or a compound nucleus, that is able to reach thermodynamical equilibrium. The compound nucleus can form if the nuclear level density of the compound nucleus is high enough at the excitation energy corresponding to the projectile incident energy so that there is an average statistical continuum superposition of available resonances. The energy of the incident particle is then shared by all the nucleons before the energy is released by de-exitation by γ emission or by particle emission. [153] The Hauser-Feshbach formalism also requires that the formation and decay of the compound nucleus are independent, i.e. the so-called Bohr hypothesis. [155–157] As this may not hold in all the cases, there are additional corrections included in TALYS. The code has been tested and compared against to similar reaction codes, like MOST, and the obtained values have shown improved results compared to the previous codes. [157] The Hauser-Feshbach formula and other equations used in TALYS can be found in [131].

In this thesis, TALYS 1.6 was used to calculate (n, γ) reaction rates for reaction ${}^{\mathrm{A}}_{\mathrm{N}}\mathrm{X}^* + \mathrm{n} \longrightarrow {}^{\mathrm{A+1}}_{\mathrm{N+1}}\mathrm{X}$, where X* denotes an isomer of the element X with N neutrons and mass number A, and X is the ground state of the same element, but another isotope with N+1 neutrons, and mass number A+1. A schematic example of a compound reaction with an isomer and a neutron is illustrated in Figure 10. As the isomeric states in NUBASE and TALYS might not have the same labelling, e.g. the one in NUBASE might imply the first isomer, but the one in TALYS would be the seventh level, a comparison was made, and if the labelling was identical, the isomer was added. The obtained values were then fitted in order to obtain the (n, γ)

reaction rates in the REACLIB format [133]:

$$\lambda = \exp\left\{\left[a_0 + \sum_{i=1}^{5} a_i T_9^{(2i-5)/3} + a_6 \ln T_9\right]\right\}. \tag{50}$$

Here a_i, $i = 0,\ldots,6$ are adjustable parameters, and T_9 is the temperature in GK. The reverse rates for reaction (γ, n) are then calculated via detailed balance theorem (see Section 3.1). Also, the reaction rates between the ground states ^{A}X and $^{A+1}$X were updated, so that the neutron capture and photodisintegration reaction rates for isomers and the corresponding ground states were both calculated using mass excesses from NUBASE2020.

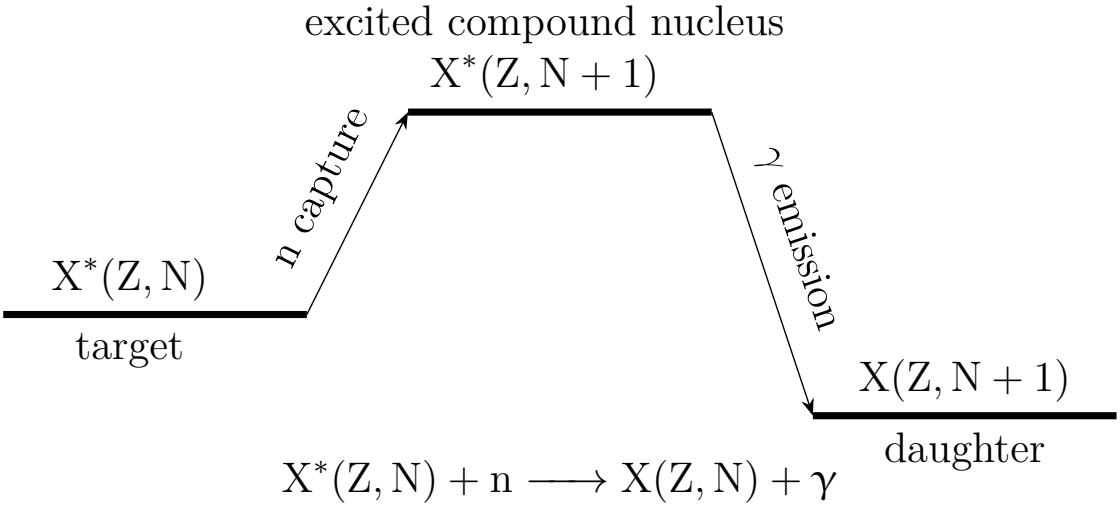

Figure 10. A simplified schematic figure of a compound reaction with a neutron capture. The target, an isomeric state $X^*(Z, N)$ is collided by a neutron. The formed compound nucleus is an excited state of $X^*(Z, N + 1)$. It decays to a daughter nucleus, which in this case is the ground state of $X(Z, N + 1)$, by γ emission.

3.4 Input files

The input files include the necessary data for basic nuclear properties, like isotope names and mass excesses, proton and neutron numbers, and also partition functions for nuclei in different temperatures. Other files include the information of different nuclear reaction properties. These are used in the data compilation part of the code. Particle reactions and their properties are listed in the Reaclib file, while decay reactions have each their own file. The reactions and decay types to be included

in the calculation, can be selected in the control file. For β- and α-decays, there are also experimental and theoretical files available. The code will primarily use experimental values, and resort to theoretical values if there are no experimental data available. Fission properties have also their own input file for each type: spontaneous, γ-induced, neutron induced, and β-delayed fission. The fission yield distributions are also included. There are also available several Reaclib files for different mass models: DZ31 (Duflo-Zuker) [158], FRDM (finite-range droplet model) [159], HFB-21 (Hartree-Fock-Bogliubov) [160], and WS3 (Weizsäcker-Skyrme) [161]. In this work, FRDM files are used. For a comparison of the effects of different mass models in the r-process, see e.g. [61].

Apart from the data files that contain nuclear properties and reaction rates, there are also so-called trajectory files which are used in the network part of the code. These files contain information about the evolution of parameters that affect the r-process nucleosynthesis.

3.4.1 Nuclear data

For this thesis, the most important data files are the Reaclib files that contain the neutron capture rates, and the β^--decay files. Neutron capture rates are needed for the r-process nucleosynthesis, while the β^--data is required for the decay phase. As the modifications to the code (Section 3.2.1) were done in the β^- files, the respective input data files had to be altered, as well, to include isomer decay values. Similarly, neutron capture reaction rates for isomers were added to the Reaclib file.

In order to separate the added isomers from ground states, they had to be named with an arbitrary two-letter name, as the code cannot handle longer names (Section 3.2.1). A separate file was created to include required names. Now every nth (1st, 2nd, and so on) isomer was a new element, and thus reactions including isomers could be added. This issue was mainly in the Reaclib file, as there the different reactants are differentiated by their chemical symbol and mass number. The beta files use proton and neutron numbers in order to distinguish different elements. Thus, an extra index had to be added in the decay files in order to differentiate isomers from the ground states.

The nuclear property files include all the possible nuclear species in the network. They list the name and the mass of each nucleus. In addition, they also list the proton and the neutron numbers, the spin, and the mass excess of each nucleus.

There are also partition function calculated in different temperatures for each nucleus. The original values are from AME2016 [162]. The added isomers use values from NUBASE2020 [52]. As the differences between the ground state values in AME2016 and NUBASE2020 are minimal, and in most of the cases non-existent, the older values can still be used without sacrificing too much accuracy. For example, there is a 0.6 keV difference in mass excess (−68024.4 keV vs −68025.0 keV) and a 0.5 ms (261.5 ms vs 261 ms) difference in half-life of the ground state ^{131}In between NUBASE2020 and AME2016. In addition, for simplicity, the partition functions of added isomers were copied from the respective ground state values. As the code does not utilise any error limits in the data files, only the measured results without uncertainties. In Appendix A, a round-up of some of the nuclear information added to the files can be found.

The Reaclib file is divided in different chapters, and each chapter has different types of reactions. For example, the first chapter has reactions of type $e_1 \longrightarrow e_2$, and the second chapter $e_1 \longrightarrow e_2 + e_3$. An example of $e_1 \longrightarrow e_2$ reaction in the Reaclib format is an electron capture $^7\mathrm{Be} + e^- \longrightarrow {}^7\mathrm{Li} + \nu_e$:

```
be7  li7                                  ec      8.62000E-01
-2.271830E+01 1.074870E-03 3.886080E-01 1.166990E+00
-1.171250E-01 9.263280E-03-1.020170E-01
```

In the first row, the reactants are listed, followed by reaction label and the Q value for the reaction. The two other rows are the seven Reaclib coefficients, defined in Equation (50) [133]. For the complete list of chapters, different flags used, and the exact format, see the Jina Reaclib Database [2].

The Reaclib coefficients for neutron capture reactions for isomers were calculated with the help of TALYS. The obtained values were then added to the Reaclib file in the correct format. The neutron capture rates and its inverse were only calculated between the ground state of a heavier isotope and a lighter isomer, i.e. $^{\mathrm{A}}_{\mathrm{N}}\mathrm{X}^* + \mathrm{n} \longleftrightarrow {}^{\mathrm{A+1}}_{\mathrm{N+1}}\mathrm{X}$, where A and N are the mass and the neutron number of the element X respectively. The asterisk * denotes isomeric state, and n is a neutron. As TALYS does not return the Reaclib coefficients directly, the obtained values were fitted so that the resulting function would give the Reaclib coefficients. A plotted example of such a fit (in light blue) and its inverse (in light orange) can be seen in Figure 11: The reaction rates for neutron capture reactions were also updated for each ground

[2] Available at `https://reaclib.jinaweb.org/index.php`

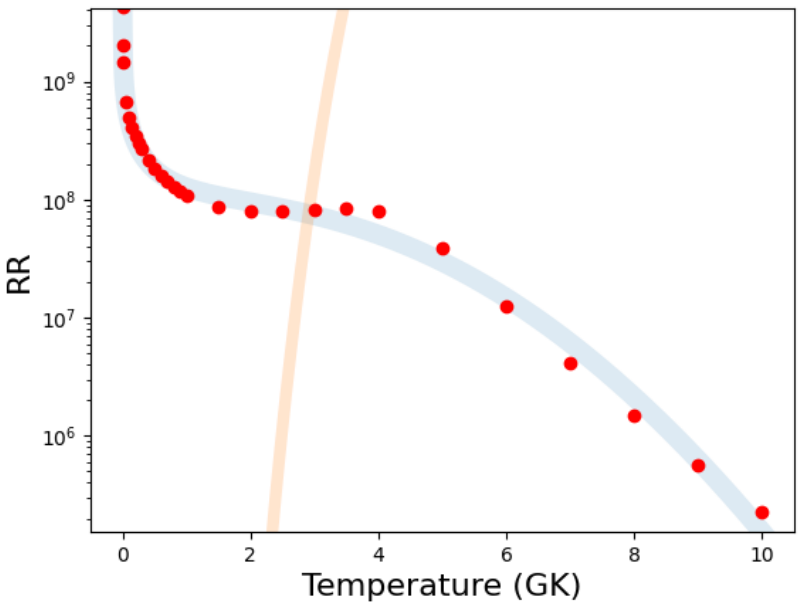

Figure 11. An example fit for the Reaclib coefficients of the reaction ^{153m1}Nd + n $\longrightarrow$ ^{154}Nd (in light blue), and its inverse (in light orange). Red dots are the data points obtained from TALYS calculation. Reaction rate is on the y-axis. Image courtesy of Stylianos Nikas.

state that has an isomer added.

The experimental β^--decay file was another file that underwent major changes in order to add isomers. Instead of element names, as was the case with the Reaclib file, the beta file handles different elements by their neutron and proton numbers. In order to distinguish isomers from the ground states, an additional index was inserted into the file. The modified code (see Section 3.2.1 and Appendix B) was then able to separate isomers from the ground states. The β file includes the half-life for each isotope, as well as the branching ratios to different daughter nuclei. The file includes branching ratio to the daughter nucleus without beta-delayed neutron emission, and branching ratios up to three beta-delayed neutrons emitted. Each of these branching ratios were split into three values: one for branching to the ground state and one for each added isomer, the 1st and the 2nd. Of course, most of these values were zeroes, as there are far less isomers added than there are beta decaying nuclei in total. Each beta decaying nuclei now had 12 possible branching ratios. The branching ratios were obtained from NUBASE2020 [52]. However, due to limited data available, most of the possible β^--decays that could have included an isomeric daughter, were still decaying completely to the ground state.

For the nuclei, for which there is no experimental half-life data available, the β^--decay rates, with β^--delayed neutron emission branchings, were obtained from the compilation of Möller et al. [163]. These values use QRPA (quasiparticle random phase approximation) calculations in addition to the FRDM mass model. Both the β^--decay values and the included neutron capture rates determine the "neutron drip line" in this work, as every reaction must be included in the input files. An illustration of the experimental β^--decay values (in blue) and the theoretical values by Möller et al. (in red) in an NZ-plane can be seen in Figure 12. The limiting "neutron drip line" is a straight line that is also visible in the r-process snapshots in Appendix C.

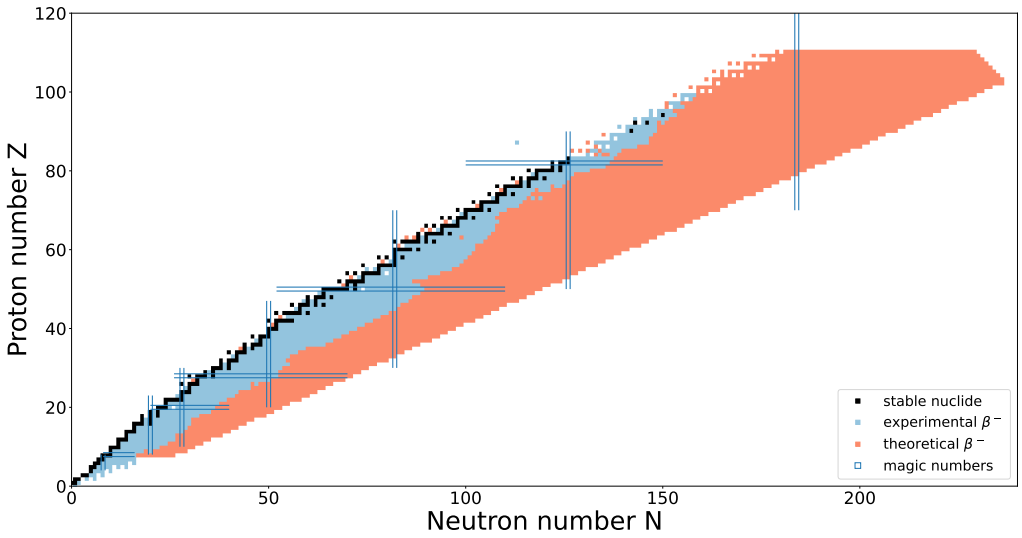

Figure 12. The included β^--decay values are illustrated in the NZ-plane. Black squares are the stable nuclides, the blue squares are nuclides with experimentally known β^--decay values, and the red squares are nuclides with theoretical β^--decay values by Möller et al. [163]. Blue vertical and horizontal lines mark the magic numbers for neutrons and protons respectively.

3.4.2 Trajectories

Trajectories are based on hydrodynamical simulations, and there are different trajectories for different events. [61] Trajectory files include necessary data so that the network can evaluate the abundances during the NSE phase before the r-process begins. In GSINet, these files list the mass of the trajectory, and the evolution of several parameters, including Y_e, temperature, density, and entropy during the first $\sim$ 40 milliseconds of simulation, before the network switches to the r-process calculations at 5 GK. Differences in these parameters lead to different outcomes of the whole nucleosynthesis. In this thesis, five different trajectories were used to test how the addition of isomers affect the outcome of nucleosynthesis. They are labelled here with numbers from 1 to 5.

The evolution of different parameters in the used trajectories are presented in Figure 13. The temperature evolution is plotted in Figure 13a. Trajectories 1 and 2 start from low temperatures, at around 0.1 GK, and the temperature stays low, apart from spikes to 1 GK, until $\sim$ 18 ms. At that point the temperature rises suddenly, in the case of Trajectory 1 to $\sim$ 15 GK, and in Trajectory 2 to 40 GK. Temperatures in Trajectory 1 fall as suddenly as they rise, and before 20 ms temperatures are

back around 0.1 GK. Also in Trajectory 2 temperatures fall quickly, however slightly slower than with Trajectory 1. In Trajectory 2, temperature fall to 0.1 GK when around 25 ms have elapsed. The other trajectories have higher initial temperatures. Trajectory 3 begins at around 1.5 GK, and the temperature rises slightly, before rising to $\sim$ 27 GK at around 19 ms. There is a sudden dip in temperature, down to $\sim$ 1 GK, before it rises to $\sim$ 15 GK at around 21 ms, after which it gradually falls below 1 GK at 40 ms. Trajectories 4 and 5 have similar initial temperature evolution, starting and staying at around 6-8 GK. Trajectory 4 is a cooler one, never reaching temperatures over 10 GK, while Trajectory 5 reaches 25 GK. Both of these cool in a similar fashion to Trajectory 3. Trajectory 4 reaches its final temperature of 0.5 GK at around 27 ms, and after reaching it, the temperature stays constant. In Trajectory 5, the temperature slowly decreases after reaching the peak value, and at 40 ms, it has fallen to around 0.9 GK.

Electron abundance (Y_e) evolution is plotted in Figure 13b. The Y_e value is significant, alongside with entropy, in determining how heavy isotopes can be produced during the r-process, as discussed in Chapter 2.2.2, as it defines the neutron abundance in the system. All these trajectories have very low initial Y_e, but already in the initial moments Trajectories 1 and 2 have the lowest Y_e values. This carries on to the end of the trajectory time scale, as Trajectory 1 has Y_e value of 0.13. In Trajectory 2, the final Y_e is 0.19. The other three trajectories have higher initial Y_e, and significantly higher final Y_e values, as in Trajectories 3 and 4 Y_e is 0.36–0.37, and in Trajectory 5 0.33.

Density (ρ) evolution is in principle rather similar in all trajectories, as can be seen in Figure 13c. They all start at a very high density, over 10^{14} g/m^3, and the density begins to exponentially fall, starting around 18 ms. Trajectory 1 becomes the least dense, with $\rho \approx 3.4 \times 10^4$ g/m^3. Trajectories 2 and 4 are in the middle ground, with final densities of 5.0×10^5 g/m^3 and 1.4×10^6 g/m^3 respectively. Trajectories 3 and 5 have the highest final densities, x and y respectively.

Entropy (S) evolution, depicted in Figure 13d, differs significantly between the trajectories. At $t = 18$ ms, in all trajectories entropy starts to increase. Trajectory 4 has a significantly higher entropy after $t = 18$ ms compared to the other trajectories, the final value being $S \approx 52$. On the other hand, Trajectory 2 has a decreasing entropy from $t = 19$ ms to $t = 24$ ms. The final entropy is $S \approx 8$, the lowest of all the trajectories. The rest are positioned around 20 J/K. Trajectories 1 and 3 have

entropies slightly below 20 J/K, $S \sim 17$–18. In Trajectory 5, the entropy rises to $S \approx 27$. As mentioned in Chapter 2.2.2, entropy alongside with Y_e have a great impact on the r-process nucleosynthesis.

In order to visualise the the differences in the nucleosynthesis evolution between the different trajectories, snapshots of the evolution of abundances in the NZ-plane are provided in Appendix C, illustrating the early moments of the r-process, advancing r-process with build-up at even and the magic neutron numbers, and the decaying matter after the r-process has ended. The snapshots present the results with the unmodified code as distinguishing the differences between the unmodified code and the one with isomers visually in an NZ-plane is difficult. Direct comparison between different time steps is also not viable as the temperatures and times of each step differ between the unmodified and modified simulations.

A comparison of abundances at 10^9 a is given in Figure 14. These results have been obtained with the unmodified code. The graph clearly shows the differences caused by different initial conditions given in the trajectory files. Trajectories 1 and 2 lead to the nucleosynthesis that includes also the heaviest nucleons, with $A > 200$. On the other hand, nucleosynthesis determined by Trajectories 3, 4, and 5 do not create isotopes with $A > 140$. Trajectories 3 and 5 have the abundance maximum at around $A \sim 80$, which coincides with the first r-process peak (Chap. 2.2.3, Fig. 6). Trajectory 4 leads to nucleosynthesis with abundance maximum at around $A = 100$. The abundance distribution of these trajectories resembles the so-called weak r-process (Section 2.3). Trajectories 1 and 2 have two main abundance peaks: one around $A = 135$, and the other one around $A = 195$. There are some differences, as Trajectory 2 leads to higher abundances at lower mass numbers, especially at $A = 130$, while Trajectory 1 has the highest abundance peak just at $A = 195$. The both trajectories also produce the elements in the rare-earth peak at around $A = 160$. The peak around $A = 130$ is the 2nd r-process peak, and the one at $A = 195$ is the 3rd peak. The 2nd and the 3rd peaks are a part of the main abundance peaks, and they are produced by the so-called main r-process. As Trajectories 1 and 2 have the lowest Y_e, they have the most neutron-rich conditions that enable the r-process to proceed to the heaviest elements. The evolution snapshots in Appendix C also support this, as with Trajectories 1 and 2, the abundance maximum reaches heavier isotopes than with the other three trajectories.

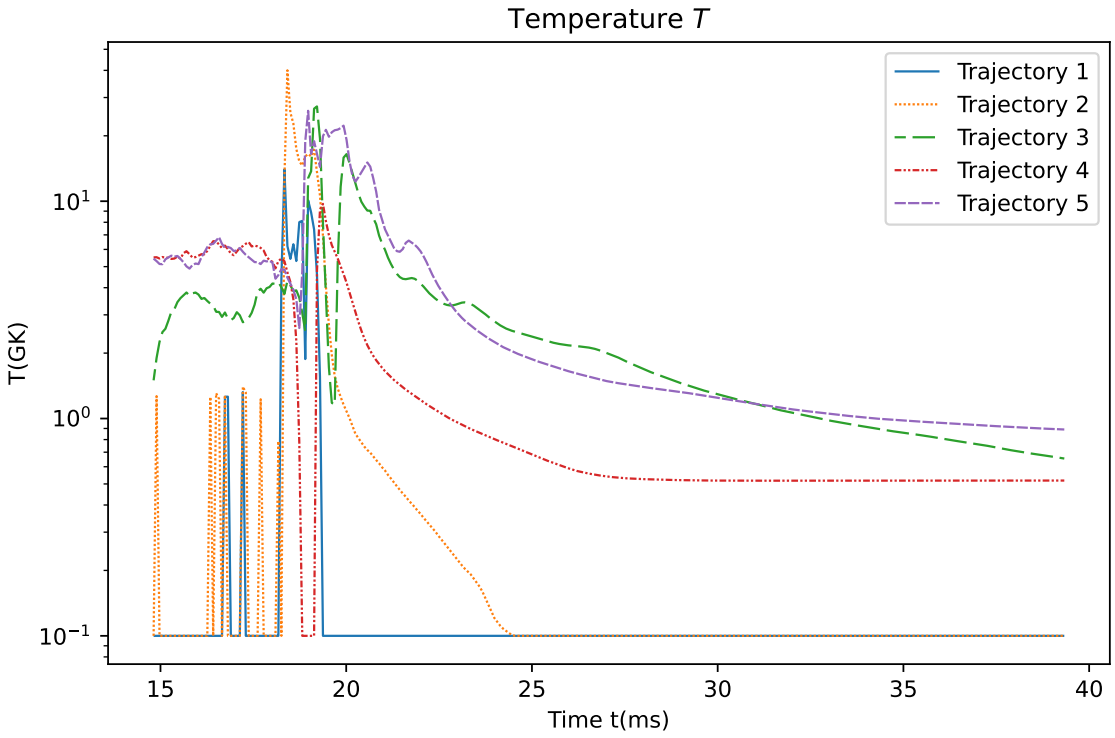

(a) Temperature evolution.

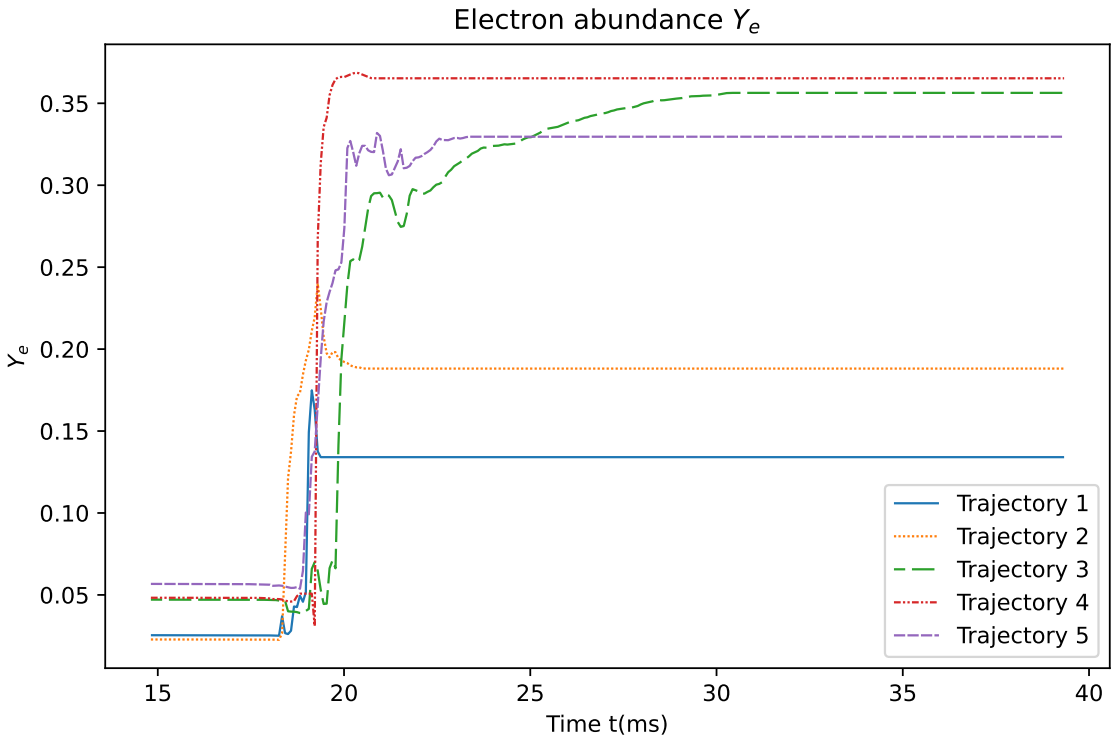

(b) Y_e evolution.

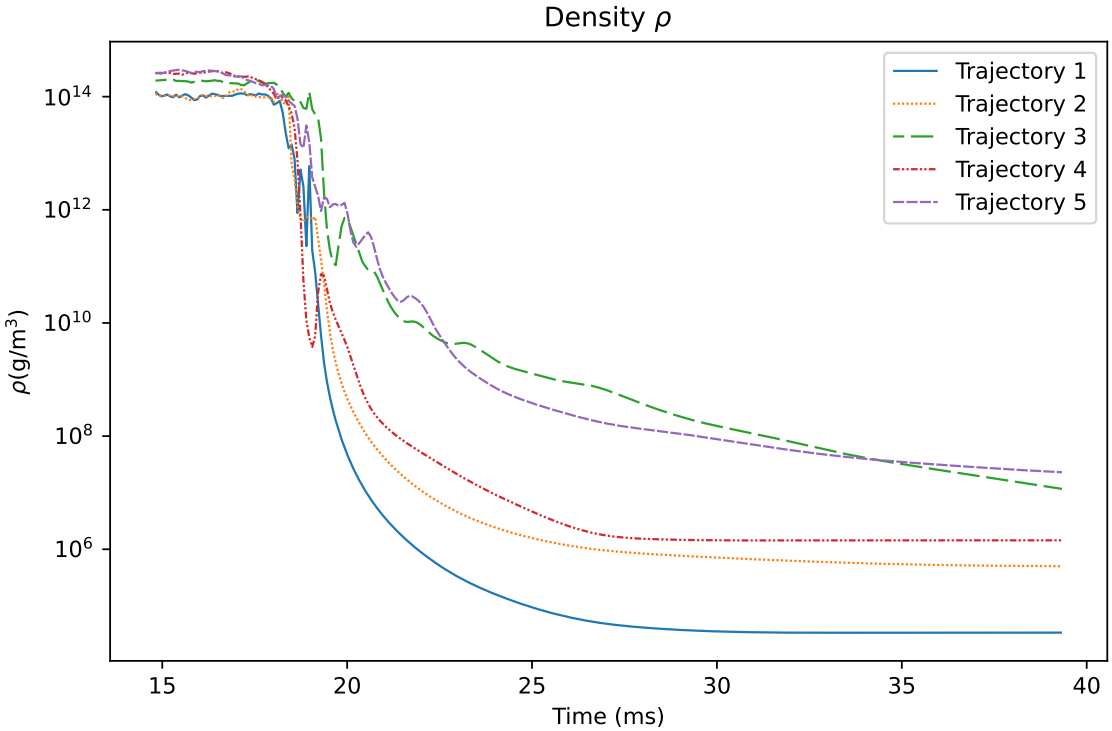

(c) Density evolution.

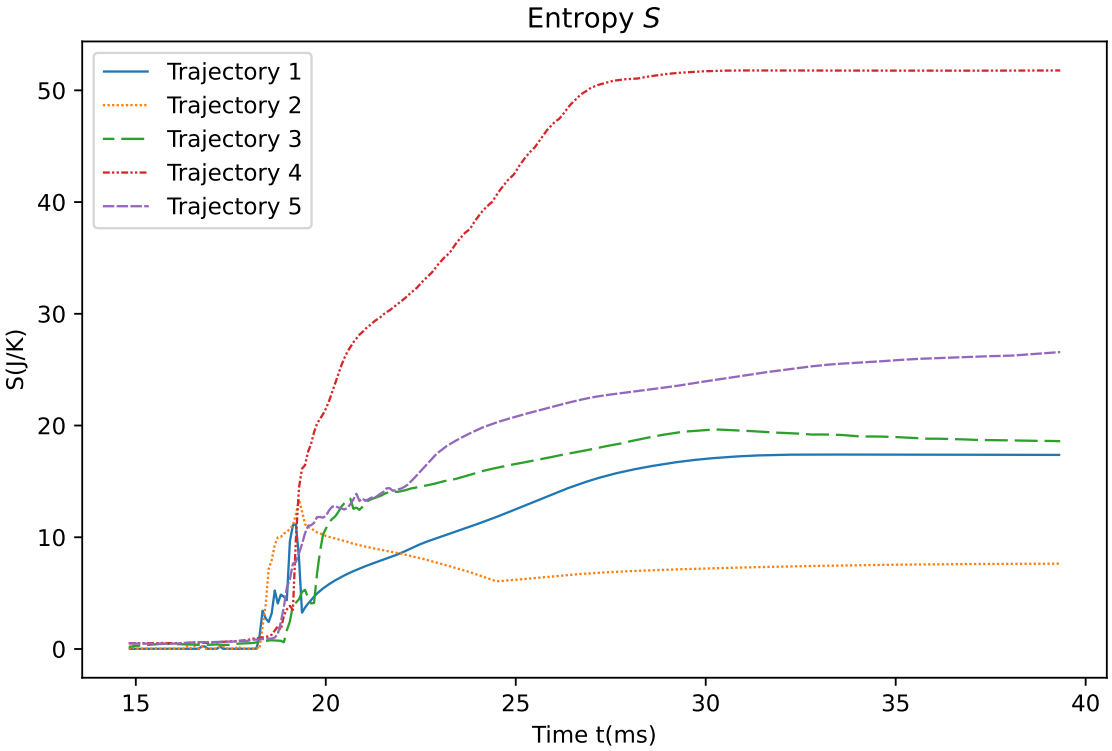

(d) Entropy evolution.

Figure 13. Evolution of different parameters of the used trajectories.

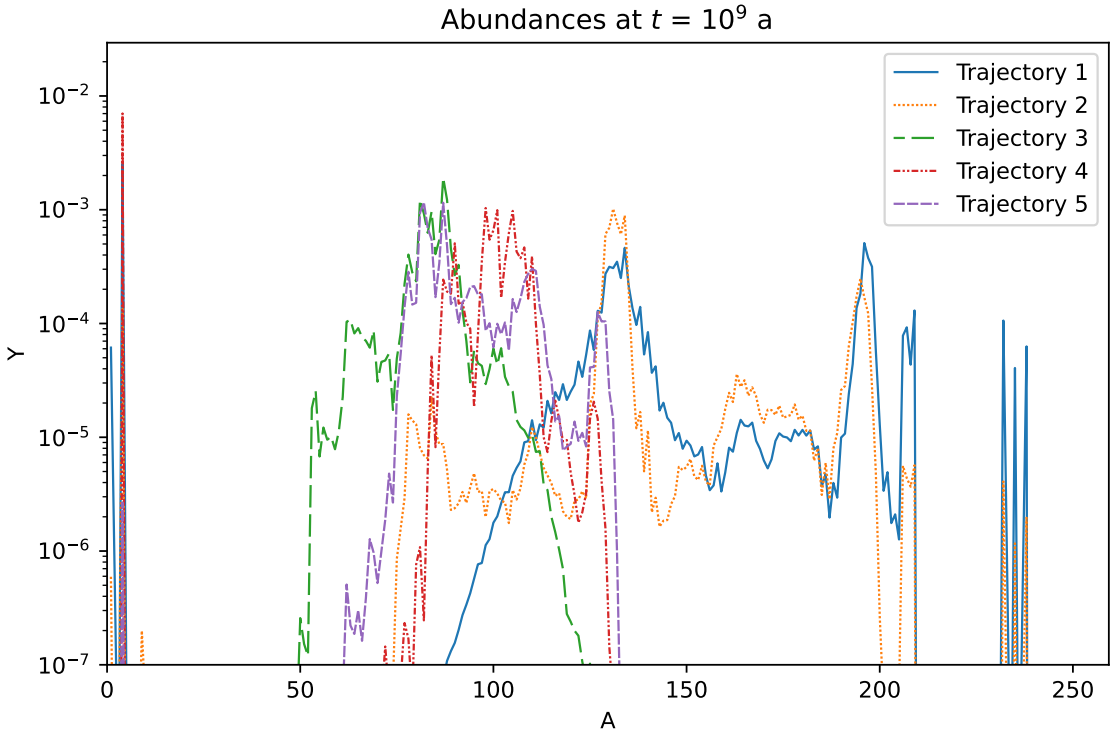

Figure 14. Abundance comparison of the trajectories at 10^9 a.

4 Results

In this chapter, the results obtained from the five different trajectories described in Chapter 3.4.2 are presented. Each trajectory uses different initial conditions and the evolution of parameters differs. This leads to varying outcomes in nucleosynthesis. For each trajectory, the unmodified code was used to give baseline results. Then the modified code with added isomers was used to obtain results with isomers. In addition, the modified code was also run with isomers and an artificial β^--branching to isomeric states. Apart from the changes in the branching ratios listed in NUBASE2020, the setup was similar to the run with the modified code. The used branching forced half of the ground state of ${}^{\mathrm{A}}_{\mathrm{N}}\mathrm{X}$ to beta decay to the first isomeric state ${}_{\mathrm{N}-1}{}^{\mathrm{A}}\mathrm{Y}^*$ and the other half to ground state ${}_{\mathrm{N}-1}{}^{\mathrm{A}}\mathrm{Y}$, in order to exaggerate the effect of the isomeric states in the final abundances. In the few cases of elements with two isomers, no changes to the branching ratios were made. Figure 15 illustrates the difference between the branching ratios obtained from NUBASE2020 and the artificial 50:50 branching ratio. With most of the added isomers, the branching in β^--decay leads to the ground state, instead of splitting the branching between the isomeric and the ground state. As in the example in Figure 15, the isomer states, especially those with noticeably longer half-lives compared to the ground state, have a property that hinders the decay. Some of these properties are discussed in Section 2.4.

Obtained numerical results from both the modified code with listed decay branchings and the 50:50 β^--decay branching are compared to the reference results without isomers. Abundances at one gigayear, with an emphasis on the solar r-process peaks as illustrated in Figure 6, and energy released by nuclear reactions, i.e. nuclear heating, during days 1 to 1000 after the merger are presented and compared as well.

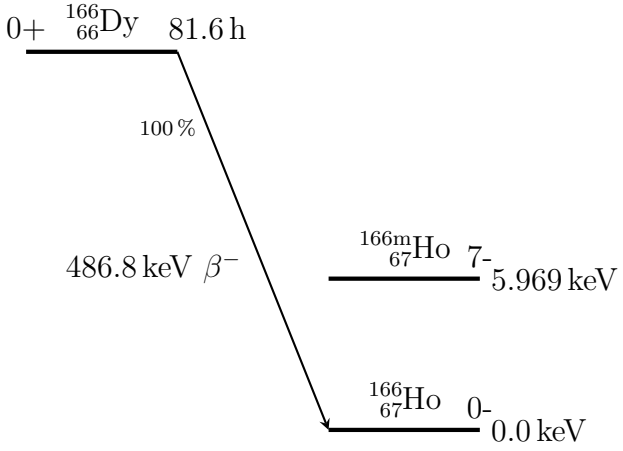

(a) β^--decay of $^{166}_{66}$Dy to the ground state of $^{166}_{67}$Ho using values listed in NUBASE2020. The decay has no branching to the isomeric state $^{166m}_{67}$Ho.

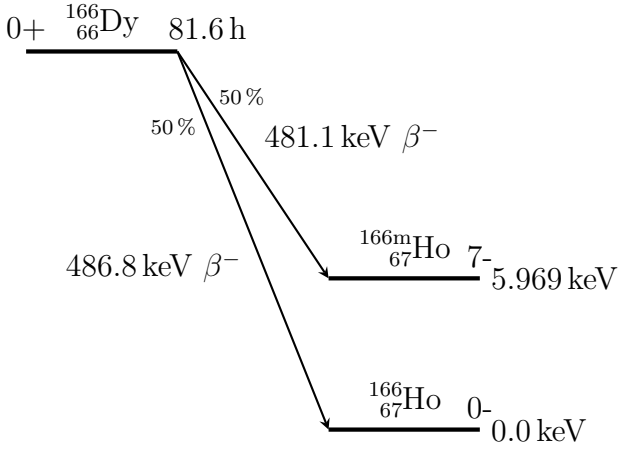

(b) β^--decay of $^{166}_{66}$Dy to the ground state $^{166}_{67}$Ho and the isomeric state $^{166m}_{67}$Ho using an artificial 50:50 branching to both of the states.

Figure 15. A decay scheme showing the difference in β^--decay using branching ratios listed in NUBASE2020 and artificial 50:50 decay branching with an example case of β^--decay of $^{166}_{66}$Dy. In this particular case, the large discrepancy between the angular momentum of $^{166}_{66}$Dy and $^{166m}_{67}$Ho hinders the β^--decay to the isomeric state. There is also a notable difference between the half-lives of $^{166}_{67}$Ho and $^{166m}_{67}$Ho, with $t_{1/2}$(g.s.) = 26.812 h and $t_{1/2}$(isom) = 1132.6 a.

4.1 Abundances and their differences at 1 Ga

A gigayear after the merger, the abundances are basically constant, with the exception of radionuclides that are part of the decay chains of the primordial radionuclides with very long half-lives (^{235}U, ^{238}U, and ^{232}Th). Most of the unstable nuclei have already decayed to the stable isotopes, and there are only a few radioisotopes left. Also the other reactions than decay reactions in unstable nuclei are negligible. In this section, abundances below 10^{-6} are ignored, and the abundance differences are calculated only for abundances over 10^{-7}. It should be noted that smaller differences at lower abundances lead to greater relative differences than similar differences at higher abundances.

Abundances with Trajectory 1 are shown in Figure 16a. The abundance distribution resembles that of the Solar System, with the exception of the first r-process peak at $A \approx 82$. The 2nd r-process peak at around $A \approx 130$ is clearly visible, as well as the the 3rd r-process peak at $A \approx 196$. The added isomers have a slight effect on the abundances. There is a noticeable drop in abundances at $A = 102$, although the abundances around $A = 100$ are around two orders of magnitude smaller than the highest abundances. The drop can also be seen in the relative differences in Figure 16b. There is around 70 % underproduction of elements at $A = 102$ with isomers. On the other hand, there is around 60 % higher abundance at $A = 103$ with isomers than without. The high percentages are partially explained by the low abundance of elements in question. As the r-process with Trajectory 1 operates near the neutron drip line (Figure 26), the difference likely stems from the decay phase, as most of the added isomers are near the stability, and thus do not have a big impact on the r-process neutron captures. This is also evident from the 50:50 results, which are similar to the results with the experimental decay branchings at $A = 102$ and $A = 103$. There are multiple short-lived niobium ($Z = 41$) isomers that might cause the necessary impact on the abundances. These can also affect the early neutron capture phase, before the abundance maximum reaches the neutron drip line.

With the added isomers, the differences to the reference simulation are rather minimal, up to $A \approx 130$, which is near the abundance peak of Trajectory 1 simulation. There are some abundance differences, albeit not as remarkable as is at $A \approx 102$. There is around 15 % less abundance with $A = 130$ with isomers than without. On the other hand, the opposite can be seen at $A = 131$, where around 20 % greater

abundance can be observed with isomers. Again, the 50:50 branching enhances this effect at the same mass numbers. There are multiple added isomers with $A \approx 130$ which are likely the origin of this behaviour.

The rest of the differences are smaller, mainly less than 10 %, with a dip in abundances with isomers at $A = 150$. However, the abundances around $A = 150$ are around two orders of magnitude smaller than in the peak around $A \approx 135$ so the absolute differences are rather small. These smaller differences can originate both from β-decay differences, and also neutron capture reaction differences.

With the 50:50 beta branching, the results have more variations. The abundance difference mostly line up with the isomeric case, but they area heavily enhanced. Especially around the abundances between $A \approx 110$ and $A \approx 130$, there are several ≈ 40 % variations in abundances in both directions, some even peaking 60 %. Of course, the abundances below $A \approx 125$ are still an order of magnitude smaller than the abundances around $A = 135$. As the changes in beta branching are the the only difference between these two simulations with isomers, with a trajectory that runs near the neutron drip line, the abundance differences are very noticeable as nearly every added isomer now affects the decay phase. This leads to these relatively large differences.

In Figure 16b, one can notice the large difference at $A = 170$ and $A = 171$ in abundances with 50:50 branching ratio that is basically non-existent with the results of a isomer simulation with decay branching from NUBASE2020. This does, however, coincidence with ^{170}Ho. Although the ground state and the isomeric state half-lives are rather short, $t_{1/2}(\text{g.s.}) = 166$ s and $t_{1/2}(\text{isom}) = 43$ s, and might not be enough to cause differences in the decay phase. However, as the differences between the abundances with isomers and the abundances without, the decay branching does have some sort of an impact.

Typical for all these differences is that with isomers, there is first underproduction of elements with some mass number, but the adjacent mass number has overproduction. This can be seen as a zigzag pattern in Figure 16b, and it is particularly notable with the 50:50 beta branching. Naturally, this is to be expected, as matter does not vanish, so the underproduction of some mass number unavoidably leads to overproduction of some other mass number. With this trajectory, as the r-process operates near the neutron drip line, differences in half-lives cause the biggest impact in abundances. As the added isomers are mainly around $A = 100$–140, it is under-

standable that the greatest differences are around the same mass numbers. The differences caused by differing neutron capture rates between the isomers and the ground state have less impact, as the r-process operates mostly at heavier isotopes than the added isomers.

In Figure 17, the results with Trajectory 2 are plotted. The simulation with Trajectory 2 also produces a wide range of elements, ranging from $A \approx 75$ to $A = 200$. However, there is a clear peak around $A = 130$–135, where the abundances are around two orders of magnitude greater than in the other mass regions, with the exception of the peaks around at $A = 165$, and $A = 195$. In Figure 17b, one can see an underproduction of around 10 % of elements with mass numbers below $A = 103$ with isomers. Similarly to the simulation with Trajectory 1, there is a dip at $A = 102$ and a peak at $A = 103$ in relative differences with isomers compared to the reference with Trajectory 2. The underproduction turns into a slight overproduction at around $A = 135$, and there is a slight excess of heavier elements with a simulation with isomers than without. Besides the dip and the spike at $A = 102$–103, that range from -80 % to $+60$ % compared to the reference abundances, the differences are rather subtle, mostly being within 10 %.

Simulation with Trajectory 2 does reach the neutron drip line during the r-process, as can be seen in Figure 27b, but the heaviest elements with $A > 200$ of Trajectory 1 simulation are missing. Again, the added niobium isomers could be the reason for the behaviour at $A = 102$–103. The abundance peak at around $A = 130$–135 is caused by the waiting point at the neutron magic number $N = 82$, and the heavier peak at $A \approx 195$ by the magic number $N = 126$. There are some minor differences, e.g. around $A = 125$ that do line up with the added isomers. As there are also small differences in the abundances of heavies elements, with the simulation with isomers producing more heavier elements, the different neutron capture rates of the isomers must have an effect on this.

The 50:50 beta branching simulation yields similar abundances compared to the one with isomers added. As can be seen in Figure 17b, when compared to the reference abundances, both the 50:50 beta branching and the isomer simulations have similar differences. However, there is again a similar zigzag pattern in relative differences as was in the simulation with Trajectory 1 with the 50:50 beta branching. Between $A = 100$ and $A = 130$, the relative differences are, in general, within 50 %. This is mainly caused by the differences in β^--decay, as the forced branching

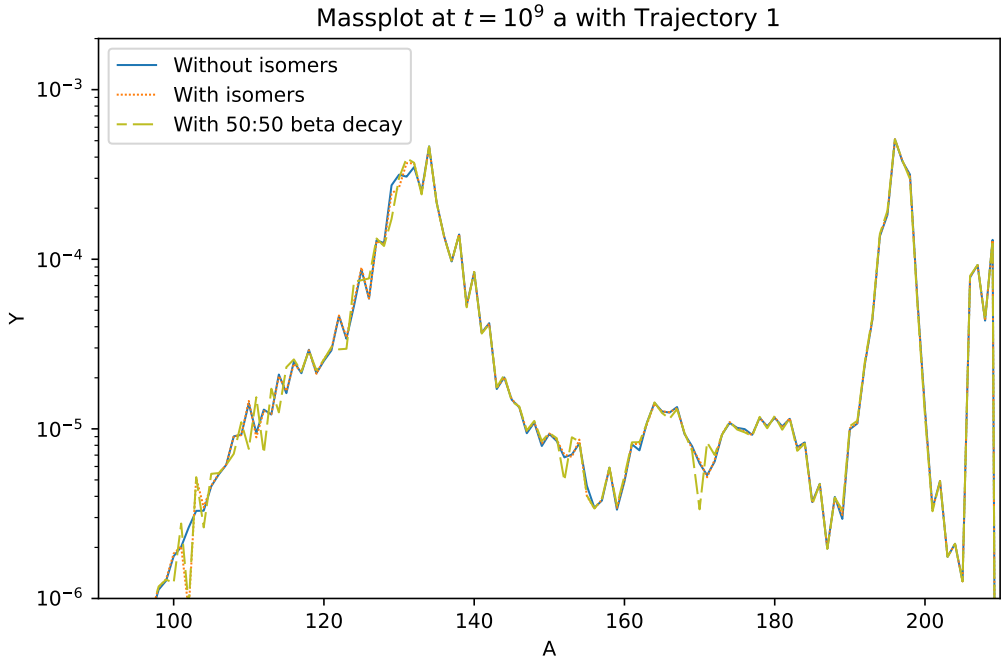

(a) Abundances at 1 Ga with Trajectory 1.

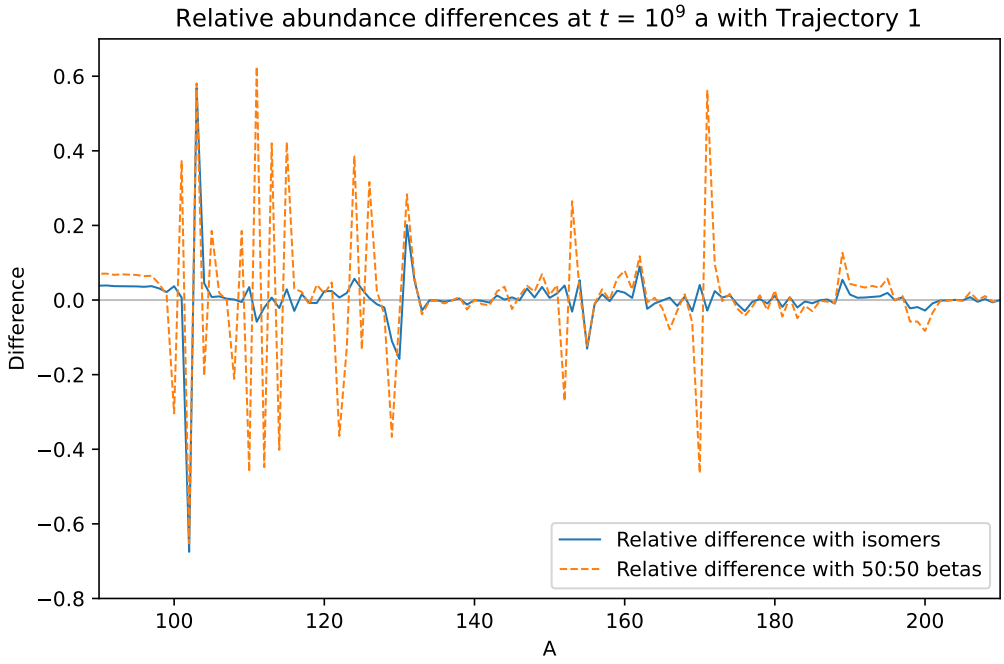

(b) Relative abundance differences compared to the reference at 1 Ga with Trajectory 1.

Figure 16. Abundances with and without isomers, and with isomers and 50:50 β branching ratio at 1 Ga are illustrated in Subfigure a. The corresponding relative abundance differences compared to the reference case without isomers are plotted in Subfigure b.

leads to higher abundances of the isomers. Slight differences can also be seen near the abundance peak at $A \approx 195$. The abundances with the 50:50 beta branching compared to the reference simulation are around 10 % higher below the peak, but on the other hand, around 10 % lower with $A > 195$. With only isomers added, the abundances are 5–10 % higher around the $A \approx 195$ peak when compared to the reference. As there are no added isomers with $A > 170$, the differences probably do not originate from different decay rates. Instead, the possible cause may be the different abundances at the freeze-out, due to different neutron capture rates.

The abundances and the relative abundance differences with Trajectory 3 are plotted in Figure 18. Trajectory 3 produces elements that are, in principle, below $A = 120$, with abundance maximum at $A \approx 80$–90. The r-process reaches the neutron drip line, but the abundance maximum never reaches the heavier nuclei above $N = 82$. The most notable differences between the simulation with isomers and the one without lie around $A = 68$ and $A = 102$ where the simulation with isomers lead to notably lower abundances (Figure 18b), with 50–70 % lower abundance at $A = 68$ and $A = 102$ compared to the reference without isomers. On the other hand, there are peaks of higher abundance at $A = 69$ and $A = 103$ when compared to the case without isomers.

At the lighter peak, there is around 25 % higher abundance, while at the $A = 103$ peak there is around double the abundance of the reference simulation. At $A = 68$–69, there are two added isomers, $^{68\mathrm{m}}$Co and $^{69\mathrm{m}}$Ni, that potentially have altered the abundance distribution. As can be seen in Appendix A, the cobalt isomer $^{68\mathrm{m}}$Co has a half-life of 1.6 s compared to the ground state half-life of 0.2 s. In ^{69}Ni, the ground state has a longer half-life, $t_{1/2}(\mathrm{g.s.}) = 11.4$ s, while the isomer has $t_{1/2}(\mathrm{isom}) = 3.5$ s. Combining the differences in half-lives and in the neutron capture rates, the added isomers have an impact on the abundances 10^9 years after the merger leading to the r-process nucleosynthesis. Similarly, there are niobium isomers with $A = 100, 102,$ and 104, and a technetium isomer $^{102\mathrm{m}}$Tc, that have affected the abundances at $A = 102$–103. The niobium isomers have half-lives that are around 1/3 to 5 times the half-lives of the corresponding ground state. As such, the effect caused by differing half-lives of the niobium isomers might not be enough. Instead, $^{102\mathrm{m}}$Tc has a much longer half-life, $t_{1/2}(\mathrm{isom}) = 261$ s compared to the ground state half-life of 5.28 s. This may explain the double abundance peak at $A = 103$. Also the differences in neutron capture rates between the isomer and the ground state

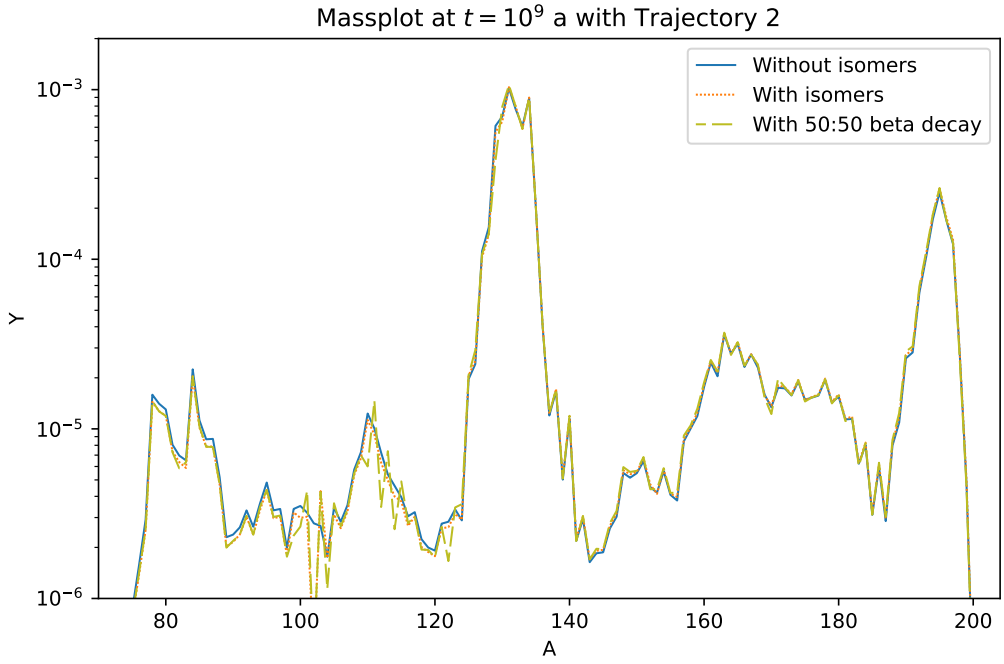

(a) Abundances at 1 Ga with Trajectory 2.

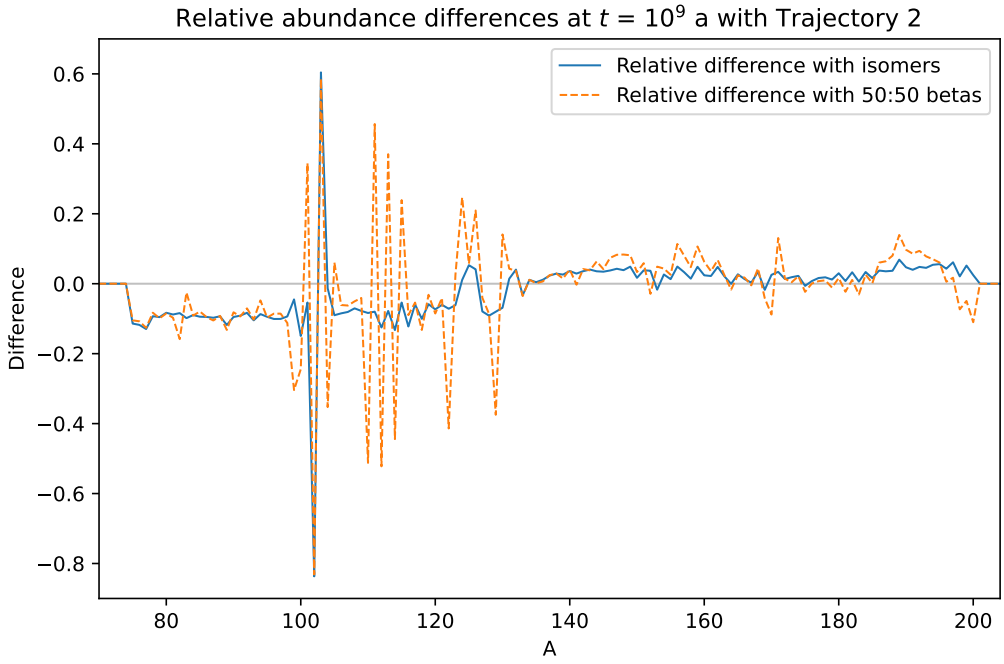

(b) Relative abundance differences compared to the reference at 1 Ga with Trajectory 2.

Figure 17. Abundances with and without isomers, and with isomers and 50:50 β branching ratio at 1 Ga are illustrated in Subfigure a. The corresponding relative abundance differences compared to the reference case without isomers are plotted in Subfigure b.

can affect the abundance maxima and minima locations as well.

Otherwise the abundance differences between the isomer simulation and the one without are quite small. With $A < 68$, abundances with isomers are slightly below the the abundances without isomers. Between the two peaks, the differences are minimal, with an exception at around $A = 75$–80, where the isomers increase the abundances by ≈ 10 % compared to the reference. With $A > 103$ abundances fell quickly, and only a small effect caused by the isomers can be seen in abundances.

Adding the 50:50 beta branching to isomer simulation leads again to a clear zigzag pattern in abundance differences around $A = 100$–120, as can be seen in Figure 18b. Similar behaviour can be observed with the simulation with isomers, but without the forced beta branching. However, the 50:50 multiplies the differences from less than 10 % to 50–70 %. As with the previous trajectories, this is caused by the several added isomers with $A = 100$–120. Another notable abundance peak, over 50 % higher abundance compared to the reference, is at $A = 101$ with the 50:50 beta branching. This is barely visible with isomers only. On the other hand, there is a slight underproduction of elements with $A = 99$ and $A = 100$ when the 50:50 beta branching is effective. There are a couple niobium isomers that probably are behind this. ^{98}Nb has a half-life of 2.86 s, while the isomer has $t_{1/2}(\text{isom}) = 3066$ s. The ground state of ^{99}Nb also has a short half-life compared to the half-life of the respective isomer, $t_{1/2}(\text{g.s.}) = 15.0$ and $t_{1/2}(\text{isom}) = 150$, as can be seen Appendix A. The longer half-lives lead to increased possibility to neutron capture reactions that shift the abundance maximum after the r-process. There are still neutrons remaining after the freeze-out, only the timescale of the neutron captures has become longer than the timescale of beta decays.

There are also a abundance minimum at $A = 71$ and a maximum a $A = 72$ with the forced beta branching which are not present in the reference simulation or in the simulation with isomers. There are a nickel and a zinc isomer ($^{71\text{m}}$Ni and ($^{71\text{m}}$Zn)) that have a matching mass number. However, of these two, the zinc isomer is a more probable culprit as the half-life of the isomer is around 10 times longer than the half-life of the ground state ($t_{1/2}(\text{isom}) = 1.493 \times 10^4$ and $t_{1/2}(\text{g.s.}) = 147$) s while with the nickel isomer the difference is around 0.2 s ($\approx 10\%$ of the half-life of the ground state). Apart from these differences, the abundance differences when compared to the reference are quite small, both with isomers only and with isomers and the 50:50 beta branching.

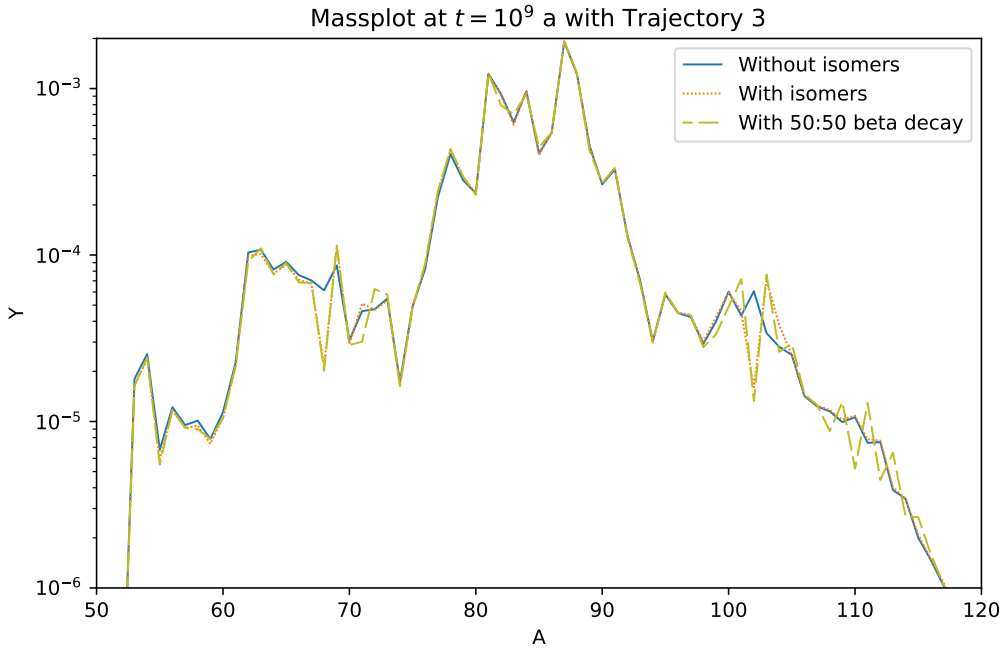

(a) Abundances at 1 Ga with Trajectory 3.

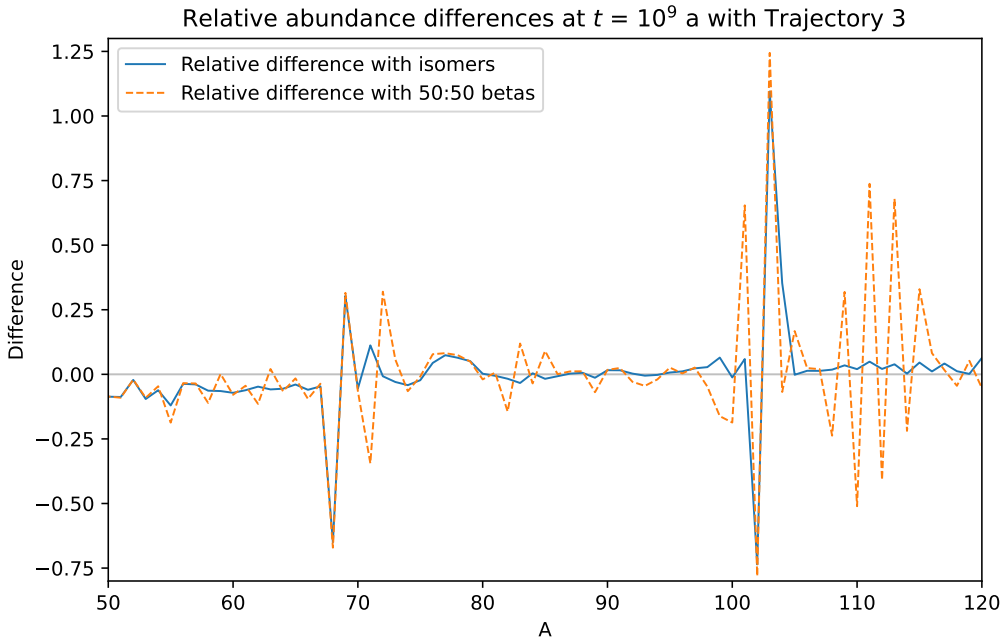

(b) Relative abundance differences compared to the reference at 1 Ga with Trajectory 3.

Figure 18. Abundances with and without isomers, and with isomers and 50:50 β branching ratio at 1 Ga are illustrated in Subfigure a. The corresponding relative abundance differences compared to the reference case without isomers are plotted in Subfigure b.

In Figure 19 the abundances with Trajectory 4 are illustrated with the relative differences compared to the reference abundances. Like Trajectory 3, this one does not produce the heaviest elements, instead the abundances rapidly drop around $A = 130$. On the other hand, there is a sharp rise in abundances at around $A = 82$. Compared to Trajectories 1 and 2, the r-process in this one advances further away from the neutron drip line, with abundance maximum never reaching $N \approx 100$.

The simulation with isomers does not differ a lot from the reference. There are three major differences at $A = 102, A = 103,$ and $A = 124$. Of these three, the one at $A = 102$ is the most notable, with 80 % less abundance with isomers than without. On the other hand, the adjacent mass number $A = 103$ has around 40 % greater abundance. The third notable abundance difference at $A = 124$ has around 40 % higher abundance with isomers than without. However, the abundance at $A = 124$ is around an order of magnitude smaller compared to the abundances at the two other difference maxima. Again, the differences at $A = 102$ and $A = 103$ can be explained with niobium isomers ^{100m}Nb, ^{102m}Nb, and ^{104m}Nb, and with the added technetium isomer ^{102m}Tc, similarly to the differences with Trajectory 3. The difference at $A = 124$ probably stems from the added indium and tin isomers ^{123m}In, ^{125m}In, ^{123m}Sn, and ^{125m}Sn. Of these, the tin isomers have several orders of magnitude shorter half-life than the ground state (^{123m}Sn: $t_{1/2}$(g.s.) $= 1.116 \times 10^7$ s, $t_{1/2}$(isom) = 2404 s, and ^{125m}Sn: $t_{1/2}$(g.s.) $= 8.324 \times 10^5$ s, $t_{1/2}$(isom) = 586 s). Along with difference in half-lives also the differences in neutron capture rates probably lead to observed abundance differences.

Adding the 50:50 beta branching changes the results somewhat. The same differences are present with the changed beta branching as they are without changes, although the drop in abundance at $A = 102$ is now lesser, around 50 % compared to the reference, and the adjacent abundance at $A = 103$ is now only around 15 % higher. There is another pair of abundance lows and highs at $A = 100$–101, with relative differences of around 15 % compared to the reference case. The niobium isomers ^{98m}Nb, ^{99m}Nb, and ^{100m}Nb are likely causing these differences, as especially with ^{98m}Nb and ^{99m}Nb, the half-lives of the respective ground states differ notably from the isomer half-lives. For example, $t_{1/2}(^{98}\text{Nb}) = 2.86$ s, and $t_{1/2}(^{98m}\text{Nb}) = 3066$ s. As with the other trajectories, there is again a zigzag pattern around $A = 110$–116, with relative differences ranging from -50 % to $+140$ % compared to the reference abundances. These differences are possibly due to rhodium, cadmium, and indium

isomers with similar mass numbers.

The abundance distribution of the simulation with Trajectory 5 (Figure 20) is similar to that of Trajectory 4. Abundances are slightly more widespread with Trajectory 5: the lightest have $A \approx 70$, and the heaviest $A \approx 132$. This can also be seen in the evolution snapshots in Figures 29 (Trajectory 4) and 30 (Trajectory 5), as the abundance maximum is at slightly heavier nuclides with Trajectory 5. The abundance maximum with Trajectory 5 is around $A = 80$–85, with somewhat lower abundances up to $A = 110$. There is an abundance minimum at around $A = 115$–125, where abundances are around two orders of magnitude lower than they are at the peak. There is a smaller peak around $A = 127$–129, with abundances about an order of magnitude greater than at the minimum.

Comparing the abundance differences with isomers reveals rather large differences at $A = 68$ and $A = 69$, with differences of nearly 100 % less abundance at $A = 68$, and around 80 % more at $A = 69$. However, one has to notice that the abundances at these mass numbers are at most 10^{-6}, so even a small change in absolute abundances can lead to a massive relative difference. This difference might be related to the isomers of ^{68}Co and ^{69}Ni, which have somewhat different half-lives than the respective ground states. The cobalt isomer has $t_{1/2}(\text{isom}) = 1.6$ s, while the ground state has $t_{1/2}(\text{g.s.}) = 0.2$ s. The nickel isomer has $t_{1/2}(\text{isom}) = 3.5$ s, while the ground state has $t_{1/2}(\text{g.s.}) = 11.4$ s. Different half-lives compiled to the differing neuron capture rates probably cause the abundance differences.

The other, and in this case more significant, difference occurs at $A = 102$–103. Similarly as with other trajectories, there is first an underproduction of elements with $A = 102$, but then an overproduction of elements with $A = 103$. Again, this can be explained by the niobium isomers $^{100\text{m}}$Nb, $^{102\text{m}}$Nb, and $^{104\text{m}}$Nb, and the added technetium isomer $^{102\text{m}}$Tc. There are also two smaller abundance differences in which isomers lead to greater abundance at $A = 125$–126, and at $A = 129$–131. These are relatively small differences, with around 15 % higher abundances with isomers. There are several indium, tin, and antimony isomers that have an effect on the abundances.

The 50:50 beta branching leads to very similar outcome as do the isomers alone. As with the other trajectories, there is a zigzag pattern in the relative abundance plot with Trajectory 5, as well. This occurs around $A = 110$–118. Possible isomers affecting this region are several rhodium, cadmium, and indium isomers. Of these, e.g. ^{115}Cd and its isomer have half-lives, $t_{1/2}(\text{g.s.}) = 1.925 \times 10^5$ s and $t_{1/2}(\text{isom}) = 3.850 \times 10^6$

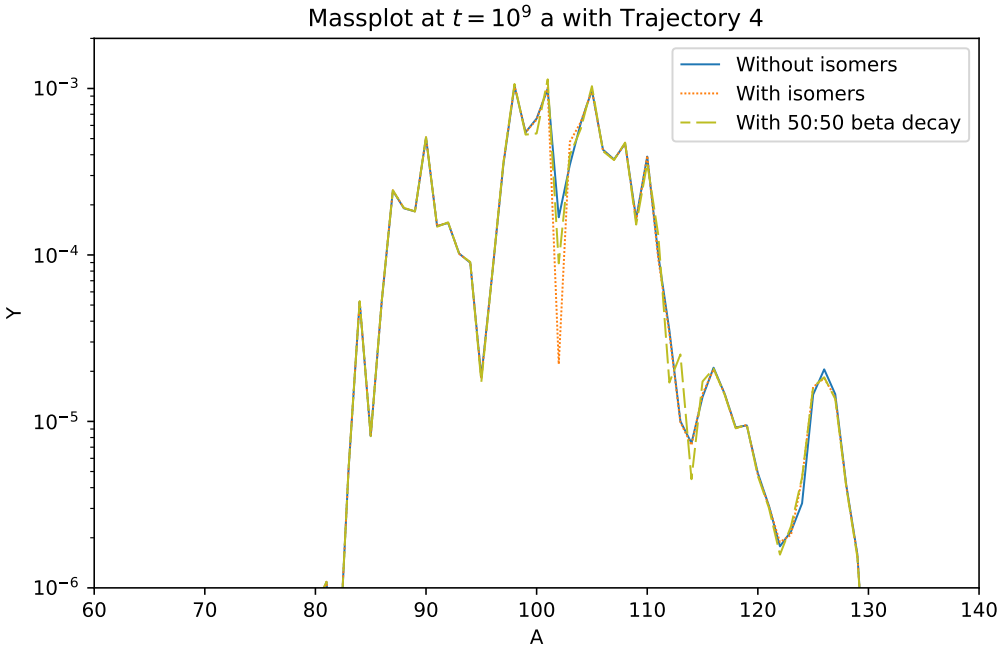

(a) Abundances at 1 Ga with Trajectory 4.

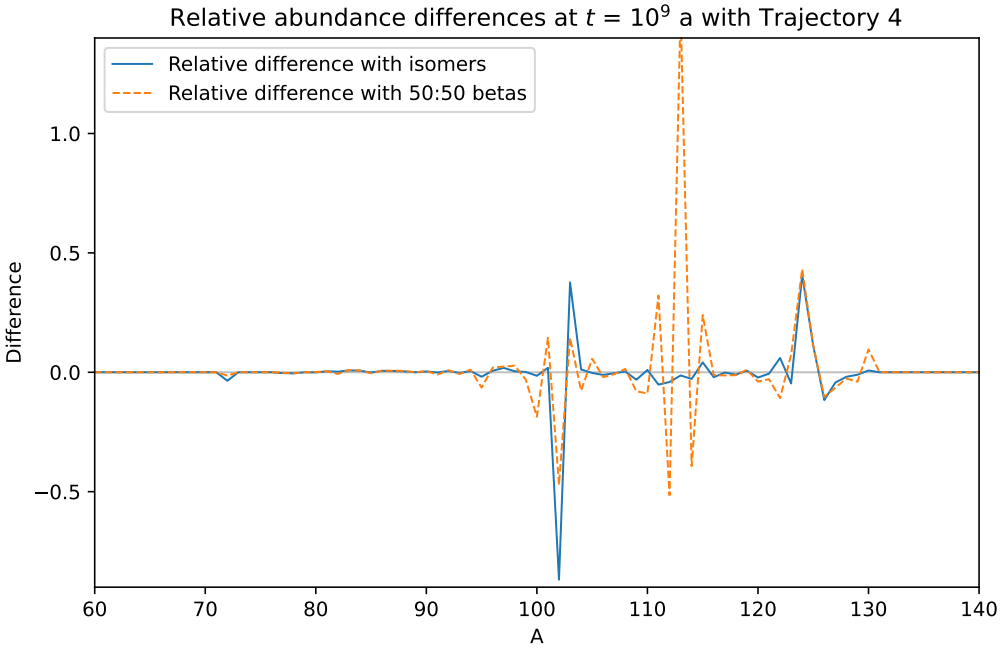

(b) Relative abundance differences compared to the reference at 1 Ga with Trajectory 4.

Figure 19. Abundances with and without isomers, and with isomers and 50:50 β branching ratio at 1 Ga are illustrated in Subfigure a. The corresponding relative abundance differences compared to the reference case without isomers are plotted in Subfigure b.

s, that could cause the observed abundance differences. Some differences not present with isomers only, can be found at $A = 100, 101$, and 104. These form a similar zigzag pattern in the relative abundances as is present at $A = 110$–118. The possible isomers affecting these are the niobium isomers with mass numbers ranging from $A = 98$ to $A = 104$. The included technetium isomer $^{102\mathrm{m}}$Tc might also affect these differences.

4.2 Heating during the first 1000 days

The total heating, or the energy released, was analysed by comparing the obtained results from the modified code to the baseline results without added isomers. As the time steps are slightly different between the unmodified and the modified simulations, interpolated values for heating were used with time values obtained with a Numpy function `numpy.logspace(-2,18,num=10000)` [164] which returns evenly spaced values on a log scale, in this case, 10000 values between 10^{-2} and 10^{18}. Interpolation of heating was done by using a Scipy function `scipy.interpolate.CubicSpline` [165] which returns a piecewise cubic polynomial that is twice continuously differentiable [166]. Interpolated values were then compared. As the r-process operates in a timescale of seconds, the heating during the first 1000 is mainly caused by decay reactions, especially by β^--decays. As such, the added isomers with different half-lives compared to the ground states cause differences in heating rate.

In the heating figures, the total heating rate $\dot{Q}_{\mathrm{tot}}$ is given in erg/s/g which is an often-used unit in astrophysics. It is given in the Gaussian centimetre-gram-second system of units (CGS), and one erg equals to 10^{-7} joules (= 100 nJ), or in MeV: 1 erg = 6.2415×10^5 MeV. [11] The values used in this section are taken from NUBASE2020 [17].

In Figure 21, the heating during the first 1000 days after the merger with Trajectory 1 can be seen. The decrease in heating during that time is over tenfold. The differences with and without isomers are barely visible in Figure 21a, but the relative heating difference graph in Figure 21b shows that during the first 10–100 seconds, the isomers increase the amount of heating by 5–8 %. However, during $t \approx 10^2$–10^5 s, the total heating is lower with isomers than it is without. The relative minimum of the heating with isomers occurs at around 300 seconds, when the difference is around -17 % when compared to the reference without isomers. During the rest of the 1000 days, the heating with isomers is slightly above the

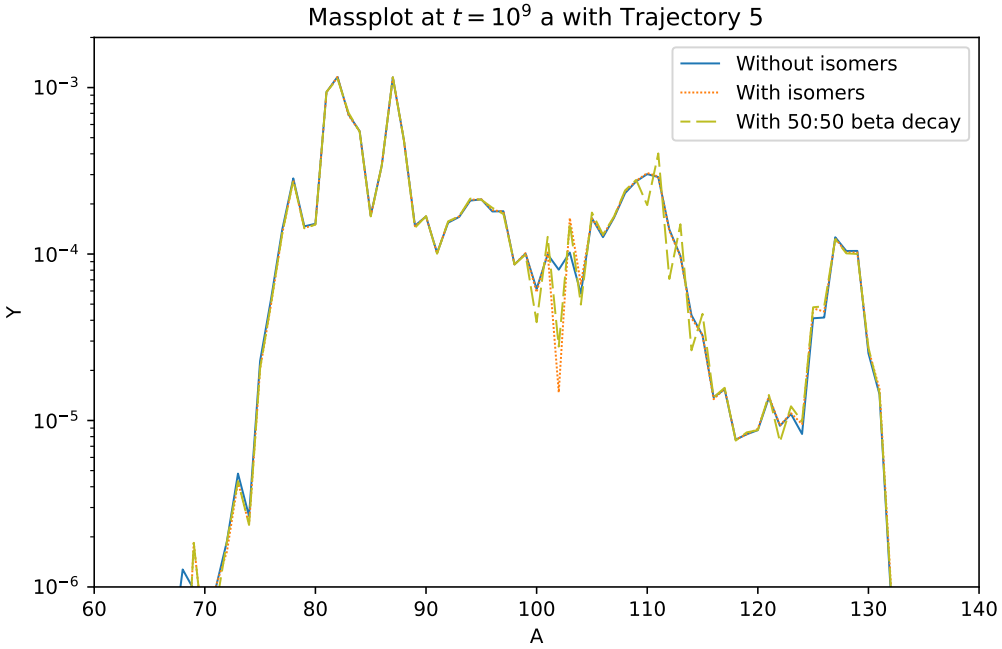

(a) Abundances at 1 Ga with Trajectory 5.

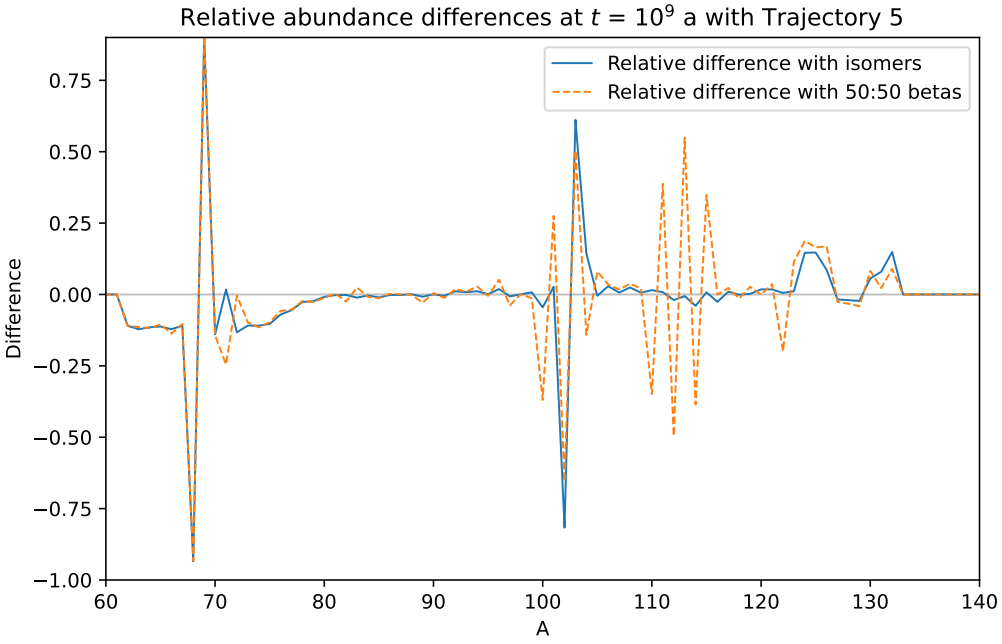

(b) Relative abundance differences compared to the reference at 1 Ga with Trajectory 5.

Figure 20. Abundances with and without isomers, and with isomers and 50:50 β branching ratio at 1 Ga are illustrated in Subfigure a. The corresponding relative abundance differences compared to the reference case without isomers are plotted in Subfigure b.

reference heating, by a few percent.

Unlike in the abundance differences, using the 50:50 beta branching does not cause drastic changes to the heating rate. The most important reason for heating differences are the differences in half-lives: with longer half-lives the energy released in β^--decay occurs during longer periods of time, and thus the heating is lower. On the other hand, the excitation energies of isomeric states are mostly rather low, a few hundred kiloelectronvolts (see Appendix A for E_{ex} values), so they do not balance the longer half-lives. Some of the added isomers do have short half-lives with $t_{1/2} \sim 1$ s. The relative heating minimum with isomers, which occurs around $t = 300$ s, is probably due to several isomers with half-lives longer and also shorter than the ground state half-lives of $\sim 10^2$–10^4 seconds, like $^{83\mathrm{m}}$Se ($t_{1/2} = 70.1$ s) and $^{166\mathrm{m}}$Ho ($t_{1/2} = 3.5718 \times 10^{10}$ s). The respective ground state half-lives are $t_{1/2}(^{83}\mathrm{Se}) = 1335$ s and $t_{1/2}(^{166}\mathrm{Ho}) = 9.6523 \times 10^4$ s. There is a nearly 10 % increase in heating compared to the reference case without isomers at $t \approx 10^7$ s. There are a few potential isomers, like $^{1115\mathrm{m}}$Cd with $t_{1/2} = 3.850 \times 10^6$ s, while the ground state has $t_{1/2}(^{115}\mathrm{Cd}) = 1.925 \times 10^5$. This is probably at least partially the reason, why the forced beta branching leads to increased heating at $t \approx 10^7$ s. Without the 50:50 branching, the isomeric states barely populate during the decay phase, as the nucleosynthesis with Trajectory 1 operates close to the neutron drip line, and the only way to populate the isomers near the stability is via beta decays.

Heating with Trajectory 2 with isomers differs a bit more from the reference than with Trajectory 1, as can be seen in Figure 22. The total decrease is slightly over tenfold. The relative differences (Figure 22b) with isomers range from -45 % to $+25$ % when compared to the reference without isomers. At first, during the first ≈ 200 seconds, the heating with isomers is higher than without. The relative minimum is again around $t \approx 300$ s, when the relative difference reaches -45 %. The outline is very similar to the one of Trajectory 1, only the relative differences are greater. After 10^5 seconds, the heating with isomers is around 5 % greater than it is without. With Trajectory 2, using the 50:50 beta branching does not change the heating rates a lot compared to the case with isomers. There is a slight increase in heating around $t = 10$–40 s, and a small decrease at $t \sim 10^4$. Otherwise, the heating rate of the simulation with isomers and with the 50:50 beta branching are basically identical, and there is no single isomer that would cause the differences. One example could be $^{130\mathrm{m}}$Sn with $t_{1/2} = 100$ s, compared to the ground state half-life of 223 s. When

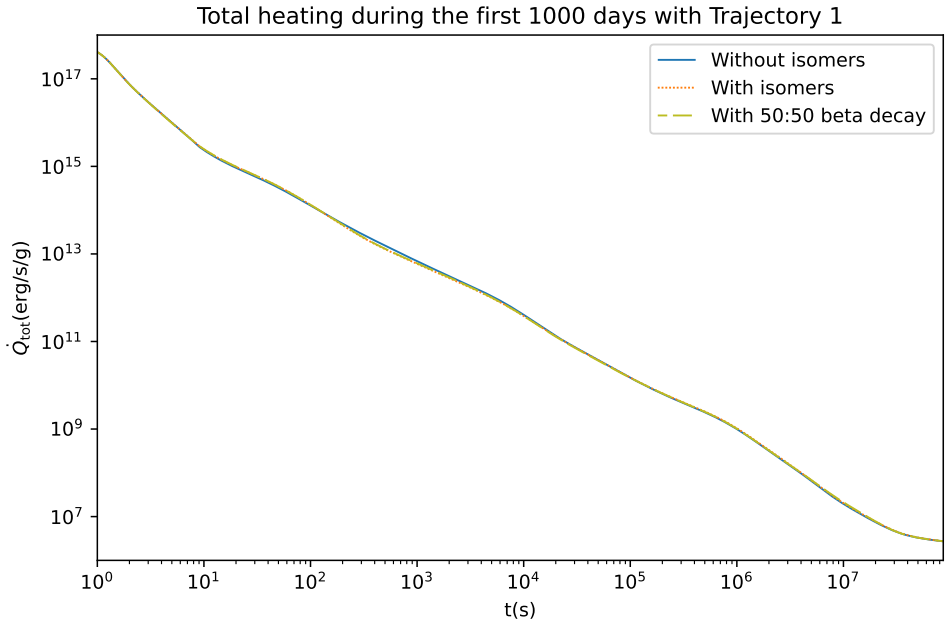

(a) Heating during the first 1000 days after the merger with Trajectory 1.

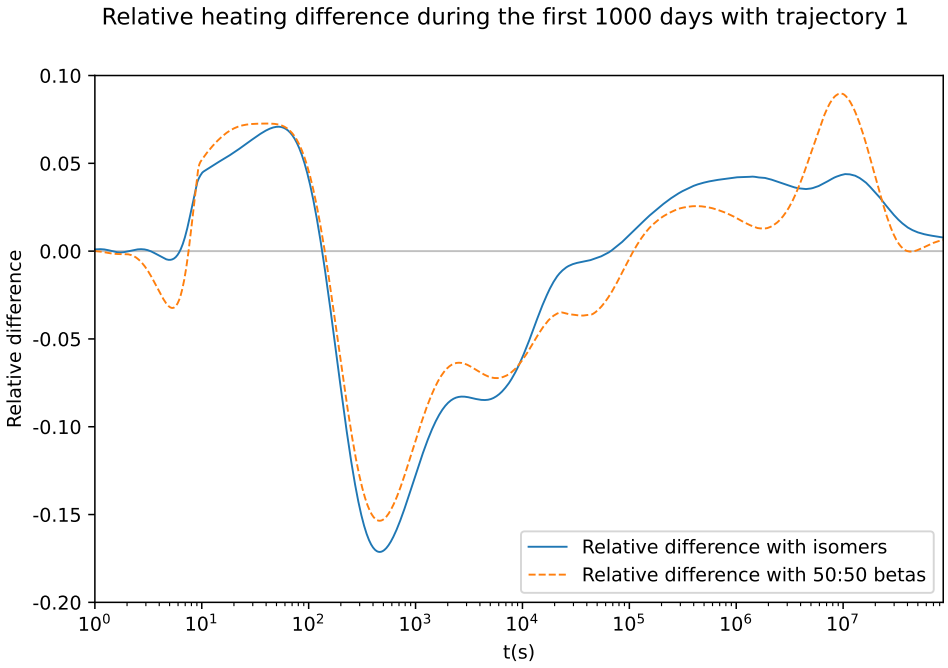

(b) Relative heating differences compared to the reference during the first 1000 days with Trajectory 1.

Figure 21. Heating with and without isomers, and with isomers and 50:50 β branching ratio during the first 1000 days are illustrated in Subfigure a. The corresponding relative heating differences compared to the reference case without isomers are plotted in Subfigure b.

comparing to the reference, the same observations hold as with Trajectory 1.

Heating with Trajectory 3 is depicted in Figure 23. The heating decreases from 10^{17} erg/s/g to 10^{6} erg/s/g. Again, the differences between different simulations are barely visible in Figure 23a. The relative differences in Figure 23b show around 30 % decrease in heating with isomers compared to the reference without isomers. There is also an increase of around 15 % during $t = 10$–500 s.As there are little elements heavier than $A = 120$ produced with Trajectory 3, there are no isomers with very long half-lives. Thus the differences between the later times heating are minimal. With the 50:50 beta branching the differences to the isomer case are rather small. This can be explained by the fact that most of the lighter elements, with $A < 120$, are relatively short lived (Appendix A). The noticeable drop in heating at $t \sim 10^3$ s is likely due to several isomers with shorter half-life than their respective ground state, like ^{83m}Se ($t_{1/2} = 70.1$ s) and ^{84m}Br ($t_{1/2} = 360$ s). The respective ground state values are ^{83}Se ($t_{1/2} = 1335$ s) and ^{84}Br ($t_{1/2} = 1906$ s).

The differences in heating are again barely visible with Trajectory 4 in Figure 24a, but the relative differences in Figure 24b show some variations. The heating rate decreases from 10^{17} erg/g/s to 10^{7} erg/g/s. The relative differences compared to the reference heating are quite small, within 10 % with isomers and within 15 % with the 50:50 beta branching. At $t \sim 10$ s and $t \sim 10^3$, the heating is slightly lower than in the reference heating without isomers. There are several isomers that are probably behind this decrease in heating, like ^{127}Sn, with $t_{1/2}$(g.s.) = 7560 s and ^{127m}Sn, with $t_{1/2}$(isom) = 248 s. At $t \approx 2 \times 10^6$ the heating with isomers is nearly 10 % higher than without. One potential isomer to affect this could be ^{115m}Cd ($t_{1/2}$(g.s.) $= 1.925 \times 10^5$ s, $t_{1/2}$(isom) $= 3.850 \times 10^6$ s. With the 50:50 beta branching there is a nearly 15 % greater heating at $t \sim 10^2$ s. This is likely due to the multiple added isomers with $t_{1/2} \sim 10^2$ s.

The total heating and the relative heating with respect to the reference heating with Trajectory 5 are shown in Figure 25. The heating decreases from $\sim 10^{17}$ erg/s/g to $\sim 10^{7}$ erg/s/g during the first 1000 days, similarly with the other trajectories. There is one notable drop in the relative heating that occurs both with isomers and with the 50:50 beta branching. The heating is around 30 % lower at $t \approx 2000$ s compared to the reference heating. This is at least partially due to the selenium and bromine isomers as was the case with Trajectory 3. On the other hand, at around $t \approx 100$ s, there is a relatively higher heating period, with ≈ 10 % higher heating

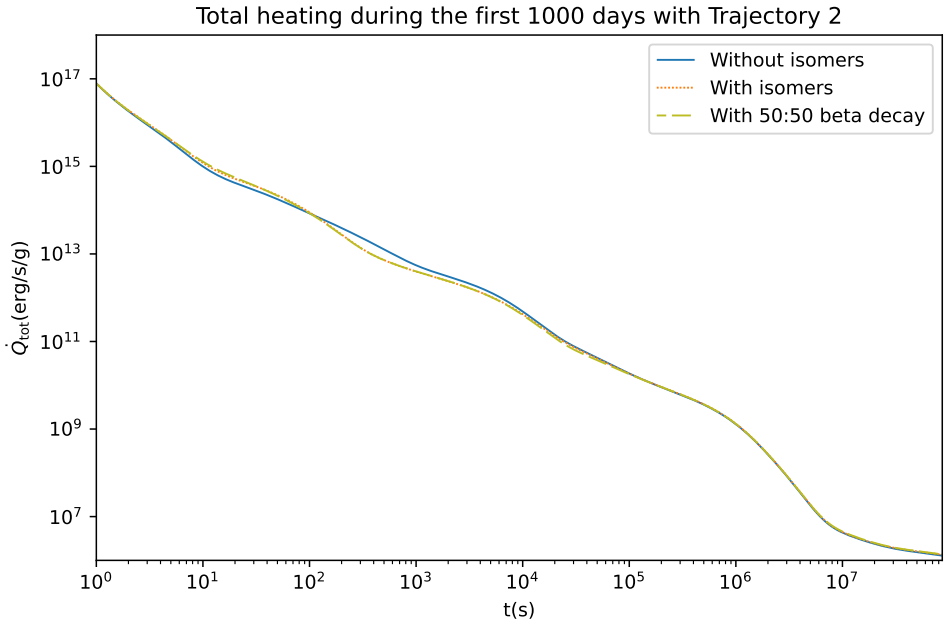

(a) Heating during the first 1000 days after the merger with Trajectory 2.

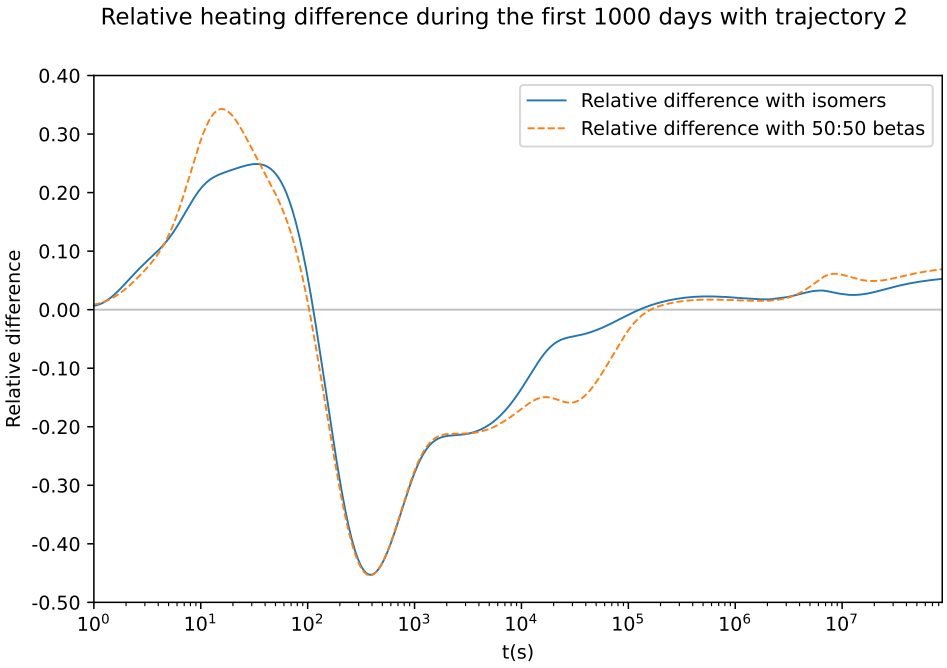

(b) Relative heating differences compared to the reference during the first 1000 days with Trajectory 2.

Figure 22. Heating with and without isomers, and with isomers and 50:50 β branching ratio during the first 1000 days are illustrated in Subfigure a. The corresponding relative heating differences compared to the reference case without isomers are plotted in Subfigure b.

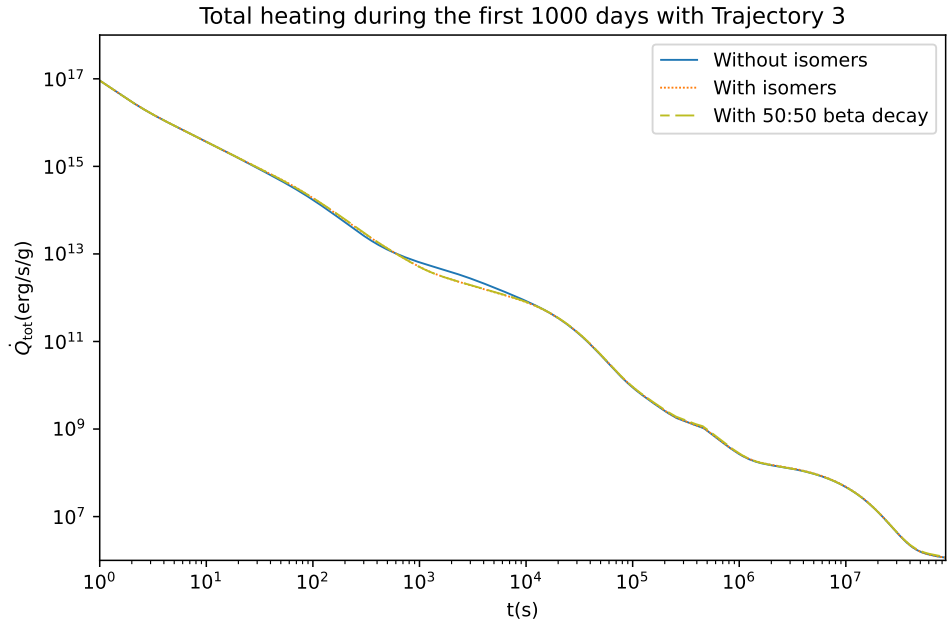

(a) Heating during the first 1000 days after the merger with Trajectory 3.

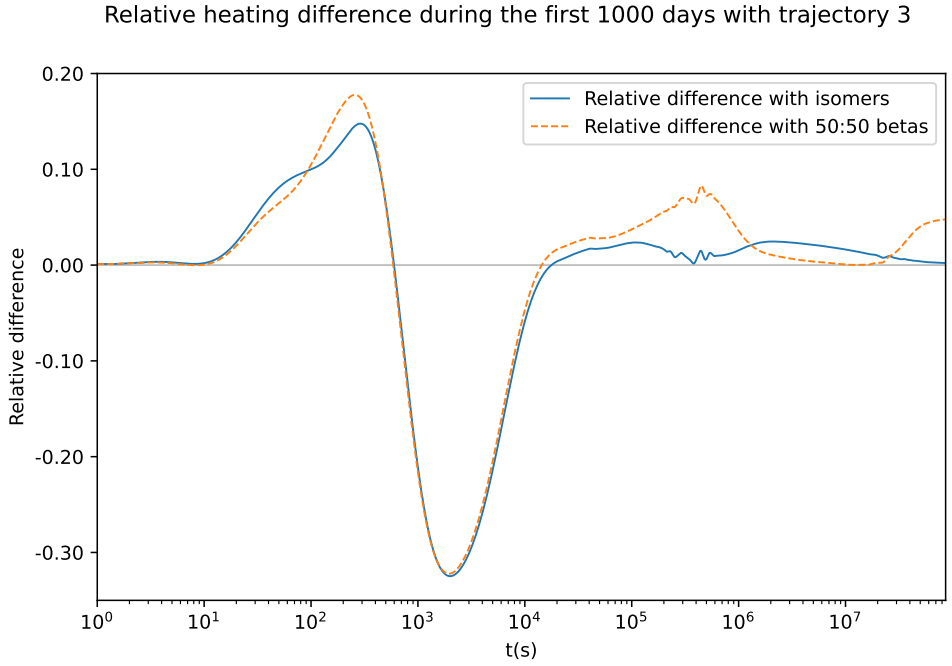

(b) Relative heating differences compared to the reference during the first 1000 days with Trajectory 3.

Figure 23. Heating with and without isomers, and with isomers and 50:50 β branching ratio during the first 1000 days are illustrated in Subfigure a. The corresponding relative heating differences compared to the reference case without isomers are plotted in Subfigure b.

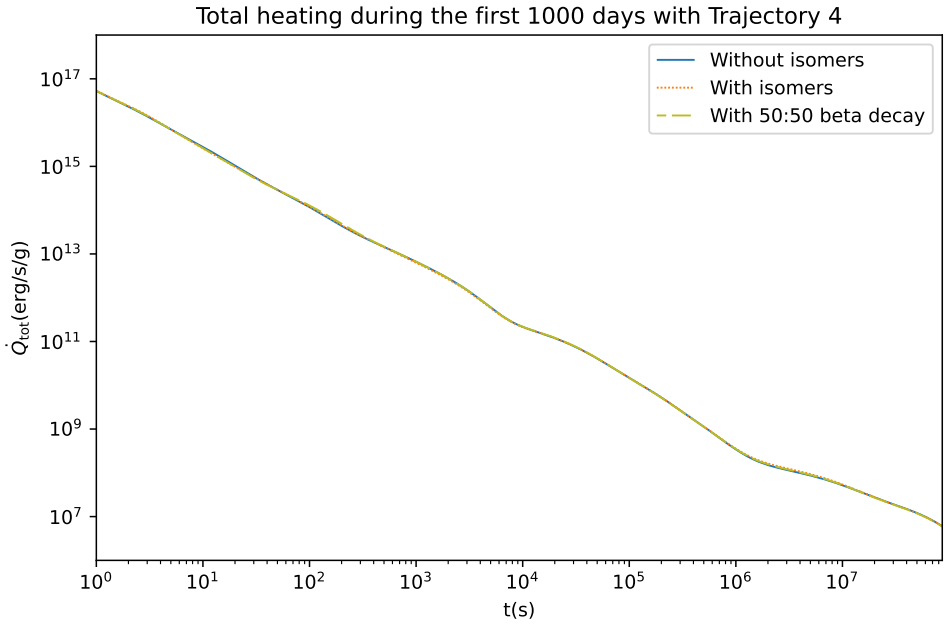

(a) Heating during the first 1000 days after the merger with Trajectory 4.

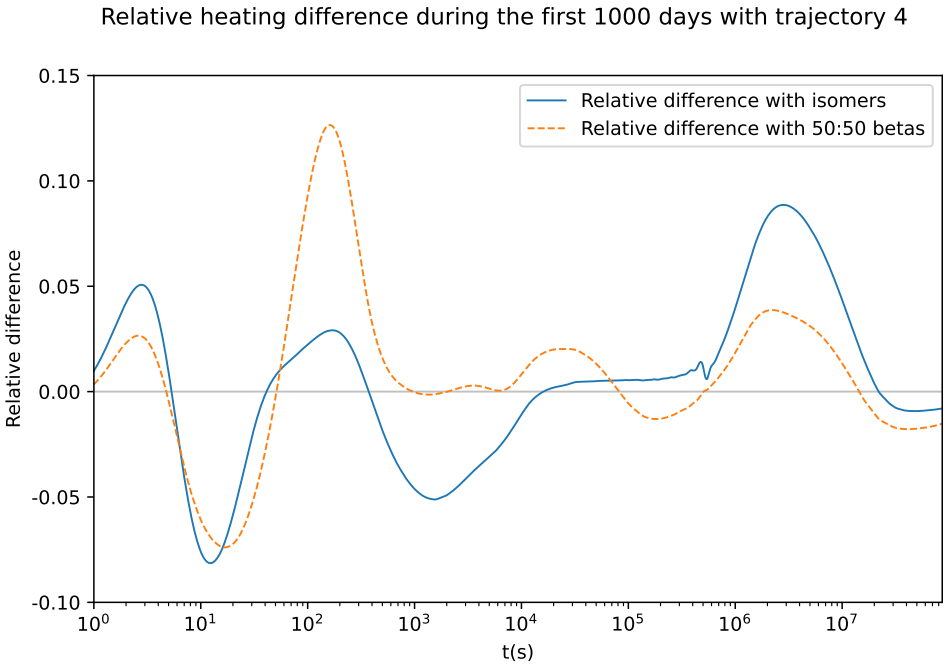

(b) Relative heating differences compared to the reference during the first 1000 days with Trajectory 4.

Figure 24. Heating with and without isomers, and with isomers and 50:50 β branching ratio during the first 1000 days are illustrated in Subfigure a. The corresponding relative heating differences compared to the reference case without isomers are plotted in Subfigure b.

compared to the reference. There are multiple isomers that may participate in heating during the first few hundred seconds. Also, at $t > 10^6$ s, the relative heating is slightly higher than the reference. For example, ^{115m}Cd with $t_{1/2} = 3.850 \times 10^6$ s is one of the isomers that has long enough half-life to affect heating after 100 days ($t \sim 10^6$). The 50:50 beta branching has a small, around 10 % decrease in heating compared to the reference at $t \approx 2 \times 10^5$ s. ^{115m}Cd is one possible isomer that is behind that decrease ($t_{1/2}$(g.s.) $= 1.925 \times 10^5, t_{1/2}$(isom) $= 3.850 \times 10^6$).

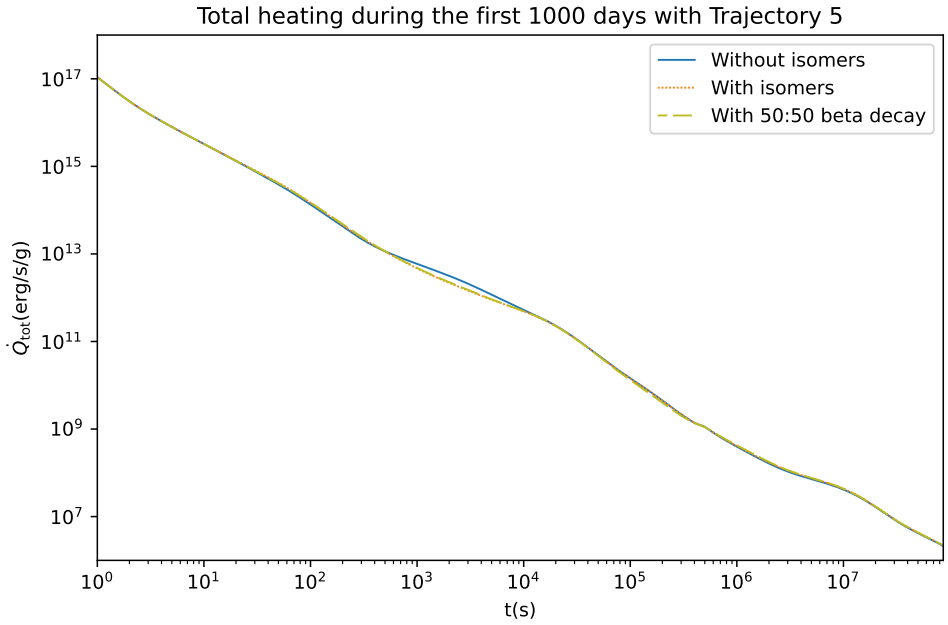

(a) Heating during the first 1000 days after the merger with Trajectory 5.

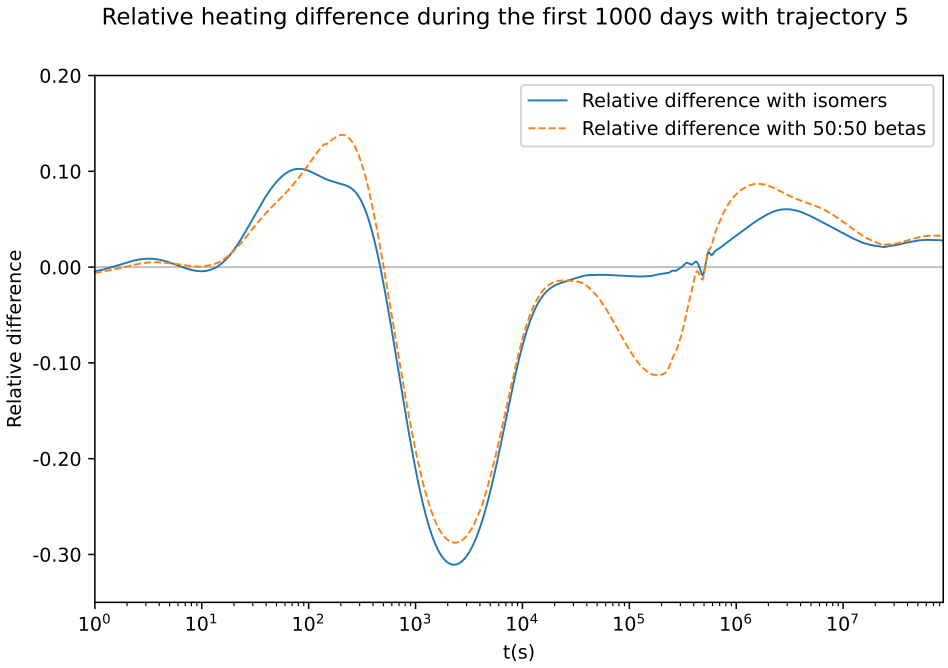

(b) Relative heating differences compared to the reference during the first 1000 days with Trajectory 5.

Figure 25. Heating with and without isomers, and with isomers and 50:50 β branching ratio during the first 1000 days are illustrated in Subfigure a. The corresponding relative heating differences compared to the reference case without isomers are plotted in Subfigure b.

5 Summary and outlook

The motivation behind this thesis was to include isomeric states in a wide scale to an r-process code as this has not been done before. The code used was a nuclear reaction network GSINet. The modified code with isomers was then tested with five different trajectories, and the results were compared to the results obtained from an unmodified code. A case with an artificial 50:50 β-branching to the ground state and an isomeric state was also investigated alongside the branching ratios from literature in order to enhance the effect of isomers in β-decays. Although the selection of added isomers is very limited compared to the list of the all known isomers (58 of 1938 listed in NUBASE2020), the obtained results were in line with the expected differences. This shows that the code can work with isomers, and the results give a glimpse of what might be the possible effects of nuclear isomers if they were used in a larger scale.

The obtained results show slight variations in abundances at one gigayear when compared to the unmodified results. In conclusion, the differences in abundances at different mass numbers were most prominent at those mass numbers that were part of or close to β-decay chains with isomeric states. Due to different half-lives and β-decay Q-values this behaviour was to be expected. Also the differing neutron capture rates during the r-process have affected the final abundances. Depending on the trajectory used, the effect of included isomers varied. For some trajectories, the r-process nucleosynthesis operated at lower mass numbers. As most of the included isomers have $A > 100$, the lightest trajectories and their associated nucleosynthesis never reached the region with the majority of isomers. This led to a smaller impact of isomers to the final abundances, as expected.

The total heating during the first 1000 days of r-process nucleosynthesis has slight differences between the simulation including isomers and the one without. Again, different trajectories affected the effect of isomers. Due to different, usually longer, half-lives in isomeric states, the heating after $t \sim 10^6 (\sim 100d)$ is, in general, slightly higher with isomers than without. On the other hand, there is usually a noticeable drop in the heating rate with isomers at some point, when compared to the reference

heating rate without isomers. This, of course, was to be expected due to differences in half-lives between isomers and the ground state. The differences in β^--decay Q-values have a little effect on the heating rate, as the excitation energies of the isomers are rather small.

The artificial 50:50 β-branching enhanced the effect of isomers in abundances, as it forced the decay to different branches that led to a new β-decay distribution. The collected literature values listed e.g. in AME2020 give decay branchings mainly completely to the ground state, ignoring the intermediate excitation levels. Using the ground states only in the daughter nucleus might not be very accurate in astrophysical conditions, as nuclei there are constantly excited and de-excited. This changes the population ratio of the ground an isomeric states. There are results indicating that decay rates may have different temperature dependency depending on the mass of a nucleus. [167] Having temperature dependent decay rates could improve the accuracy of the results. However, the relative differences in the heating rate, when compared to the reference heating without isomers, were rather similar between the simulation with isomers and the simulation with isomers and the 50:50 beta branching.

The most important improvement to the results obtained in this work would be the inclusion of (nearly) all of the known isomers. This, however, requires the handling of internal transitions in nuclei in the code as isomeric transitions are the main decay channel in most of the isomers. This would also make thermal transitions possible. Including the internal transitions would also enable proper research of possible astromers and their effects in the r-process nucleosynthesis. In the scope of this work, this was omitted as creating a whole new decay type would require creating new modules to the code, which was not easily achievable without excessive modifications.

Some minor updates and improvements can be done to the input files. They are partially outdated, for example, the ground states use AME2016 masses instead of masses from AME2020. While they are mostly unchanged in the stable and nearly stable isotopes, they may have significant changes in the least stable nuclei between t he different Atomic Mass Evaluations. Of course, these are limited to those isotopes that can be studied experimentally. FRDM has been used for the isotopes not available in Atomic Mass Evaluations. The partition functions used for isomers were also identical to the ground state partition functions. In order to get more accurate results, these should also be computed for isomers. G. W. Micsh

and M. R. Mumpower have listed in their article [168] isomers that have missing experimental data which would be needed for finding more potential astromers, and their effects. With many isomers, branching information for decay feeding from a parent nucleus is missing.

The Reaclib values used in the code could be updated as well, as the accuracy of reaction rates affect the outcome [27]. Also the neutron capture rates of isomeric states could be expanded to include rates for reaction ${}^{A-1}\mathrm{X} + \mathrm{n} \rightleftharpoons {}^{A}\mathrm{X}\cdot$ so that the isomeric states could be accessed also from an adjacent lighter isotope. Due to the data in the input files, the drip line is basically a straight line as the input files that have theoretical reaction and decay rates are calculated up to the assumed drip line. Using different models could lead to different outcomes, especially if the r-process advances near or at the neutron drip line. The accuracy of theoretical masses varies also between different mass models, and this is especially noticeable near the neutron drip line as the masses there are based on theoretical models. [29]

References

[1] A. S. Eddington. “The Internal Constitution of the Stars”. In: *Nature* 106.2653 (Sept. 1920), pp. 14–20. ISSN: 1476-4687. DOI: 10.1038/106014a0.

[2] H. A. Bethe and C. L. Critchfield. “The Formation of Deuterons by Proton Combination”. In: *Physical Review* 54 (4 Aug. 1938), pp. 248–254. DOI: 10.1103/PhysRev.54.248.

[3] F. von Weizsäcker. “Uber Elementumwandlungen im Innern der Sterne, II”. In: *Physikalische Zeitschrift* 39 (1938), pp. 633–646.

[4] H. A. Bethe. “Energy Production in Stars”. In: *Physical Review* 55 (5 Mar. 1939), pp. 434–456. DOI: 10.1103/PhysRev.55.434.

[5] F. Hoyle. “On Nuclear Reactions Occuring in Very Hot Stars.I. the Synthesis of Elements from Carbon to Nickel.” In: *The Astrophysical Journal Supplement Series* 1 (Sept. 1954), p. 121. DOI: 10.1086/190005.

[6] E. E. Salpeter. “Nuclear Reactions in Stars Without Hydrogen.” In: *Astrophysical Journal* 115 (Mar. 1952), pp. 326–328. DOI: 10.1086/145546.

[7] E. E. Salpeter. “A Generalist Looks Back”. In: *Annual Review of Astronomy and Astrophysics* 40.1 (2002), pp. 1–25. DOI: 10.1146/annurev.astro.40.060401.093901.

[8] R. A. Alpher, H. Bethe, and G. Gamow. “The Origin of Chemical Elements”. In: *Physical Review* 73 (7 Apr. 1948), pp. 803–804. DOI: 10.1103/PhysRev.73.803.

[9] F. Hoyle. “The Synthesis of the Elements from Hydrogen ⋆”. In: *Monthly Notices of the Royal Astronomical Society* 106.5 (Oct. 1946), pp. 343–383. ISSN: 0035-8711. DOI: 10.1093/mnras/106.5.343.

[10] E. M. Burbidge et al. “Synthesis of the Elements in Stars”. In: *Reviews of Modern Physics* 29 (4 Oct. 1957), pp. 547–650. DOI: 10.1103/RevModPhys.29.547.

[11] C. Iliadis. *Nuclear Physics of Stars*. Jan. 2007. ISBN: 9783527406029. DOI: 10.1002/9783527618750.ch4.

[12] A. Arcones and F.-K. Thielemann. "Origin of the elements". In: *The Astronomy and Astrophysics Review* 31.1 (Dec. 2022), p. 1. ISSN: 1432-0754. DOI: 10.1007/s00159-022-00146-x.

[13] R. Shurtleff and E. Derringh. "The most tightly bound nucleus". In: *American Journal of Physics* 57 (June 1989), pp. 552–552. DOI: 10.1119/1.15970.

[14] M. P. Fewell. "The atomic nuclide with the highest mean binding energy". In: *American Journal of Physics* 63.7 (July 1995), pp. 653–658. ISSN: 0002-9505. DOI: 10.1119/1.17828.

[15] C. Fröhlich et al. "Neutrino-Induced Nucleosynthesis of A > 64 Nuclei: The νp Process". In: *Physical Review Letters* 96 (14 Apr. 2006), p. 142502. DOI: 10.1103/PhysRevLett.96.142502.

[16] S. E. Woosley et al. "The ν-Process". In: *Astrophysical Journal* 356 (June 1990), p. 272. DOI: 10.1086/168839.

[17] M. Wang et al. "The AME 2020 atomic mass evaluation (II). Tables, graphs and references*". In: *Chinese Physics C* 45.3 (Mar. 2021), p. 030003. DOI: 10.1088/1674-1137/abddaf.

[18] B. Abbott et al. "GW170817: Observation of Gravitational Waves from a Binary Neutron Star Inspiral". In: *Physical Review Letters* 119.16 (Oct. 2017). DOI: 10.1103/physrevlett.119.161101.

[19] B. P. Abbott et al. "Gravitational Waves and Gamma-Rays from a Binary Neutron Star Merger: GW170817 and GRB 170817A". In: *The Astrophysical Journal* 848.2 (Oct. 2017), p. L13. DOI: 10.3847/2041-8213/aa920c.

[20] B. Margalit and B. D. Metzger. "Constraining the Maximum Mass of Neutron Stars from Multi-messenger Observations of GW170817". In: *The Astrophysical Journal* 850.2 (Nov. 2017), p. L19. DOI: 10.3847/2041-8213/aa991c.

[21] B. P. Abbott et al. "Multi-messenger Observations of a Binary Neutron Star Merger". In: *The Astrophysical Journal* 848.2 (Oct. 2017), p. L12. DOI: 10.3847/2041-8213/aa91c9.

[22] L.-X. Li and B. Paczyski. "Transient Events from Neutron Star Mergers". In: *The Astrophysical Journal* 507.1 (Nov. 1998), pp. L59–L62. ISSN: 0004-637X. DOI: 10.1086/311680.

[23] I. Arcavi et al. "Optical emission from a kilonova following a gravitational-wave-detected neutron-star merger". In: *Nature* 551.7678 (Nov. 2017), pp. 64–66. ISSN: 1476-4687. DOI: 10.1038/nature24291.

[24] E. Pian et al. "Spectroscopic identification of r-process nucleosynthesis in a double neutron-star merger". In: *Nature* 551.7678 (Nov. 2017), pp. 67–70. ISSN: 1476-4687. DOI: 10.1038/nature24298.

[25] S. J. Smartt et al. "A kilonova as the electromagnetic counterpart to a gravitational-wave source". In: *Nature* 551.7678 (Nov. 2017), pp. 75–79. ISSN: 1476-4687. DOI: 10.1038/nature24303.

[26] F.-K. Thielemann et al. "What are the astrophysical sites for the r-process and the production of heavy elements?" In: *Progress in Particle and Nuclear Physics* 66.2 (2011). Particle and Nuclear Astrophysics, pp. 346–353. ISSN: 0146-6410. DOI: https://doi.org/10.1016/j.ppnp.2011.01.032.

[27] G. W. Misch et al. "Astromers: Nuclear Isomers in Astrophysics". In: *The Astrophysical Journal Supplement Series* 252.1 (Dec. 2020), p. 2. DOI: 10.3847/1538-4365/abc41d.

[28] G. W. Misch, T. M. Sprouse, and M. R. Mumpower. "Astromers in the Radioactive Decay of r-process Nuclei". In: *The Astrophysical Journal Letters* 913.1 (May 2021), p. L2. DOI: 10.3847/2041-8213/abfb74.

[29] M. Arnould, S. Goriely, and K. Takahashi. "The r-process of stellar nucleosynthesis: Astrophysics and nuclear physics achievements and mysteries". In: *Physics Reports* 450.4-6 (Sept. 2007), pp. 97–213. DOI: 10.1016/j.physrep.2007.06.002.

[30] T. Rauscher. *Essentials of Nucleosynthesis and Theoretical Nuclear Astrophysics*. 2514-3433. IOP Publishing, 2020. ISBN: 978-0-7503-1149-6. DOI: 10.1088/2514-3433/ab8737.

[31] C. Freiburghaus et al. “The Astrophysical r-Process: A Comparison of Calculations following Adiabatic Expansion with Classical Calculations Based on Neutron Densities and Temperatures”. In: *The Astrophysical Journal* 516.1 (May 1999), p. 381. DOI: 10.1086/307072.

[32] T. A. Thompson, A. Burrows, and B. S. Meyer. “The Physics of Proto-Neutron Star Winds: Implications for r-Process Nucleosynthesis”. In: *The Astrophysical Journal* 562.2 (Dec. 2001), pp. 887–908. DOI: 10.1086/323861.

[33] K. Farouqi et al. “Neutron captures and the r-process”. In: *AIP Conference Proceedings* 819.1 (Mar. 2006), pp. 419–422. ISSN: 0094-243X. DOI: 10.1063/1.2187894.

[34] F. Käppeler et al. “Time-Scales of the s Process: from Minutes to Ages”. In: *Publications of the Astronomical Society of Australia* 26.3 (2009), pp. 209–216. DOI: 10.1071/as08052.

[35] M. Wang et al. “The AME2012 atomic mass evaluation (II). Tables, graphs and references”. In: *Chinese Physiscs C* 36 (2012), p. 1603.

[36] F. Kappeler, H. Beer, and K. Wisshak. “s-process nucleosynthesis-nuclear physics and the classical model”. In: *Reports on Progress in Physics* 52.8 (Aug. 1989), p. 945. DOI: 10.1088/0034-4885/52/8/002.

[37] J. J. Cowan et al. “Origin of the heaviest elements: The rapid neutron-capture process”. In: *Reviews of Modern Physics* 93.1 (Feb. 2021). DOI: 10.1103/revmodphys.93.015002.

[38] G. Martínez-Pinedo and K. Langanke. “Nuclear quests for the r-process”. In: *The European Physical Journal A* 59.4 (Apr. 2023), p. 67. ISSN: 1434-601X. DOI: 10.1140/epja/s10050-023-00987-9.

[39] M. Reichert et al. *The nuclear reaction network WinNet*. 2023. arXiv: 2305.07048 [astro-ph.IM].

[40] A. I. Chugunov, H. E. DeWitt, and D. G. Yakovlev. “Coulomb tunneling for fusion reactions in dense matter: Path integral Monte Carlo versus mean field”. In: *Physical Review D* 76.2 (July 2007). DOI: 10.1103/physrevd.76.025028.

[41] W. Hix and F.-K. Thielemann. “Computational methods for nucleosynthesis and nuclear energy generation”. In: *Journal of Computational and Applied Mathematics* 109.1 (1999), pp. 321–351. ISSN: 0377-0427. DOI: https://doi.org/10.1016/S0377-0427(99)00163-6.

[42] M. D. Delano and A. G. W. Cameron. “Nucleosynthesis in neutron rich supernova ejecta”. In: *Astrophysics and Space Science* 10 (1971), pp. 203–226. DOI: 10.1007/BF00704083.

[43] F.-K. Thielemann et al. “Neutron Star Mergers and Nucleosynthesis of Heavy Elements”. In: *Annual Review of Nuclear and Particle Science* 67.1 (Oct. 2017), pp. 253–274. DOI: 10.1146/annurev-nucl-101916-123246.

[44] S. E. Woosley and R. D. Hoffman. “The α-Process and the r-Process”. In: *Astrophysical Journal* 395 (Aug. 1992), p. 202. DOI: 10.1086/171644.

[45] L. F. Roberts, S. E. Woosley, and R. D. Hoffman. “Integrated nucleosynthesis in neutrino-driven winds”. In: *The Astrophysical Journal* 722.1 (Sept. 2010), pp. 954–967. DOI: 10.1088/0004-637x/722/1/954.

[46] K. Farouqi et al. “Charged-particle and neutron-capture processes in the high-entropy wind of core-collapse supernovae”. In: *The Astrophysical Journal* 712.2 (Mar. 2010), p. 1359. DOI: 10.1088/0004-637X/712/2/1359.

[47] J. Lippuner and L. F. Roberts. “r-process lanthanide production and heating rates in kilonovae”. In: *The Astrophysical Journal* 815.2 (Dec. 2015), p. 82. DOI: 10.1088/0004-637x/815/2/82.

[48] J. Görres, M. Wiescher, and F. K. Thielemann. “Bridging the waiting points: The role of two-proton capture reactions in the *rp* process”. In: *Physical Review C Nuclear Physics* 51.1 (Jan. 1995), pp. 392–400.

[49] F.-K. Thielemann et al. “Massive Stars and Their Supernovae”. In: *Astronomy with Radioactivities*. Ed. by R. Diehl, D. H. Hartmann, and N. Prantzos. Berlin, Heidelberg: Springer Berlin Heidelberg, 2011, pp. 153–231. ISBN: 978-3-642-12698-7. DOI: 10.1007/978-3-642-12698-7_4.

[50] M. Wiescher and T. Rauscher. “Nuclear Reactions”. In: *Astronomy with Radioactivities*. Ed. by R. Diehl, D. H. Hartmann, and N. Prantzos. Berlin, Heidelberg: Springer Berlin Heidelberg, 2011, pp. 461–489. ISBN: 978-3-642-12698-7. DOI: 10.1007/978-3-642-12698-7_9.

[51] "Differential and Difference Equations". In: *Numerical Methods for Ordinary Differential Equations*. John Wiley & Sons, Ltd, 2016. Chap. 1, pp. 1–53. ISBN: 9781119121534. DOI: https://doi.org/10.1002/9781119121534.ch1.

[52] F. Kondev et al. "The NUBASE2020 evaluation of nuclear physics properties *". In: *Chinese Physics C* 45.3 (Mar. 2021), p. 030001. DOI: 10.1088/1674-1137/abddae.

[53] A. G. W. Cameron, J. J. Cowan, and J. W. Truran. "The Waiting Point Approximation in R-Process Calculations". In: *Astrophysics and Space Science* 91.2 (Apr. 1983), pp. 235–243. DOI: 10.1007/BF00656112.

[54] S. Shibagaki et al. "Relative Contributions of the Weak, Main, and Fission-recycling r-process". In: *The Astrophysical Journal* 816.2 (Jan. 2016), p. 79. DOI: 10.3847/0004-637X/816/2/79.

[55] S. Goriely et al. "The r-process nucleosynthesis during the decompression of neutron star crust material". In: *Journal of Physics: Conference Series* 665.1 (Jan. 2016), p. 012052. DOI: 10.1088/1742-6596/665/1/012052.

[56] P. Walker and J. Carroll. "Feature Article: Nuclear Isomers: Recipes from the Past and Ingredients for the Future". In: *Nuclear Physics News* 17 (June 2007), pp. 11–15. DOI: 10.1080/10506890701404206.

[57] K.-L. Kratz. "Measurements of r-process nuclei". In: *Nuclear Physics A* 688.1-2 (May 2001), pp. 308–317. DOI: 10.1016/s0375-9474(01)00719-9.

[58] R. Surman et al. "Source of the Rare-Earth Element Peak in r-Process Nucleosynthesis". In: *Physical Review Letters* 79 (1997), pp. 1809–1812. DOI: 10.1103/PhysRevLett.79.1809.

[59] M. Eichler et al. "The Role of Fission in Neutron Star Mergers and its Impact on the r-Process Peaks". In: *The Astrophysical Journal* 808.1 (July 2015), p. 30. DOI: 10.1088/0004-637X/808/1/30.

[60] S. Goriely et al. "New Fission Fragment Distributions and r-Process Origin of the Rare-Earth Elements". In: *Physical Review Letters* 111.24 (Dec. 2013). DOI: 10.1103/physrevlett.111.242502.

[61] J. de Jesús Mendoza-Temis et al. "Nuclear robustness of the r process in neutron-star mergers". In: *Physical Review C* 92.5 (Nov. 2015). DOI: 10.1103/physrevc.92.055805.

[62] S. A. Giuliani et al. “Fission and the r-process nucleosynthesis of translead nuclei in neutron star mergers”. In: *Physical Review C* 102.4 (Oct. 2020). DOI: 10.1103/physrevc.102.045804.

[63] S. Goriely and G. Martínez Pinedo. “The production of transuranium elements by the r-process nucleosynthesis”. In: *Nuclear Physics A* 944 (Dec. 2015), pp. 158–176. DOI: 10.1016/j.nuclphysa.2015.07.020.

[64] S. Nikas, G. M. Pinedo, and A. Sieverding. “The creation of the first r-process peak elements; effects of beta decay rates and nuclear masses”. In: *Journal of Physics: Conference Series* 1668.1 (Oct. 2020), p. 012029. DOI: 10.1088/1742-6596/1668/1/012029.

[65] K. Lodders. “Relative Atomic Solar System Abundances, Mass Fractions, and Atomic Masses of the Elements and Their Isotopes, Composition of the Solar Photosphere, and Compositions of the Major Chondritic Meteorite Groups”. In: *Space Science Reviews* 217.3 (Apr. 2021), p. 44. ISSN: 1572-9672. DOI: 10.1007/s11214-021-00825-8.

[66] A. Arcones and G. Martínez-Pinedo. “Dynamical r-process studies within the neutrino-driven wind scenario and its sensitivity to the nuclear physics input”. In: *Physical Review C* 83.4 (Apr. 2011). DOI: 10.1103/physrevc.83.045809.

[67] S. Wanajo. “Cold r-Process in Neutrino-driven Winds”. In: *The Astrophysical Journal* 666.2 (Aug. 2007), pp. L77–L80. DOI: 10.1086/521724.

[68] B. D. Metzger et al. “Neutron-powered precursors of kilonovae”. In: *Monthly Notices of the Royal Astronomical Society* 446.1 (Nov. 2014), pp. 1115–1120. ISSN: 0035-8711. DOI: 10.1093/mnras/stu2225.

[69] S. Honda et al. “Neutron-Capture Elements in the Very Metal Poor Star HD 122563”. In: *The Astrophysical Journal* 643.2 (June 2006), pp. 1180–1189. DOI: 10.1086/503195.

[70] J. J. Cowan and C. Sneden. “Heavy element synthesis in the oldest stars and the early Universe”. In: *Nature* 440.7088 (Apr. 2006), pp. 1151–1156.

[71] R. Surman et al. “Sensitivity studies for the weak r process: neutron capture rates”. In: *AIP Advances* 4.4 (Feb. 2014). 041008. ISSN: 2158-3226. DOI: 10.1063/1.4867191.

[72] K. Maeda. “Stellar Evolution, Sn Explosion, and Nucleosynthesis”. In: *Handbook of X-ray and Gamma-ray Astrophysics*. Springer Nature Singapore, Nov. 2022, pp. 1–41. DOI: 10.1007/978-981-16-4544-0_85-1.

[73] H. A. Bethe and J. R. Wilson. “Revival of a stalled supernova shock by neutrino heating”. In: *Astrophysical Journal* 295 (Aug. 1985), pp. 14–23. DOI: 10.1086/163343.

[74] Akram, Waheed et al. “Nucleosynthesis of light trans-Fe isotopes in ccSNe: Implications from presolar SiC-X grains”. In: *EPJ Web of Conferences* 227 (2020), p. 01009. DOI: 10.1051/epjconf/202022701009.

[75] A. Arcones and F. Montes. “Production of Light-element Primary Process Nuclei in Neutrino-driven Winds”. In: *The Astrophysical Journal* 731.1 (Mar. 2011), p. 5. DOI: 10.1088/0004-637X/731/1/5.

[76] L. F. Roberts. “A New Code for Proto-Neutron Star Evolution”. In: *The Astrophysical Journal* 755.2 (Aug. 2012), p. 126. DOI: 10.1088/0004-637X/755/2/126.

[77] T. Fischer et al. “Neutrino signal from proto-neutron star evolution: Effects of opacities from charged-currentneutrino interactions and inverse neutron decay”. In: *Physical Review C* 101.2 (Feb. 2020). DOI: 10.1103/physrevc.101.025804.

[78] A. Mirizzi et al. “Supernova neutrinos: production, oscillations and detection”. In: *La Rivista del Nuovo Cimento* 39.1 (Jan. 2016), pp. 1–112. ISSN: 1826-9850. DOI: 10.1393/ncr/i2016-10120-8.

[79] M. Eichler et al. “Nucleosynthesis in 2D core-collapse supernovae of 11.2 and 17.0 $M_\odot$ progenitors: implications for Mo and Ru production”. In: *Journal of Physics G: Nuclear and Particle Physics* 45.1 (Dec. 2017), p. 014001. DOI: 10.1088/1361-6471/aa8891.

[80] S. Jones, R. Hirschi, and K. Nomoto. “The Final Fate of Stars that Ignite Neon and Oxygen Off-center: Electron Capture or Iron Core-collapse Supernova?” In: *The Astrophysical Journal* 797.2 (Dec. 2014), p. 83. DOI: 10.1088/0004-637X/797/2/83.

[81] S. Wanajo, H.-T. Janka, and B. Müller. "Electron-capture supernovae as the origin of elements beyond iron". In: *The Astrophysical Journal Letters* 726.2 (Dec. 2010), p. L15. DOI: 10.1088/2041-8205/726/2/L15.

[82] Jones, S. et al. "Do electron-capture supernovae make neutron stars? - First multidimensional hydrodynamic simulations of the oxygen deflagration". In: *Astronomy & Astrophysics* 593 (2016), A72. DOI: 10.1051/0004-6361/201628321.

[83] O. S. Kirsebom et al. "Discovery of an Exceptionally Strong β-Decay Transition of ^{20}F and Implications for the Fate of Intermediate-Mass Stars". In: *Physical Review Letters* 123 (26 Dec. 2019), p. 262701. DOI: 10.1103/PhysRevLett.123.262701.

[84] P. Banerjee et al. "Neutrino-Induced Nucleosynthesis in Helium Shells of Early Core-Collapse Supernovae". In: *EPJ Web of Conferences* 109 (2016). Ed. by W.-P. Liu et al., p. 06001. DOI: 10.1051/epjconf/201610906001.

[85] I. Sagert et al. "Signals of the QCD Phase Transition in Core-Collapse Supernovae". In: *Physical Review Letters* 102 (8 Feb. 2009), p. 081101. DOI: 10.1103/PhysRevLett.102.081101.

[86] T. Fischer et al. "Core-collapse supernova explosions triggered by a quark-hadron phase transition during the early post-bounce phase". In: *The Astrophysical Journal Supplement Series* 194.2 (May 2011), p. 39. DOI: 10.1088/0067-0049/194/2/39.

[87] T. Fischer et al. "Core-collapse Supernova Explosions Driven by the Hadron-quark Phase Transition as a Rare r-process Site". In: *The Astrophysical Journal* 894.1 (Apr. 2020), p. 9. DOI: 10.3847/1538-4357/ab86b0.

[88] V. M. Kaspi and A. M. Beloborodov. "Magnetars". In: *Annual Review of Astronomy and Astrophysics* 55.1 (Aug. 2017), pp. 261–301. DOI: 10.1146/annurev-astro-081915-023329.

[89] E. M. D. Symbalisty, D. N. Schramm, and J. R. Wilson. "An expanding vortex site for the r-process in rotating stellar collapse". In: *The Astrophysical Journal Letters* 291 (Apr. 1985), pp. L11–L14. DOI: 10.1086/184448.

[90] J. Greiner et al. “A very luminous magnetar-powered supernova associated with an ultra-long γ-ray burst”. In: *Nature* 523.7559 (July 2015), pp. 189–192. DOI: 10.1038/nature14579.

[91] C. Winteler et al. “Magnetorotationally driven Supernovae as the origin of early galaxy r-process elements?” In: *The Astrophysical Journal* 750.1 (Apr. 2012), p. L22. DOI: 10.1088/2041-8205/750/1/l22.

[92] N. Nishimura et al. “The Intermediate r-process in Core-collapse Supernovae Driven by the Magneto-rotational Instability”. In: *The Astrophysical Journal Letters* 836.2 (Feb. 2017), p. L21. DOI: 10.3847/2041-8213/aa5dee.

[93] D. M. Siegel, J. Barnes, and B. D. Metzger. “Collapsars as a major source of r-process elements”. In: *Nature* 569.7755 (May 2019), pp. 241–244. ISSN: 1476-4687. DOI: 10.1038/s41586-019-1136-0.

[94] J. M. Lattimer and M. Prakash. “The Physics of Neutron Stars”. In: *Science* 304.5670 (Apr. 2004), pp. 536–542. DOI: 10.1126/science.1090720.

[95] A. Heger et al. “How Massive Single Stars End Their Life”. In: *The Astrophysical Journal* 591.1 (July 2003), p. 288. DOI: 10.1086/375341.

[96] J. Piekarewicz. *The Nuclear Physics of Neutron Stars*. Jan. 2024. DOI: 10.1093/acrefore/9780190871994.013.91.

[97] J. M. Lattimer and D. N. Schramm. “Black-Hole-Neutron-Star Collisions”. In: *The Astrophysical Journal Letters* 192 (Sept. 1974), p. L145. DOI: 10.1086/181612.

[98] J. M. Lattimer and D. N. Schramm. “The tidal disruption of neutron stars by black holes in close binaries.” In: *Astrophysical Journal* 210 (Dec. 1976), pp. 549–567. DOI: 10.1086/154860.

[99] M. Shibata and K. Taniguchi. “Merger of binary neutron stars to a black hole: Disk mass, short gamma-ray bursts, and quasinormal mode ringing”. In: *Physical Review D* 73.6 (Mar. 2006). DOI: 10.1103/physrevd.73.064027.

[100] S. Rosswog et al. “The long-term evolution of neutron star merger remnants - I. The impact of r-process nucleosynthesis”. In: *Monthly Notices of the Royal Astronomical Society* 439.1 (Jan. 2014), pp. 744–756. DOI: 10.1093/mnras/stt2502.

[101] A. Bauswein, S. Goriely, and H.-T. Janka. "Systematics of dynamical mass ejection, nucleosynthesis, and radioactively powered electromagnetic signals from neutron-star mergers". In: *The Astrophysical Journal* 773.1 (July 2013), p. 78. DOI: 10.1088/0004-637x/773/1/78.

[102] O. Korobkin et al. "On the astrophysical robustness of the neutron star merger r-process". In: *Monthly Notices of the Royal Astronomical Society* 426.3 (Oct. 2012), pp. 1940–1949. DOI: 10.1111/j.1365-2966.2012.21859.x.

[103] R. Fernández et al. "Long-term GRMHD simulations of neutron star merger accretion discs: implications for electromagnetic counterparts". In: *Monthly Notices of the Royal Astronomical Society* 482.3 (Oct. 2018), pp. 3373–3393. DOI: 10.1093/mnras/sty2932.

[104] S. Wanajo et al. "Production of all the r-process nuclides in the dynamical ejecta of neutron star mergers". In: *The Astrophysical Journal* 789.2 (June 2014), p. L39. DOI: 10.1088/2041-8205/789/2/l39.

[105] S. Goriely et al. "Impact of weak interactions of free nucleons on the r-process in dynamical ejecta from neutron star mergers". In: *Monthly Notices of the Royal Astronomical Society* 452.4 (Aug. 2015), pp. 3894–3904. ISSN: 0035-8711. DOI: 10.1093/mnras/stv1526.

[106] D. Martin et al. "Neutrino-driven Winds in the Aftermath of a Neutron Star Merger: Nucleosynthesis and Electromagnetic Transients". In: *The Astrophysical Journal* 813.1 (Oct. 2015), p. 2. DOI: 10.1088/0004-637X/813/1/2.

[107] S. Fujibayashi et al. "Mass Ejection from the Remnant of a Binary Neutron Star Merger: Viscous-radiation Hydrodynamics Study". In: *The Astrophysical Journal* 860.1 (June 2018), p. 64. DOI: 10.3847/1538-4357/aabafd.

[108] R. Ciolfi et al. "General relativistic magnetohydrodynamic simulations of binary neutron star mergers forming a long-lived neutron star". In: *Physical Review D* 95 (6 Mar. 2017), p. 063016. DOI: 10.1103/PhysRevD.95.063016.

[109] R. Fernández and B. D. Metzger. "Delayed outflows from black hole accretion tori following neutron star binary coalescence". In: *Monthly Notices of the Royal Astronomical Society* 435.1 (Aug. 2013), pp. 502–517. ISSN: 0035-8711. DOI: 10.1093/mnras/stt1312.

[110] A. M. Beloborodov and M. Axelsson. “Hyper-accreting black holes”. In: *AIP Conference Proceedings*. AIP, 2008. DOI: 10.1063/1.3002509.

[111] B. D. Metzger and R. Fernández. “Red or blue? A potential kilonova imprint of the delay until black hole formation following a neutron star merger”. In: *Monthly Notices of the Royal Astronomical Society* 441.4 (May 2014), pp. 3444–3453. ISSN: 0035-8711. DOI: 10.1093/mnras/stu802.

[112] P. Walker and Z. Podolyák. “100 years of nuclear isomers — then and now”. In: *Physica Scripta* 95.4 (Feb. 2020), p. 044004. DOI: 10.1088/1402-4896/ab635d.

[113] F. Soddy. “The Stability of Lead Isotopes from Thorium”. In: *Nature* 99.2482 (May 1917), pp. 244–245. ISSN: 1476-4687. DOI: 10.1038/099244c0.

[114] O. Hahn. “Über eine neue radioaktive Substanz im Uran”. In: *Berichte der deutschen chemischen Gesellschaft (A and B Series)* 54.6 (1921), pp. 1131–1142. DOI: https://doi.org/10.1002/cber.19210540602.

[115] C. F. v. Weizsäcker. “Metastabile Zustände der Atomkerne”. In: *Naturwissenschaften* 24.51 (Dec. 1936), pp. 813–814. ISSN: 1432-1904. DOI: 10.1007/BF01497732.

[116] F. Kondev, G. Dracoulis, and T. Kibédi. “Configurations and hindered decays of K isomers in deformed nuclei with A>100”. In: *Atomic Data and Nuclear Data Tables* 103-104 (2015), pp. 50–105. ISSN: 0092-640X. DOI: https://doi.org/10.1016/j.adt.2015.01.001.

[117] P. Walker and G. Dracoulis. “Energy traps in atomic nuclei”. In: *Nature* 399.6731 (May 1999), pp. 35–40. ISSN: 1476-4687. DOI: 10.1038/19911.

[118] P. M. Walker and G. D. Dracoulis. “Exotic Isomers in Deformed Atomic Nuclei”. In: *Hyperfine Interactions* 135.1 (July 2001), pp. 83–107. ISSN: 1572-9540. DOI: 10.1023/A:1013915200556.

[119] D. Belic et al. “Photoactivation of $^{180}\mathrm{Ta}^{m}$ and Its Implications for the Nucleosynthesis of Nature’s Rarest Naturally Occurring Isotope”. In: *Physical Review Letters* 83 (25 Dec. 1999), pp. 5242–5245. DOI: 10.1103/PhysRevLett.83.5242.

[120] E. der Mateosian. “Nuclear Isomerism and Yrast Traps*”. In: *Transactions of the New York Academy of Sciences* 40.1 Series II (1980), pp. 65–70. DOI: https://doi.org/10.1111/j.2164-0947.1980.tb02999.x.

[121] T. Døssing. et al. “Structure of Yrast Traps”. In: *Physical Review Letters* 39 (22 Nov. 1977), pp. 1395–1397. DOI: 10.1103/PhysRevLett.39.1395.

[122] A. Gadea et al. “Hindered E4 decay of the 12+12+ yrast trap in 52Fe”. In: *Physics Letters B* 619 (July 2005), pp. 88–94. DOI: 10.1016/j.physletb.2005.05.073.

[123] P. V. Isacker. “Seniority isomers in nuclei”. In: *Journal of Physics: Conference Series* 322.1 (Oct. 2011), p. 012003. DOI: 10.1088/1742-6596/322/1/012003.

[124] B. Maheshwari, D. Choudhury, and A. K. Jain. “Generalized seniority isomers in and around Z=82 closed shell: A survey of Hg, Pb and Po isotopes”. In: *Nuclear Physics A* 1014 (Oct. 2021), p. 122277. DOI: 10.1016/j.nuclphysa.2021.122277.

[125] K. Wisshak et al. “Fast neutron capture on the Hf isotopes: Cross sections, isomer production, and stellar aspects”. In: *Physical Review C* 73 (4 Apr. 2006), p. 045807. DOI: 10.1103/PhysRevC.73.045807.

[126] S. Okumura et al. “235U(n, f) Independent fission product yield and isomeric ratio calculated with the statistical HauserFeshbach theory”. In: *Journal of Nuclear Science and Technology* 55.9 (2018), pp. 1009–1023. DOI: 10.1080/00223131.2018.1467288.

[127] A. Couture et al. *Measurement of the excitation energy of the 5^+ isomeric state in ^{128}Sb for r-process nucleosynthesis*. Tech. rep. Geneva: CERN, 2021. URL: https://cds.cern.ch/record/2766563.

[128] S.-i. Fujimoto and M.-a. Hashimoto. “The impact of isomers on a kilonova associated with neutron star mergers”. In: *Monthly Notices of the Royal Astronomical Society: Letters* 493.1 (Feb. 2020), pp. L103–L107. DOI: 10.1093/mnrasl/slaa016.

[129] R. A. Ward and W. A. Fowler. “Thermalization of long-lived nuclear isomeric states under stellar conditions”. In: *Astrophysical Journal* 238 (May 1980), pp. 266–286. DOI: 10.1086/157983.

[130] A. Coc, M.-G. Porquet, and F. Nowacki. “Lifetimes of ^{26}Al and ^{34}Cl in an astrophysical plasma”. In: *Physical Review C* 61 (1 Dec. 1999), p. 015801. DOI: 10.1103/PhysRevC.61.015801.

[131] A. Koning, S. Hilaire, and S. Goriely. “TALYS: modeling of nuclear reactions”. In: *The European Physical Journal A* 59.6 (June 2023), p. 131. ISSN: 1434-601X. DOI: 10.1140/epja/s10050-023-01034-3.

[132] W. A. Fowler, G. R. Caughlan, and B. A. Zimmerman. “Thermonuclear Reaction Rates”. In: *Annual Review of Astronomy and Astrophysics* 5.1 (1967), pp. 525–570. DOI: 10.1146/annurev.aa.05.090167.002521.

[133] R. Cyburt et al. “The jina reaclib database: Its recent updates and impact on type-I X-ray bursts”. In: *The Astrophysical Journal Supplement Series* 189 (Aug. 2010), pp. 240–252. DOI: 10.1088/0067-0049/189/1/240.

[134] F. X. Timmes. “Integration of Nuclear Reaction Networks for Stellar Hydrodynamics”. In: *The Astrophysical Journal Supplement Series* 124.1 (Sept. 1999), pp. 241–263. DOI: 10.1086/313257.

[135] W. R. Hix and B. S. Meyer. “Thermonuclear kinetics in astrophysics”. In: *Nuclear Physics A* 777 (Aug. 2006), pp. 188–207. ISSN: 0375-9474. DOI: 10.1016/j.nuclphysa.2004.10.009.

[136] D. D. Clayton. *Principles of stellar evolution and nucleosynthesis : with a new preface*. University of Chicago Press ed. Chicago: University of Chicago Press Chicago, 1983. ISBN: 9780226109534.

[137] W. D. Arnett and D. D. Clayton. “Explosive Nucleosynthesis in Stars”. In: *Nature* 227.5260 (Aug. 1970), pp. 780–784. ISSN: 1476-4687. DOI: 10.1038/227780a0.

[138] J. Lippuner and L. F. Roberts. “SkyNet: A Modular Nuclear Reaction Network Library”. In: *The Astrophysical Journal Supplement Series* 233.2 (Dec. 2017), p. 18. DOI: 10.3847/1538-4365/aa94cb.

[139] G. Bader and P. Deuflhard. “A semi-implicit mid-point rule for stiff systems of ordinary differential equations”. In: *Numerische Mathematik* 41.3 (Oct. 1983), pp. 373–398. ISSN: 0945-3245. DOI: 10.1007/BF01418331.

[140] C. Winteler. "Light element production in the big bang and the synthesis of heavy elements in 3D MHD jets from core-collapse supernovae". PhD thesis. University of Basel, Switzerland, Feb. 2014. DOI: 10.5451/unibas-006194131.

[141] O. Schenk and K. Gärtner. "Solving unsymmetric sparse systems of linear equations with PARDISO". In: *Future Generation Computer Systems* 20.3 (2004). Selected numerical algorithms, pp. 475–487. ISSN: 0167-739X. DOI: https://doi.org/10.1016/j.future.2003.07.011.

[142] B. D. Metzger et al. "Electromagnetic counterparts of compact object mergers powered by the radioactive decay of r-process nuclei: Transients from compact object mergers". In: *Monthly Notices of the Royal Astronomical Society* 406.4 (June 2010), pp. 2650–2662. ISSN: 0035-8711. DOI: 10.1111/j.1365-2966.2010.16864.x.

[143] C. Freiburghaus, S. Rosswog, and F.-K. Thielemann. "r-Process in Neutron Star Mergers". In: *The Astrophysical Journal* 525.2 (Oct. 1999), p. L121. DOI: 10.1086/312343.

[144] S. Wanajo. "Physical Conditions for the r-process. I. Radioactive Energy Sources of Kilonovae". In: *The Astrophysical Journal* 868.1 (Nov. 2018), p. 65. ISSN: 1538-4357. DOI: 10.3847/1538-4357/aae0f2.

[145] M.-R. Wu et al. "Fingerprints of Heavy-Element Nucleosynthesis in the Late-Time Lightcurves of Kilonovae". In: *Physical Review Letters* 122.6 (Feb. 2019). ISSN: 1079-7114. DOI: 10.1103/physrevlett.122.062701.

[146] J. Barnes et al. "Radioactivity and thermalization in the ejecta of compact object mergers and their impact on kilonova light curves". In: *The Astrophysical Journal* 829.2 (Nov. 2016), p. 110. ISSN: 1538-4357. DOI: 10.3847/0004-637x/829/2/110.

[147] E. E. Salpeter. "Electron Screening and Thermonuclear Reactions". In: *Australian Journal of Physics* 7.3 (1954), pp. 373–388. DOI: 10.1071/PH540373.

[148] D. G. Yakovlev et al. "Fusion reactions in multicomponent dense matter". In: *Physical Review C* 74 (3 Sept. 2006), p. 035803. DOI: 10.1103/PhysRevC.74.035803.

[149] S. Ichimaru. “Nuclear fusion in dense plasmas”. In: *Reviews of Modern Physics* 65 (2 Apr. 1993), pp. 255–299. DOI: 10.1103/RevModPhys.65.255.

[150] P. A. Kravchuk and D. G. Yakovlev. “Strong plasma screening in thermonuclear reactions: Electron drop model”. In: *Physical Review C* 89 (1 Jan. 2014), p. 015802. DOI: 10.1103/PhysRevC.89.015802.

[151] I. R. Seitenzahl et al. “Nucleosynthesis in thermonuclear supernovae with tracers: convergence and variable mass particles”. In: *Monthly Notices of the Royal Astronomical Society* 407.4 (July 2010), pp. 2297–2304. ISSN: 0035-8711. DOI: 10.1111/j.1365-2966.2010.17106.x.

[152] S. Nikas. “Nucleosynthesis on the aftermath of neutron star mergers: The creation of the first r-process peak”. PhD thesis. Darmstadt: Technische Universität, 2021, p. 111. DOI: https://doi.org/10.26083/tuprints-00019937.

[153] D. Rochman et al. “Radiative neutron capture: Hauser Feshbach vs. statistical resonances”. In: *Physics Letters B* 764 (2017), pp. 109–113. ISSN: 0370-2693. DOI: https://doi.org/10.1016/j.physletb.2016.11.018.

[154] W. Hauser and H. Feshbach. “The Inelastic Scattering of Neutrons”. In: *Physical Review* 87 (2 July 1952), pp. 366–373. DOI: 10.1103/PhysRev.87.366.

[155] P. A. Moldauer. “Why the Hauser-Feshbach formula works”. In: *Physical Review C* 11 (2 Feb. 1975), pp. 426–436. DOI: 10.1103/PhysRevC.11.426.

[156] F. Käppeler et al. “The *s* process: Nuclear physics, stellar models, and observations”. In: *Reviews of Modern Physics* 83 (1 Apr. 2011), pp. 157–193. DOI: 10.1103/RevModPhys.83.157.

[157] S. Goriely, S. Hilaire, and A. J. Koning. “Improved predictions of nuclear reaction rates with the TALYS reaction code for astrophysical applications”. In: *Astronomy & Astrophysics* 487.2 (June 2008), pp. 767–774. DOI: 10.1051/0004-6361:20078825.

[158] J. Duflo and A. Zuker. “Microscopic mass formulas”. In: *Physical Review C* 52 (1 July 1995), R23–R27. DOI: 10.1103/PhysRevC.52.R23.

[159] P. Möller et al. “Nuclear ground-state masses and deformations: FRDM(2012)”. In: *Atomic Data and Nuclear Data Tables* 109-110 (2016), pp. 1–204. ISSN: 0092-640X. DOI: https://doi.org/10.1016/j.adt.2015.10.002.

[160] S. Goriely, N. Chamel, and J. M. Pearson. “Further explorations of Skyrme-Hartree-Fock-Bogoliubov mass formulas. XII. Stiffness and stability of neutron-star matter”. In: *Physical Review C* 82 (3 Sept. 2010), p. 035804. DOI: 10.1103/PhysRevC.82.035804.

[161] N. Wang and M. Liu. “An improved nuclear mass formula: WS3”. In: *Journal of Physics: Conference Series* 420 (Mar. 2013), p. 012057. ISSN: 1742-6596. DOI: 10.1088/1742-6596/420/1/012057.

[162] M. Wang et al. “The AME2016 atomic mass evaluation (II). Tables, graphs and references”. In: *Chinese Physics C* 41.3 (2017), p. 030003. DOI: 10.1088/1674-1137/41/3/030003.

[163] P. Möller, B. Pfeiffer, and K.-L. Kratz. “New calculations of gross β-decay properties for astrophysical applications: Speeding-up the classical r process”. In: *Physical Review C* 67 (5 May 2003), p. 055802. DOI: 10.1103/PhysRevC.67.055802.

[164] C. R. Harris et al. “Array programming with NumPy”. In: *Nature* 585.7825 (Sept. 2020), pp. 357–362. DOI: 10.1038/s41586-020-2649-2.

[165] P. Virtanen et al. “SciPy 1.0: Fundamental Algorithms for Scientific Computing in Python”. In: *Nature Methods* 17 (2020), pp. 261–272. DOI: 10.1038/s41592-019-0686-2.

[166] M. Marsden. “Cubic spline interpolation of continuous functions”. In: *Journal of Approximation Theory* 10.2 (1974), pp. 103–111. ISSN: 0021-9045. DOI: https://doi.org/10.1016/0021-9045(74)90109-9.

[167] M. A. Famiano et al. “Effects of β-decays of excited-state nuclei on the astrophysical r-process”. In: *Journal of Physics G: Nuclear and Particle Physics* 35.2 (Jan. 2008), p. 025203. ISSN: 1361-6471. DOI: 10.1088/0954-3899/35/2/025203.

[168] G. W. Misch and M. R. Mumpower. “Astromers: status and prospects”. In: *The European Physical Journal Special Topics* (Apr. 2024). ISSN: 1951-6401. DOI: 10.1140/epjs/s11734-024-01136-z.

[169] G. D. Dracoulis, P. M. Walker, and F. G. Kondev. "Review of metastable states in heavy nuclei". In: *Reports on Progress in Physics* 79.7 (May 2016), p. 076301. DOI: 10.1088/0034-4885/79/7/076301.

[170] R. Reifarth et al. "Treatment of isomers in nucleosynthesis codes". In: *International Journal of Modern Physics A* 33.09 (2018), p. 1843011. DOI: 10.1142/S0217751X1843011X.

A Included isomers

Isotope	A	Z	N	J	$t_{1/2}$ (s)	$\Delta M(Z,N)$ (MeV)	E_{ex} (MeV)
$^{58}_{33}$Mn	58	25	33	3.0	3.0	-55.827	
$^{58m}_{33}$Mn	58	25	33	2.0	65.4	-55.756	0.071
$^{62}_{35}$Co	62	27	35	2.0	92.4	-61.424	
$^{62m}_{35}$Co	62	27	35	2.5	831.6	-61.402	0.022
$^{68}_{41}$Co	68	27	41	4.0	0.2	-51.924	
$^{68m}_{41}$Co	68	27	41	1.0	1.6	-51.490	0.434
$^{69}_{41}$Ni	69	28	41	4.5	11.4	-59.979	
$^{69m}_{41}$Ni	69	28	41	0.5	3.5	-59.658	0.321
$^{71}_{43}$Ni	71	28	43	1.5	2.56	-55.406	
$^{71m}_{43}$Ni	71	28	43	0.5	2.3	-55.406	0.000
$^{71}_{41}$Zn	71	30	41	0.5	147	-67.329	
$^{71m}_{41}$Zn	71	30	41	4.5	1.493×10^4	-67.171	0.158
$^{81}_{49}$Ge	81	32	49	4.5	9	-66.291	
$^{81m}_{49}$Ge	81	32	49	0.5	6	-65.613	0.678
$^{82}_{49}$As	82	33	49	1.0	19.1	-70.103	
$^{82m}_{49}$As	82	33	49	2.5	13.6	-69.973	0.130

Continued on next page

Table 2. Added isomers and their properties. Ground state values are from AME2016 [162], with the exception of half-life which uses values from NUBASE2020 [52]. All the isomer values are from NUBASE2020.

Isotope	A	Z	N	J	$t_{1/2}$ (s)	$\Delta M(Z,N)$ (MeV)	E_{ex} (MeV)
$^{83}_{49}$Se	83	34	49	4.5	1335	-75.340	
$^{83m}_{49}$Se	83	34	49	0.5	70.1	-75.112	0.228
$^{84}_{49}$Br	84	35	49	2.0	1906	-77.784	
$^{84m}_{49}$Br	84	35	49	3.0	360	-77.470	0.314
$^{98}_{57}$Nb	98	41	57	1.0	2.86	-83.530	
$^{98m}_{57}$Nb	98	41	57	2.5	3066	-83.441	0.089
$^{99}_{58}$Nb	99	41	58	4.5	15.0	-82.332	
$^{99m}_{58}$Nb	99	41	58	0.5	150	-81.970	0.362
$^{100}_{59}$Nb	100	41	59	1.0	1.5	-79.804	
$^{100m}_{59}$Nb	100	41	59	2.5	2.99	-79.478	0.326
$^{102}_{61}$Nb	102	41	61	1.0	4.3	-76.311	
$^{102m}_{61}$Nb	102	41	61	0.5	1.31	-76.204	0.107
$^{104}_{63}$Nb	104	41	63	1.0	0.98	-71.825	
$^{104m}_{63}$Nb	104	41	63	0.0	4.9	-71.801	0.024
$^{102}_{59}$Tc	102	43	59	1.0	5.28	-84.571	
$^{102m}_{59}$Tc	102	43	59	2.0	261	-84.520	0.051
$^{106}_{61}$Rh	106	45	61	1.0	30.07	-86.362	
$^{106m}_{61}$Rh	106	45	61	3.0	7860	-86.231	0.131
$^{108}_{63}$Rh	108	45	63	5.0	16.8	-85.032	
$^{108m}_{63}$Rh	108	45	63	2.5	360	-84.917	0.115

Continued on next page

Table 2. Added isomers and their properties. Ground state values are from AME2016 [162], with the exception of half-life which uses values from NUBASE2020 [52]. All the isomer values are from NUBASE2020. (Continued)

Isotope	A	Z	N	J	$t_{1/2}$ (s)	$\Delta M(Z,N)$ (MeV)	E_{ex} (MeV)
$^{110}_{65}$Rh	110	45	65	1.0	3.35	-82.829	
$^{110\text{m}}_{65}$Rh	110	45	65	3.0	28.5	-82.610	0.219
$^{112}_{67}$Rh	112	45	67	1.0	3.4	-79.733	
$^{112\text{m}}_{67}$Rh	112	45	67	3.0	6.73	-79.390	0.343
$^{114}_{69}$Rh	114	45	69	1.0	1.85	-75.713	
$^{114\text{m}}_{69}$Rh	114	45	69	3.5	1.85	-75.510	0.203
$^{116}_{71}$Rh	116	45	71	1.0	0.685	-70.739	
$^{116\text{m}}_{71}$Rh	116	45	71	3.0	0.570	-70.540	0.199
$^{122}_{75}$Ag	122	47	75	3.0	0.529	-71.110	
$^{122\text{m1}}_{75}$Ag	122	47	75	0.5	0.55	-71.030	0.080
$^{122\text{m2}}_{75}$Ag	122	47	75	4.5	0.2	-71.030	0.080
$^{115}_{67}$Cd	115	48	67	0.5	1.925×10^5	-88.084	
$^{115\text{m}}_{67}$Cd	115	48	67	5.5	3.850×10^6	-87.903	0.181
$^{117}_{69}$Cd	117	48	69	0.5	9011	-86.419	
$^{117\text{m}}_{69}$Cd	117	48	69	5.5	1.239×10^4	-86.282	0.137
$^{119}_{71}$Cd	119	48	71	1.5	161	-83.976	
$^{119\text{m}}_{71}$Cd	119	48	71	5.5	132	-83.830	0.146
$^{121}_{73}$Cd	121	48	73	1.5	13.5	-81.073	
$^{119\text{m}}_{71}$Cd	121	48	73	5.5	8.3	-80.859	0.214
$^{116}_{67}$In	116	49	67	1.0	14.10	-88.250	
$^{116\text{m}}_{67}$In	116	49	67	2.5	3257	-88.122	0.128

Continued on next page

Table 2. Added isomers and their properties. Ground state values are from AME2016 [162], with the exception of half-life which uses values from NUBASE2020 [52]. All the isomer values are from NUBASE2020. (Continued)

Isotope	A	Z	N	J	$t_{1/2}$ (s)	$\Delta M(Z,N)$ (MeV)	E_{ex} (MeV)
$^{118}_{69}$In	118	49	69	1.0	5.0	-87.230	
$^{118\mathrm{m}}_{69}$In	118	49	69	2.5	261.8	-87.130	0.100
$^{120}_{71}$In	120	49	71	1.0	3.08	-85.727	
$^{120\mathrm{m1}}_{71}$In	120	49	71	2.5	46.2	-85.680	0.047
$^{120\mathrm{m2}}_{71}$In	120	49	71	4.0	47.3	-85.430	0.297
$^{122}_{73}$In	122	49	73	1.0	1.5	-83.574	
$^{122\mathrm{m1}}_{73}$In	122	49	73	2.5	10.3	-83.530	0.044
$^{122\mathrm{m2}}_{73}$In	122	49	73	4.0	10.8	-83.280	0.294
$^{123}_{74}$In	123	49	74	4.5	6.17	-83.433	
$^{123\mathrm{m}}_{74}$In	123	49	74	0.5	47.4	-83.102	0.331
$^{125}_{76}$In	125	49	76	4.5	2.36	-80.480	
$^{125\mathrm{m}}_{76}$In	125	49	76	0.5	12.2	-80.060	0.420
$^{126}_{77}$In	126	49	77	0.0	1.53	-77.769	
$^{126\mathrm{m}}_{77}$In	126	49	77	4.0	1.64	-77.719	0.050
$^{127}_{78}$In	127	49	78	4.5	1.086	-76.898	
$^{127\mathrm{m1}}_{78}$In	127	49	78	0.5	3.618	-76.486	0.412
$^{127\mathrm{m2}}_{78}$In	127	49	78	10.5	1.04	-75.110	1.788
$^{129}_{80}$In	129	49	80	4.5	0.570	-72.835	
$^{129\mathrm{m}}_{80}$In	129	49	80	0.5	1.23	-72.384	0.451

Continued on next page

Table 2. Added isomers and their properties. Ground state values are from AME2016 [162], with the exception of half-life which uses values from NUBASE2020 [52]. All the isomer values are from NUBASE2020. (Continued)

Isotope	A	Z	N	J	$t_{1/2}$ (s)	$\Delta M(Z,N)$ (MeV)	E_{ex} (MeV)
$^{130}_{81}$In	130	49	81	0.0	0.273	-69.884	
$^{130\mathrm{m1}}_{81}$In	130	49	81	5.0	0.54	-69.840	0.044
$^{130\mathrm{m2}}_{81}$In	130	49	81	2.5	0.54	-69.521	0.363
$^{131}_{82}$In	131	49	82	4.5	0.2615	-68.022	
$^{131\mathrm{m1}}_{82}$In	131	49	82	0.5	0.328	-67.648	0.374
$^{131\mathrm{m2}}_{82}$In	131	49	82	10.5	0.322	-64.280	3.742
$^{133}_{84}$In	133	49	84	4.5	0.1630	-59.030	
$^{133\mathrm{m}}_{84}$In	133	49	84	0.5	0.167	-57.360	1.670
$^{123}_{73}$Sn	123	50	73	5.5	1.116×10^7	-87.815	
$^{123\mathrm{m}}_{73}$Sn	123	50	73	1.5	2404	-87.790	0.025
$^{125}_{75}$Sn	125	50	75	5.5	8.324×10^5	-85.893	
$^{125\mathrm{m}}_{75}$Sn	125	50	75	1.5	586	-85.866	0.027
$^{127}_{77}$Sn	127	50	77	5.5	7560	-83.470	
$^{127\mathrm{m}}_{77}$Sn	127	50	77	1.5	248	-83.465	0.005
$^{129}_{79}$Sn	129	50	79	1.5	134	-80.607	
$^{129\mathrm{m}}_{79}$Sn	129	50	79	5.5	410	-80.556	0.051
$^{130}_{80}$Sn	130	50	80	0.0	223	-80.136	
$^{130\mathrm{m}}_{80}$Sn	130	50	80	3.5	100	-78.185	1.951
$^{131}_{81}$Sn	131	50	81	1.5	56.0	-77.275	
$^{131\mathrm{m}}_{81}$Sn	131	50	81	5.5	58.4	-77.200	0.075

Continued on next page

Table 2. Added isomers and their properties. Ground state values are from AME2016 [162], with the exception of half-life which uses values from NUBASE2020 [52]. All the isomer values are from NUBASE2020. (Continued)

Isotope	A	Z	N	J	$t_{1/2}$ (s)	$\Delta M(Z,N)$ (MeV)	E_{ex} (MeV)
$^{130}_{79}$Sb	130	51	79	8.0	2370	-82.288	
$^{130\mathrm{m}}_{79}$Sb	130	51	79	2.0	380	-82.281	0.007
$^{132}_{81}$Sb	132	51	81	4.0	167	-79.636	
$^{132\mathrm{m}}_{81}$Sb	132	51	81	4.0	246	-79.490	0.146
$^{134}_{83}$Sb	134	51	83	0.0	0.674	-74.023	
$^{134\mathrm{m}}_{83}$Sb	134	51	83	3.5	10.01	-73.740	0.283
$^{146}_{89}$La	146	57	89	2.0	9.9	-69.051	
$^{146\mathrm{m}}_{89}$La	146	57	89	0.5	6.08	-69.080	-0.029
$^{152}_{91}$Pm	152	61	91	1.0	247	-71.253	
$^{152\mathrm{m}}_{91}$Pm	152	61	91	2.0	451	-71.110	0.143
$^{166}_{99}$Ho	166	67	99	0.0	9.6523×10^4	-63.069	
$^{166\mathrm{m}}_{99}$Ho	166	67	99	3.5	3.5718×10^{10}	-63.064	0.005
$^{170}_{103}$Ho	170	67	103	6.0	166	-56.243	
$^{170\mathrm{m}}_{103}$Ho	170	67	103	0.5	43	-56.140	0.103

Table 2. Added isomers and their properties. Ground state values are from AME2016 [162], with the exception of half-life which uses values from NUBASE2020 [52]. All the isomer values are from NUBASE2020. (Continued)

B Added and modified codes

Here are listed some of the most notable code additions and changes. These are written in Fortran90. The first one is used for distinguishing the isomers from output files, while the rest are used to compile the input files. File `isomers_fortran.dat` is a precompiled list of names given to every possible isomer found in NUBASE2020. The codes shown here are entirely self-written except the last one, in which the greyed parts are original code.

```
subroutine find_iso(elem, isom)
  !---------------------------------------------------------------------
  !  This routine returns the isomer number (0=g.s., 1=1st isom state,
  !  and so on) for the given element.
  !---------------------------------------------------------------------
  implicit none

  character(5), intent(in) :: elem
  integer, intent(out) :: isom
  character(2), dimension (0:6, 0:120) :: isomers
  character(2) :: elname
  integer :: ierr, i, j

  !  Read isomers from file to array
  open(222,file='network_data/isomers_fortran.dat',status='old')
  read(222,'(7(A2,1X))',iostat=ierr) isomers
  close(222)

  ! Get the element name from the input
  call find_name(elem, elname)
  isom = 0
  do i = 0, size(isomers, 2)-1   ! element
```

```
    do j = 0, size(isomers, 1)-1 ! isomer
      if (isomers(j, i) .eq. 'XX') exit
      if (isomers(j, i) .eq. elname) then
        if (i .eq. 0 .or. i .eq. 1) return ! n can be both neutron
        isom = j                           ! and nitrogen, both are
        return                             ! g.s.
      end if
    end do
  end do
end subroutine find_iso
```

```
subroutine mapname_mod(zn,zp,nam,ind)
!-----------------------------------------------------------------------
! zn....intent in: neutron number
! zp....intent in: proton number
! nam..intent out: name corresponding to zn, zp
! Determines name of nucleus from proton and neutron number
! Correct format: right bound, length 5 characters, name+mass number
! Modded to include the isomers
!-----------------------------------------------------------------------
  implicit none

  integer, intent(in) :: zn
  integer, intent(in out) :: zp,ind
  character(5), intent(out) :: nam
  integer, parameter :: zmax=120
  character(2) :: hname
  character(3) :: cza
  character(2) :: nname(2:zmax)
  character(2) :: nmassnr(0:9)
  character(2) :: inname(2:zmax)
  integer :: za,hza
  integer :: i,j,k0
  integer :: IERR

  character(2), dimension (0:6, 0:120) :: isomers
  data nmassnr/'0','1','2','3','4','5','6','7','8','9'/
  open(12, file='./inputs/isomers_fortran.dat')

  read(12,'(7(A2,1X))',iostat=IERR) isomers

  close(12)
  ! Read in values

  nam='     '
```

```
  if(zp >= 2) then
    !ind=0
    hname=isomers(ind,zp)
    !print *, hname
    za=zp+zn
    write(cza,'(I3)') za
    cza=adjustl(cza)
    nam=adjustr(hname//cza)
  else if (zp >= 0 .and. zp < 2) then
    !ind=0
    if(zp == 0) nam='    n'
    if(zp == 1 .and. zn == 0) nam='    p'
    if(zp == 1 .and. zn == 1) nam='    d'
    if(zp == 1 .and. zn == 2) nam='    t'
  end if
  return
end subroutine mapname_mod
```

```
subroutine iisomer(neut,prot,iso)
!-----------------------------------------------------------------
!  This subroutine finds the number of isomers in the daughter
!  nucleus in beta decay by reading a file created from fpbmex.
!-----------------------------------------------------------------
  use inputcontrol
  implicit none
  integer, intent(in)          :: neut,prot
  integer, intent(out)         :: iso
  integer                      :: i,k,ind,lmax,nmax,fline,lline,line=1
  integer                      :: zz,nn,aa,iiso
  real(8)                      :: rbeta,thalf              ! half-life
  real(8)                      :: brbth(12)
  integer                      :: ibr=4
  character(len=21)            :: str
  integer                      :: ios
  logical                      :: fexist,fexist2

  inquire(file='./out/isomers', exist=fexist)
  inquire(file='./out/isomers_fortran.dat', exist=fexist2)

  open(601,file='./inputs/'//trim(fpbmex),status='old')
  open(602,file='./out/isomers',status='unknown')
  open(603,file='./inputs/isomers_fortran.dat',status='old')
  open(604,file='./out/isomers_fortran.dat',status='unknown')

! Create file for number of isomers for each isotope if it does not
! exist yet
  if(.not. fexist) then
    call countlines(601,fline)
    nmax=fline
    do i=1,nmax
      read(601,*) zz,nn,ind,iiso,thalf,(brbth(k),k=1,ibr*3)
      !nn = aa - zz
```

```
      if(iiso == 0) then
        write(602,*) zz,nn,iiso
      else if(iiso > 0 .and. ind == 0) then
        write(602,*) zz,nn,iiso
      end if
    end do
  end if

! Copy fortran_isomers.dat to 'out' directory if the file does not
! exist there yet
  if(.not. fexist2) then
    call countlines(603,fline)
    nmax=fline
    do i=1,nmax
      read(603, '(A)', iostat=ios) str
      write(604,'(A)') str
    end do
  end if

! Read the number of isomers from the file ./out/isomers
  call countlines(602,lline)
  lmax=lline
  do i=1,lmax
    read(602,*) zz,nn,iiso
    if(zz == prot .and. nn == neut) then
      iso=iiso
      exit
    end if
  end do

  close(601)
  close(602)

end subroutine
```

```
subroutine beta_exp_data
!-------------------------------------------------------------
! Reads input files for beta decay data
!-------------------------------------------------------------
...
  ! i,j: indices, k: number of isomers
  ! l: 2nd index in 2d array, nmax: total number of isotopes
  ! in beta input file, fline: number of lines in input file
  integer :: i,j,k,l,nmax,fline
  ! zz,nn,aa: nuclear properties
  integer :: zz,nn,aa
  ! rbeta: decay constant, thalf: half-life
  real(8) :: rbeta,thalf
  ! ibr: number of branching channels in beta-delayed neutron
  ! emission (1=no beta-delayed neutrons)
  integer :: ibr=4
  ! imers: the maximum number of isomeric states considered
  ! in each isotope
  integer :: imers=2
  ! brbex: a 2D array containing beta branching rates
  real(8), dimension(4,3) :: brbex(1:4, 0:2)  ! now a 2D array
  ! ind,iiso,isom,idx,n: indices used in do-loops
  integer :: ind,iiso,isom,idx,n
...
  do i=1,nmax
    ! Read beta decay file which lists beta-delayed neutrons
    ! (up to 4) and possible decays to isomeric states.
    read(501,*) zz,nn,ind,iiso,thalf,(brbex(1,k),k=0,imers),
    ↪  (brbex(2,k),k=0,imers),(brbex(3,k),k=0,imers),
    ↪  (brbex(4,k),k=0,imers)
    rbeta=log(2.0d0)/thalf
    call mapname_mod(nn,zz,namreac(1),ind)
    call benam(namreac(1),inamreac(1))
    if(inamreac(1)>0) then
```

```
      if(iexp(inamreac(1))==2) then
        write(505,*) namreac(1), inamreac(1)
        cycle
      end if
      do k=1,ibr
        call iisomer(nn-k,zz+1,isom)
        do n=0,isom
          idx=n
          if(brbex(k,idx)>0.0) then
            call mapname_mod(nn-k,zz+1,namreac(2),idx)
            call benam(namreac(2),inamreac(2))
...
          end if
        end do
      end do
    end if
  end do
...
end subroutine
```

C Abundance evolution with different trajectories

The following figures illustrate the abundance evolution with different trajectories at the beginning of the r-process when neutron captures begin, during the r-process when the matter accumulates at even, and particularly at magic neutron numbers, and after the neutron captures have ended and the matter decays to the stability. Abundance (Y) of each isotope is marked with a red hue, the darkest being the most abundant isotopes. The scale is logarithmic. Black squares represent stable isotopes, and vertical and horizontal blue lines mark the magic neutron and proton numbers. The temperature (T) and time (t) of each snapshot can be found in the lower right-hand corner of each plot.

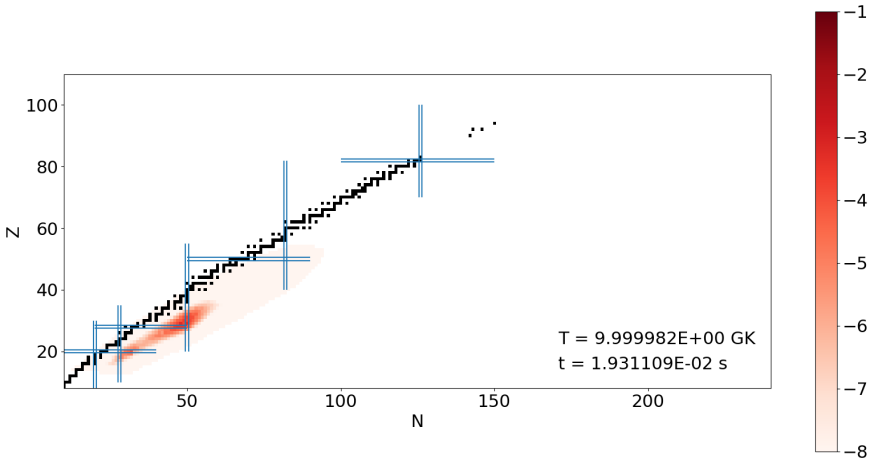

(a) At the beginning of neutron captures.

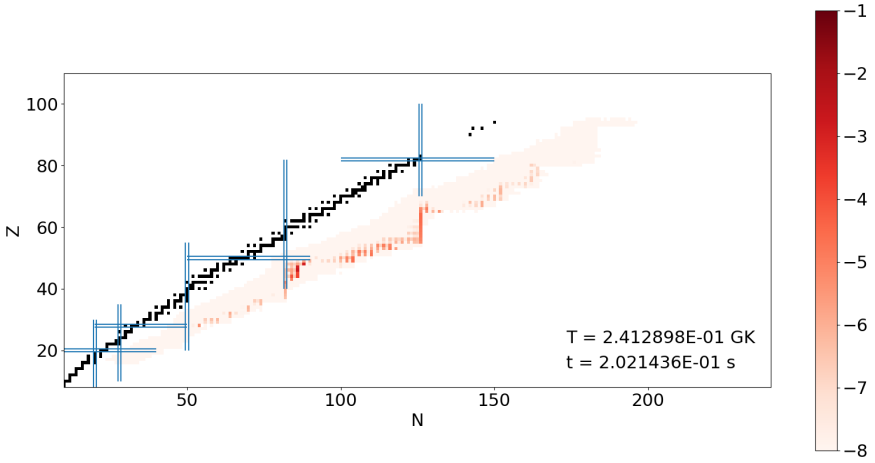

(b) During the r-process as matter accumulates at magic neutron numbers.

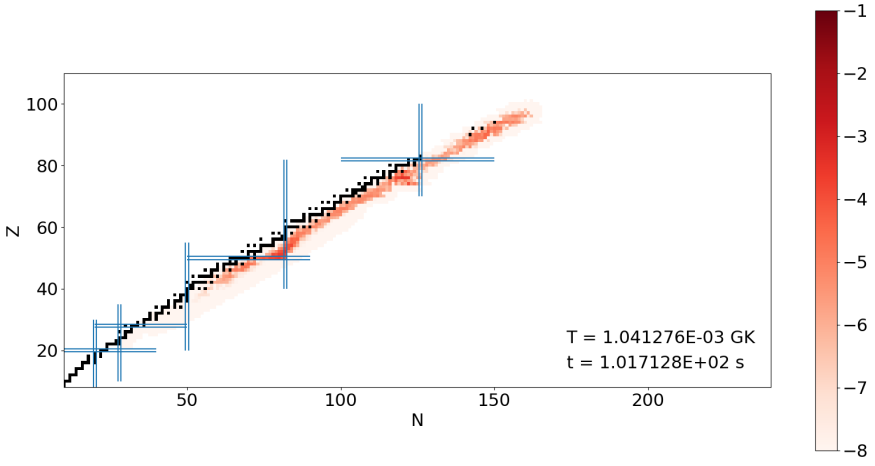

(c) After the neutron captures have ended, and the matter has nearly decayed to the stability.

Figure 26. Abundance evolution of Trajectory 1.

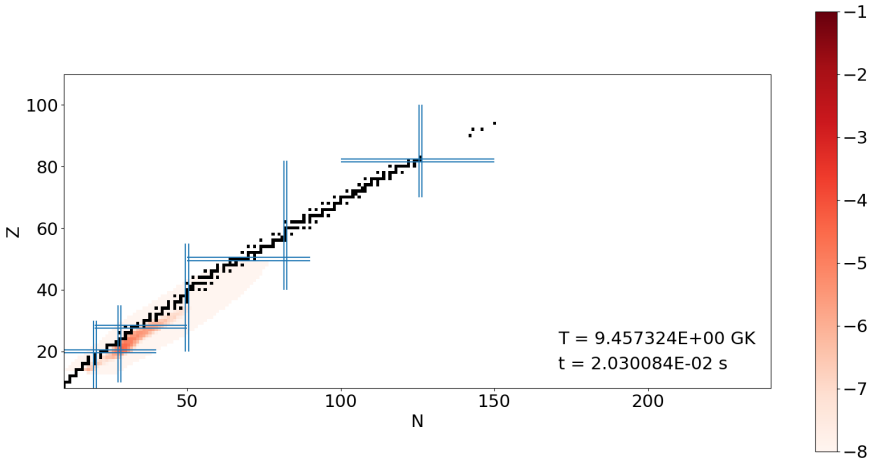

(a) At the beginning of neutron captures.

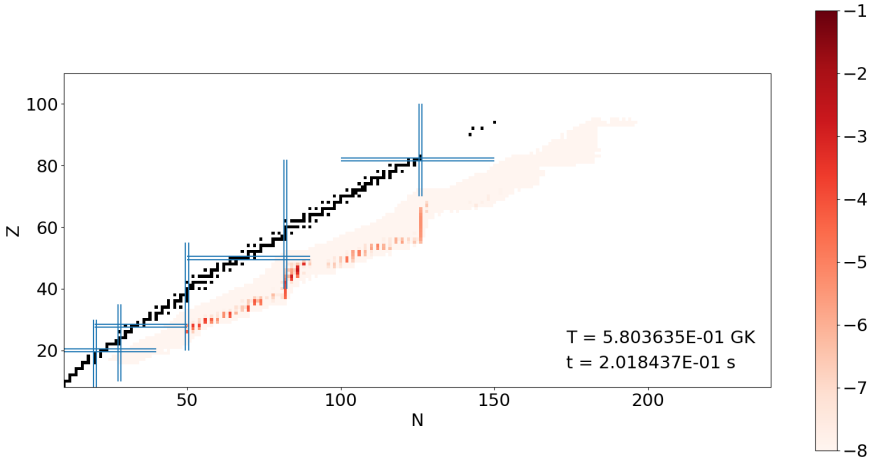

(b) During the r-process as matter accumulates at magic and even neutron numbers.

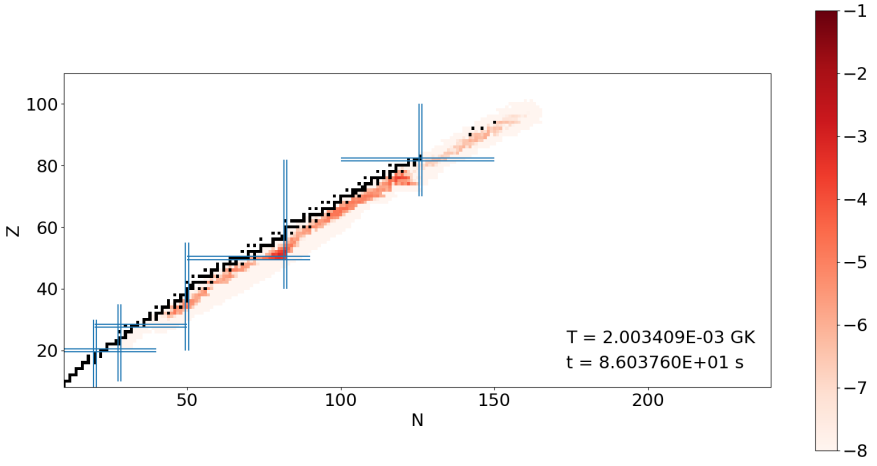

(c) After the neutron captures have ended, and the matter has nearly decayed to the stability.

Figure 27. Abundance evolution of Trajectory 2.

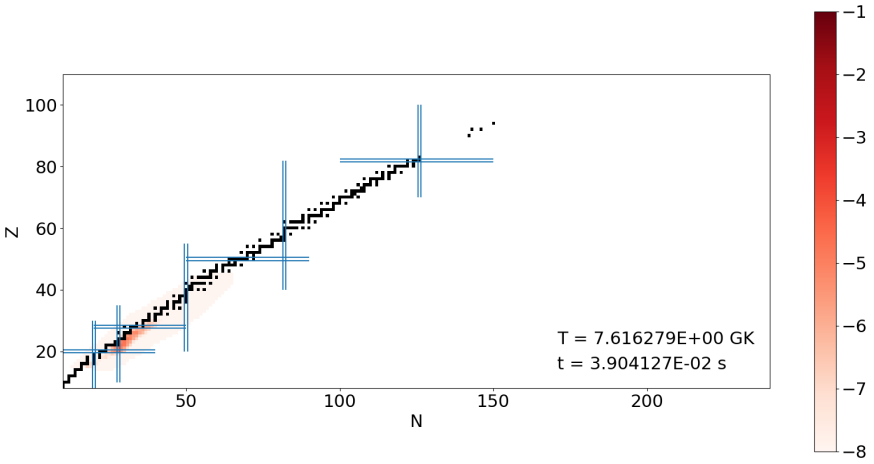

(a) At the beginning of neutron captures.

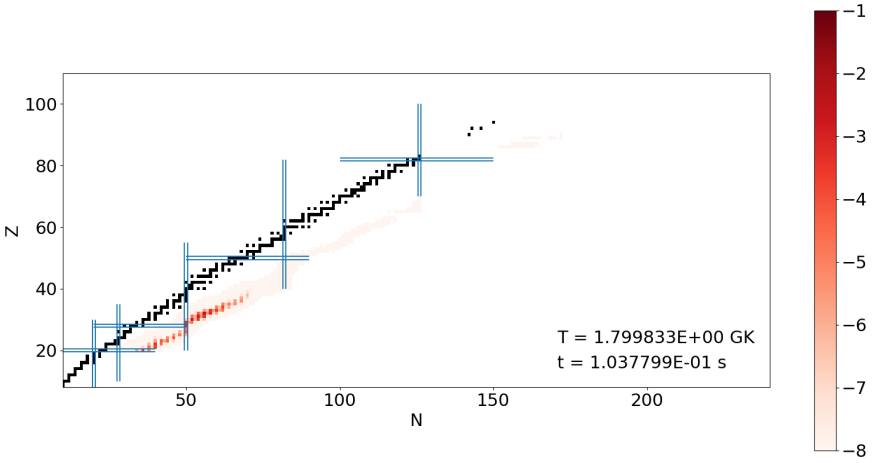

(b) During the r-process as matter accumulates at magic and even neutron numbers.

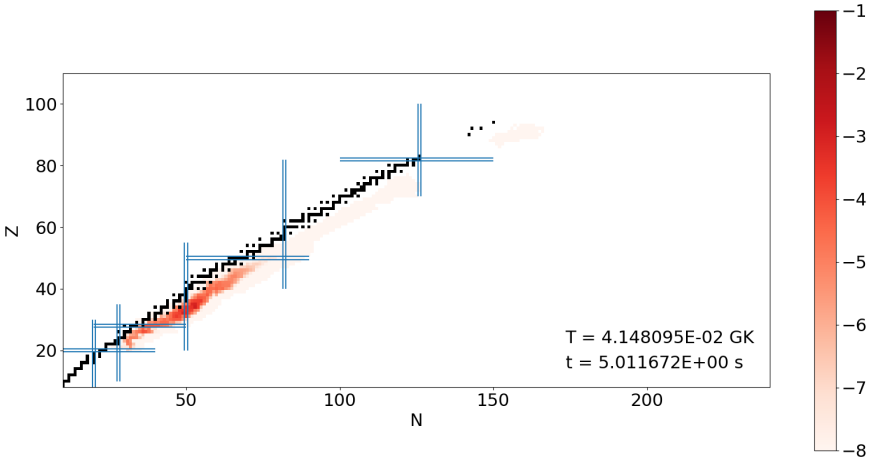

(c) After the neutron captures have ended, and the matter has nearly decayed to the stability.

Figure 28. Abundance evolution of Trajectory 3.

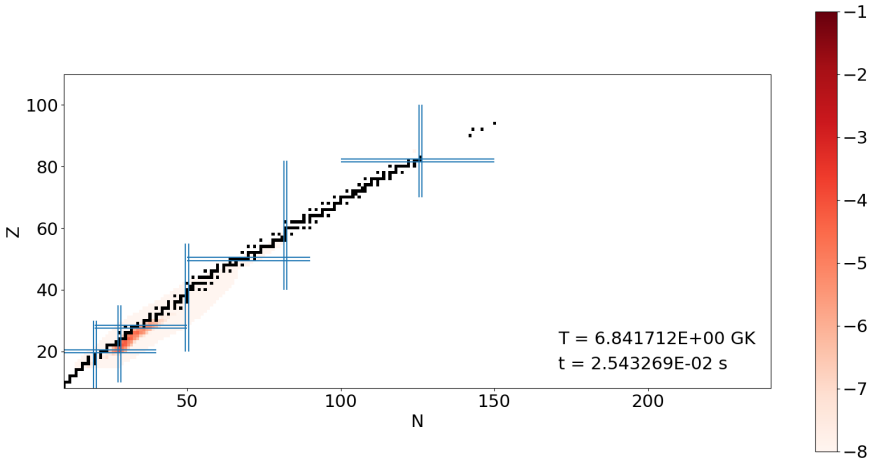

(a) At the beginning of neutron captures.

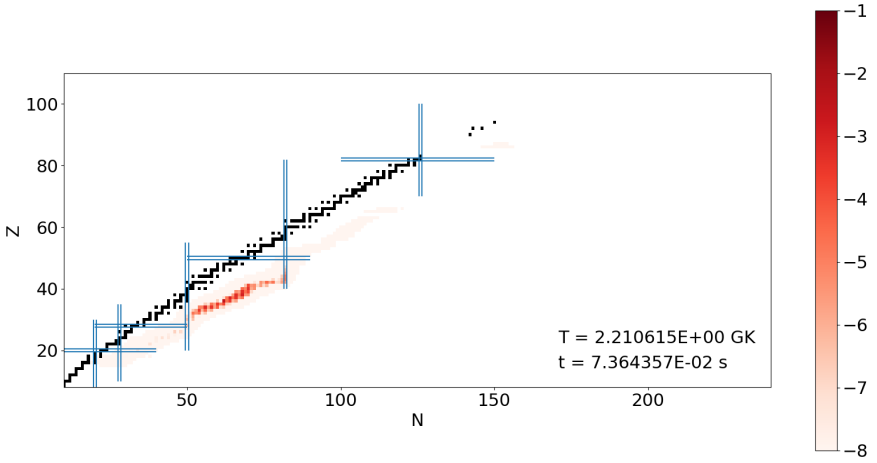

(b) During the r-process as matter accumulates at even neutron numbers.

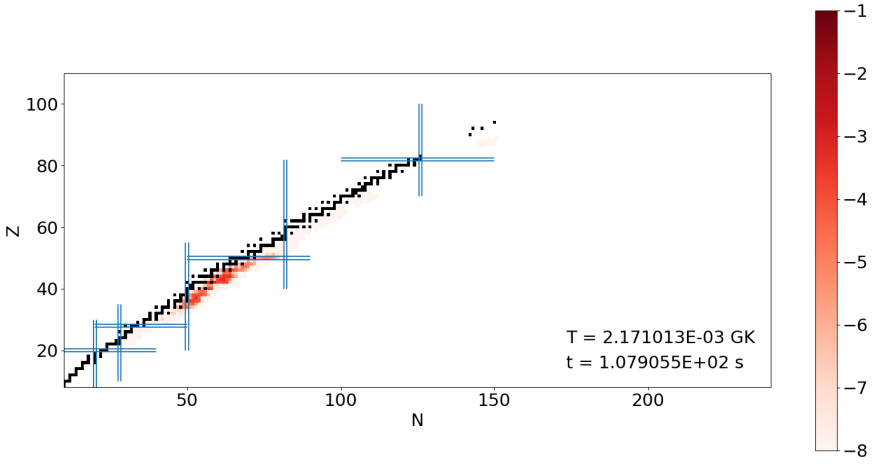

(c) After the neutron captures have ended, and the matter has nearly decayed to the stability.

Figure 29. Abundance evolution of Trajectory 4.

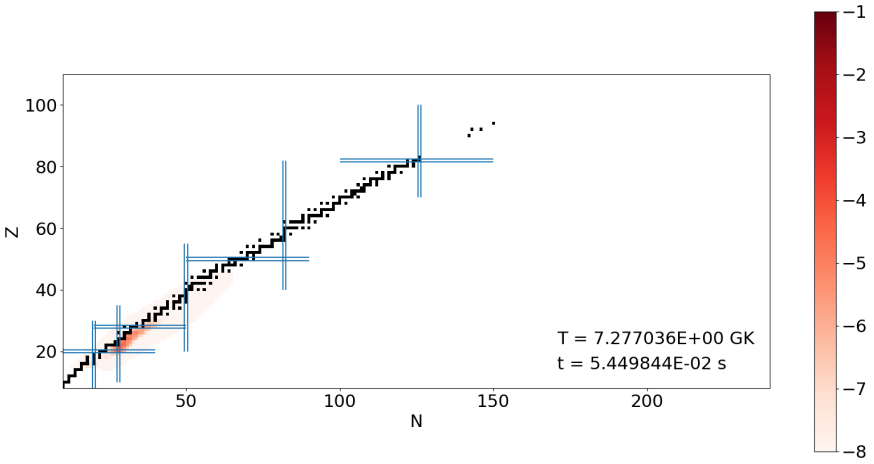

(a) At the beginning of neutron captures.

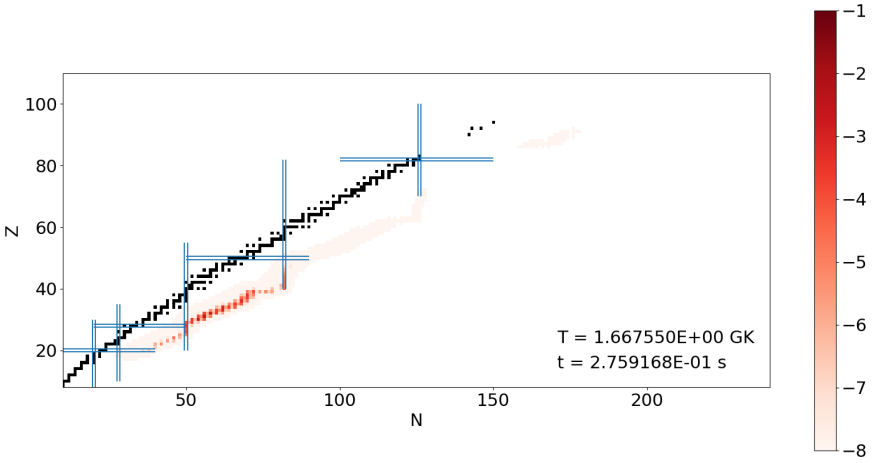

(b) During the r-process as matter accumulates at even neutron numbers.

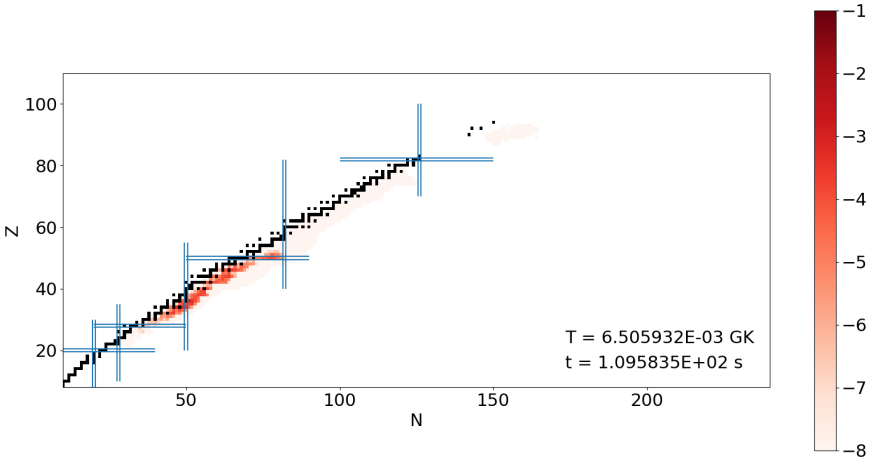

(c) After the neutron captures have ended, and the matter has nearly decayed to the stability.

Figure 30. Abundance evolution of Trajectory 5.